Fatigue Behaviour of 6061 Aluminium Alloy and Its Composite

By

Ping Hwa LIM, BEng (Honours)

This thesis is submitted to Dublin City University as the fulfilment of the requirement for the award of the degree of

Master in Engineering

Supervisor: Dr. Lisa Looney

School of Mechanical and Manufacturing Engineering
Dublin City University
September 2001

DECLARATION

I hereby certify that this material, which I now submit for assessment on the programme of study leading to the award of *Master in Engineering*, is entirely my own work and has not been taken from the work of others save and to the extent that such work has been cited and acknowledge within the text of my work.

Signed: 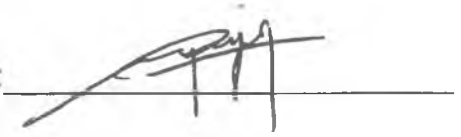

Date: 23rd September 2001

Ping Hwa LIM
ID: 98970917

Acknowledgements

I would like to take this opportunity to acknowledge the contribution of those who assisted me in completing this project. In particular:

My academic supervisor, Dr. Lisa Looney of Dublin City University (DCU) for her guidance, support, encouragement, time and limitless energy for useful discussion and thesis evaluation.

Professor Saleem Hashmi of the School of Mechanical and Manufacturing Engineering DCU, for the funding, without which this project would not have been possible.

Christopher Crouch, Jim Barry, Keith Hickey, Liam Domican, Martin Johnson, Michael May and all the technical and academic staff involved in this work, for their assistance and providing me with all I requested.

All the postgraduates within the department of Mechanical and Manufacturing Engineering, Dublin City University. Special thanks to Amy O'Callaghan, Annmarie Byrne, Anthony Comer, Brian O'Sullivan, Clint Carolan, David Chua and Joseph Stokes for their assistance, support and friendship.

Finally, to my parents, brothers and sisters for their endless source of encouragement and optimism; thanks.

Abstract

Fatigue Behaviour of 6061 Aluminium Alloy and Its Composite

Ping Hwa LIM, BEng (Honours)

Fatigue behaviour of an artificial aged powder metallurgy 6061 aluminium alloy, and a composite made of this alloy with 15% volume fraction of SiC_P was investigated. The alloy was subjected to T6 heat treatment, as was the composite material chosen (which incorporated SiC particles of average size 30μm). An extensive experimental programme was carried out in which fatigue lives were determined using load-controlled axial loading of unnotched cylindrical samples, at stress ratios of –1 and 0.1. Tensile properties of both materials were also established.

The tensile behaviour of the alloy is in agreement with other published data for this material, and the significant influence of mean stress on fatigue behaviour found, is consistent with that normally observed in metals. The relationship between number of cycles to failure and stress found for the alloy is within the range of scatter usually seen in such tests, and corresponds with available data. However, it has been found that while stiffness of the composite material is higher than that of the matrix, tensile strength and fatigue life are lower in the composite, as is ductility. At each stress ratio, the composite material exhibits shorter fatigue life at low and intermediate stresses, compared with the unreinforced aluminium alloy. While a number of these trends are consistent with expectations for ceramic reinforced metal composites, the relatively low strength of the materials is not.

Standard metallographic techniques, as well as fractographic observation under a scanning electron microscope were used to further investigate material behaviour. Particularly large particles of SiC are identified as having contributed to fracture behaviour, along with poor interfacial properties.

Table of Contents

Chapter 1: Introduction

For many years there has been a continuous quest for high performance materials to operate in ever more extreme conditions of temperature and environment, without incurring a high weight penalty. These conditions arise in critical areas such as aerospace/defence and the nuclear sectors, as well as in civilian sectors such as automotive and other general applications.

Aluminium alloys are among the traditional engineering materials considered to fulfil the above requirements, and have been used extensively to successfully meet many of the needs of industry. The major advantages of aluminium alloys are reported as their low weight, low density, good coefficient of linear expansion, good strength and good fatigue behaviour compared to other metallic alloys [1-3]. In recent years, increase in demands for high specific strength, good stiffness, and high fatigue strength materials that can work in different environments have stimulated aluminium alloy related research in academic communities and government sectors [4-5]. Because of the additional requirement for materials to operate under conditions of multidirectional stress and strain, much of this research has focused on the advanced materials: particulate ceramic reinforced metal matrix composites (PMMCs).

Various aluminium alloys reinforced with SiC particles (SiC_p) have been shown to provide improved strength, stiffness, wear resistance, creep behaviour and lower thermal expansion compared to the corresponding monolithic aluminium alloy [6-9]. In addition to their isotropic mechanical properties, SiC particulate reinforced aluminium alloys can be fabricated economically by conventional metallurgical and mechanical processes. As the production of aluminium based metal matrix composite

(AMMC) increases consecutively every year, and its commercial application becomes rather wide, there is a need for more extensive knowledge of AMMCs. Areas which merit study include processing techniques and mechanical behaviour as well as fatigue properties which included cyclic deformation response, fatigue strength and fatigue related fracture behaviour.

1.1 Fatigue Behaviour of Aluminium and Its Composites

Over the past two decades, many researchers all around the world have carried out studies on the fatigue properties of aluminium alloys and its composites. Numerous reports on fatigue and fatigue related fracture of these materials have been published. However, various conclusions in this area have been well received and sometimes very controversial results from different research groups have been reported. There are published results showing the superiority of aluminium based composites over its matrix alloy in terms of fatigue strength or fatigue lifetime, as well as increases in yield and ultimate tensile strength [10-13]. However, some researches show contrary results, or the improvement of material properties is not as pronounced [14, 15]. Hence, the question "are the MMCs really superior to the conventional alloy in terms of fatigue properties"? is still not satisfactorily answered.

The answer to the question is not easily established, as a variety of factors are involved in fatigue in metallic alloys, a complex process. Factors which may lead to variations in results for seemingly similar materials include the following [16-18]:

- The differences in processing techniques may introduce different processing defects in AMMCs products from different manufacturers.

- The size, distribution, shape and aspect ratio of reinforced particulate may differ between manufacturers, and often only mean particulate characteristics are given.

1.2 Present Research

In this context of incomplete understanding of fatigue behaviour of MMCs, the present research focuses on the mechanical and fatigue fracture behaviour of 6061 aluminium alloy and its composite. The composite system investigated in the experimental analyses for this research consists of silicon carbide (SiC) particle reinforced 6061 aluminium alloy. The aim of this work is to investigate and to understand the mechanical and fatigue behaviour of composite compared to those of the conventional aluminium alloy.

Specifically, the fatigue behaviour of an artificial aged, powder metallurgy 6061 aluminium alloy, and a composite made of this alloy with 15% volume fraction of SiC_P was investigated. The alloy was subjected to T6 heat treatment, as was the composite material chosen (which incorporated SiC particles of average size 30μm). An extensive experimental programme was carried out in which fatigue lives were determined using load-controlled axial loading of unnotched cylindrical samples, at stress ratios of –1 and 0.1. Tensile properties of both materials were also established. Further investigation included microstructural analysis - the study of metallographic and fractography samples.

1.3 Overview of Thesis

Following from this introduction, Chapter 2 summarises the literature survey carried out for this research and includes the topics of MMCs, MMC processing and fatigue behaviour of aluminium and aluminium based composites. The literature survey mainly focuses on aluminium based composite systems since the materials used in the present research are an aluminium alloy and its composite. Chapter 3 describes the experimental equipment and work carried out, and includes descriptions of the materials, tensile and fatigue testing equipment, and the test procedures used. The results obtained from the experimental work described in Chapter 3 are presented in Chapter 4. This chapter includes discussion based on experimental results of tensile and fatigue tests, metallography and fractography of material surfaces investigated under optical microscope and scanning electron microscope (SEM). Finally, Chapter 5 summarises conclusions from the present research and lists recommendation to further this research.

Chapter 2: Literature Review

2.1 Metal Matrix Composites

A composite material can be described as a mixture of component materials. It is designed to meet a specific engineering requirement by exploiting the desirable properties of the components, whilst minimising the harmful effects of their less desirable properties. It is often composed of a matrix material to which is added one or more reinforcement. The classification of composite material is according to the type of matrix material employed, such as metallic, polymeric, glass and ceramic composites etc [16-18].

Metal matrix composites (MMCs) are defined as the combination of two or more chemically different materials to produce a third, which has unique properties when compared to the monolithic material properties [21]. There is a broad family of MMCs materials which aim to achieve an enhanced combination of properties such as low density, good specific strength and stiffness, high thermal conductivity, high temperature capabilities, low coefficients of thermal expansion, good corrosion and wear resistance and increased fatigue strength. They have a wide range of applications in many major industries all over the world [6, 8, 19-20].

The first MMCs were developed during the 1960s [16]. The development of continuous carbon and boron fibres of aluminium composites led to considerable research in the period of 1960s and 1970s under the space project by NASA and the department of defence in the Unite States of America [16, 21]. But the problems of

complex reinforcement processes, the high cost of boron fibres and their production route and also the limited types of fibres that could be compatible with the matrix have limited its commercial engineering application. Hence, no significant further attention was paid to these materials [1]. On the other hand, polymer matrix composites became the dominant materials in the early 1970s.

The late 1970s and 1980s saw a surge of interest in MMCs due to the development of a wide range of low cost, and superior quality reinforcements. These led to increased interest in low cost industries and in others sectors such as aerospace and military [18, 21]. It is mainly during the last decade that MMCs have really been developed most intensively. The space industry was the pioneer in terms of interest in the usage of MMC's, followed by the aerospace and automotive sectors who found this materials to have economic importance [22]. Other applications of MMC's to date have included sports and leisure products.

The future of MMCs is bright; more research and development projects are ongoing all over the globe in terms of improving or inventing new technology in MMCs processing. Besides that, better understanding of fatigue and fracture behaviour is needed in order to ensure the adoption of this material in future.

MMCs as a class of materials can have both advantages and disadvantages compared with other materials. There are summarised below.

Comparison with un-reinforced metal [18, 19]:

- Advantages - higher specific strength.
  - higher specific stiffness.
  - improved high temperature creep resistance.
  - improved wear resistance.

- Disadvantages - lower toughness and ductility.
  - more complicated and expensive production methods.

Compared to polymer matrix composites [21, 37]:

- Advantages - higher transverse strength.
  - higher toughness.
  - higher thermal and electrical conductivity.
  - higher temperature capability.
  - improved environment resistance.
  - better damage tolerance.

- Disadvantages - less developed technology.
  - higher cost.
  - smaller data base of properties.

Compared to ceramics matrix composites [21, 28]:

- Advantages - lower cost.
  - higher toughness and ductility.
  - greater ease of fabrication.

Disadvantages - inferior high temperature strength.

2.1.1 Classification of MMCs

As is well accepted, MMCs can be divided into two categories ;

- Continuous reinforcement:
  -Reinforcement by long continuous or broken fibres with diameters of around 100 μm.

- Discontinuous reinforcement which includes three different types [18, 21]:
  -Reinforcement by whiskers that is, substantially defect free material, or chopped fibres with diameters of around 1μm.

  -Reinforcement by particulates, which are discontinuous and approximately equiaxed particles.

  -Platelets reinforcements have also been used which are in a form intermediate between whiskers and particles.

In addition, reinforcements are also employed in the form of laminates. Each of these types of MMCs is associated with particular characteristics in terms of available production fabrication routes, resultant physical mechanical properties and corresponding applications.

The continuous fibre reinforcements, which have a high aspect ratio (length/diameter) are used to hold and to align the matrix and fibres in the desired stress direction. The mechanical properties of the composites are dependent upon the efficiency of the matrix in transferring the load to the reinforcement fibres. Therefore, fibre reinforced MMC's properties are highly related to the interfacial bonding strength of the fibres/matrix [23, 24]. In addition, the matrix in the composites sometimes acts to provide protection for the fibres from mechanical damage; for example, against oxidation [23].

The increase in tensile strength in discontinuous short fibre or whisker reinforcements is usually related to the critical aspect ratio of the reinforcement (length to diameter). Whisker reinforcement, in the form of single crystal, confers superior tensile strength. Whereas, discontinuous reinforcement such as particulate, polycrystalline flakes or chopped fibres, when present in medium or high volume fractions (20% or more) in MMCs, are not as strong as whisker reinforcement [25]

In general, continuous fibre reinforced MMCs offer superior properties to other MMC classes but their high cost in terms of both fibre and composite production has limited their use to the more exotic and advanced applications related to aerospace and defence sectors [26]. On the other hand, discontinuous fibre and particulate reinforcement MMCs achieve an increase in strength and stiffness over monolithic alloys, with lower additional cost than continuous reinforcement. Furthermore, discontinuous reinforced MMCs offer flexibility in terms of composition fabrication method, isotropic properties and can also be subjected to secondary working with conventional techniques such as forging and extrusion. These techniques are of limited use for continuous reinforced MMCs [24].

Each of the continuous and discontinuous reinforced MMCs offers their own particular advantages and disadvantages as stated in the following [16, 21].

Continuous MMC:

- Advantages – the offers maximum improvement over monolithic alloys in terms of mechanical properties such as yield and ultimate tensile stress.
- Disadvantages - more expensive and difficult to produce properties generally anisotropic.

Discontinuous MMC:

- Advantage – relatively inexpensive to produce with isotropic properties.
- Disadvantages - inferior mechanical properties compare to continuous reinforcement.
  - limited secondary formability.

2.1.2 Reinforcement Materials and Structure

As already mentioned, metal matrix composite can, depending on the specific application, be reinforced with continuous (fibres) or discontinuous reinforcements as show in table 2.1. However, reinforcement can be further subdivided into four major categories: continuous fibres (monofilament), short fibres (staple fibres), whiskers and particulate (or platelet) as shown in figure 2.1.

All of the reinforcements are ceramics, typically oxides, carbides and nitrides. The most common reinforcements in MMCs are the discontinuous types of silicon carbide (SiC) and alumina (Al_2O_3) but also titanium carbide (TiC), B_4C, boron (B) and graphite [21, 41].

Reinforcement	Categories
Fibres	Continuous
Short fibres (that are polycrystalline)	Discontinuous
Particulates (Platelets)	Discontinuous
Whiskers (that are monocrystalline)	Discontinuous

Table 2.1. Four reinforcements types used to produce MMCs materials.

Continuous Reinforcement

Continuous reinforcements materials are usually based on fibres called filaments, which can be supplied as monofilament (single fibres) or multifilament (single yarn or two or three-dimension weaves). The common continuous fibres include boron, carbon, alumina-silica and silicon carbide [23, 26].

Continuous fibres such as silicon-carbide fibres, namely Nicalon and Tyranno are widely used mainly in the aerospace industry due to their attractive combination of strength, stiffness and handling characteristics [18]. Due to the technology required to produce continuous fibres and the high production cost, this form of reinforcement is very expensive and relatively limited its application.

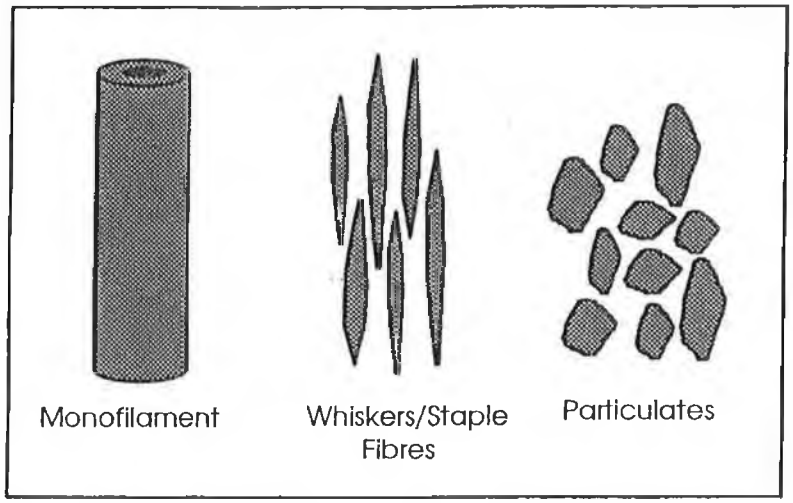

Figure 2.1. Different forms of reinforcement used in MMCs [88].

Discontinuous Reinforcement

The interest in discontinuous reinforcement of metal alloys relates primarily to producing improvements in strength and stiffness, combined with a reduction in density as well as an improvement of the materials wear resistance.

The three forms of discontinuous reinforcement used in MMCs processing are particulate, whiskers and short fibres. The ability to produce particulate and whiskers at low cost has stimulated the search for low cost routes facilitating the discontinuous reinforcement of metal. Also the secondary processes such as forging, rolling and extrusion which are relatively easily in employed on discontinuous reinforced MMCs have brought advantages in its production and fabrication routes over continuous reinforced MMCs [1, 29, 37].

Particulate reinforcement offers low cost with significant stiffness improvement when incorporated into a matrix material. It also shows an advantage over other forms of reinforcements giving isotropic material properties. Another advantage is that particulates are compatible with most conventional processing such as casting and powder metallurgy. Producing a wide range of MMCs product is relatively inexpensive compared to continuously reinforced MMCs [30]. However, strength improvements are not very pronounced and the strain to failure and fracture toughness are low compared to those for matrix material [30, 38].

There are wide ranges of particulate types available with different shape, size, morphology, mechanical properties, cost and reinforcement compatibility. The range of the particle diameter is generally from 1μm to 150μm and the most commonly used particulate reinforcements in MMCs are SiC, Al_2O_3, TiC and B_4C. It has been found that finer particles form a strong interfacial bond and higher strength composites as compared to larger particles [32, 40].

Silicon carbide particles are the most common discontinuous reinforcement in MMCs; in particular they are used to reinforce aluminium alloy due to their compatibility [30, 40]. Al_2O_3 is an attractive reinforcement of aluminium alloys because of its chemical inertness relative to aluminium, and its oxidation resistance. SiC/Al is used for applications where a modulus as high as that of steel is needed, but with reduced strength requirements while Al_2O_3/Al is used for its high strength and modulus, which is about twice that of aluminium [1, 30].

In order to produce a low cost, higher strength and wide application range of MMCs, the following criteria's are vital on selected reinforcement types with matrix alloy [36, 41]:

- Elastic modulus
- Tensile strength
- Density
- Melting temperature

- Thermal stability
- Coefficient of thermal expansion
- Size and shape
- Compatibility with matrix material
- Cost
- Health and safety hazards

Whiskers are single-crystal with typically diameter ranges from 0.1μm to 1μm, which have almost no crystalline defects and a high tensile strength. Numerous materials, including metals, oxides, carbides, and organic compounds have been prepared under controlled conditions in the form of whiskers. Discontinuous ceramic whiskers generally have an aspect ratio (length/diameter) of between 10 and several hundred. Among the commonly used whiskers such as silicon carbide, silicon nitride, carbon and potassium titanate, silicon carbide whiskers seem to offer the best opportunity for MMC reinforcement due to their outstanding specific mechanical characteristics and relatively low production cost [30, 40].

In general, whisker based composites offer higher strength, but their production cost is higher than for particulate-based ones [42]. Single crystal whiskers usually offer much greater tensile strength in discontinuous reinforced MMCs compared to other reinforcement types, such as polycrystalline flakes, particulates or chopped fibres [2]. However, initial interest in whisker reinforcement declined because of the health hazard posed in their handling which caused irritation when touched, inhaled or ingested [33]. The use of ceramic reinforcement in MMCs has increased over the last decade due to the improvement in mechanical properties of whisker based composites [43-46].

Short fibres are polycrystalline fibres which are usually available in large diameters but their aspect ratio is relatively small compared to whiskers [26]. Short fibres such as oxide fibres are mainly used for refractory insulation purposes. Saffil and Kaowool

are used for the reinforcement of automobile engine components due to their low strength which cheaper than both fibres and whiskers. A reduction in the health and safety risk in handling short fibres compared to whiskers has made them one of the acceptable alternative reinforcements. On the other hand, the disadvantage is the lead to a reduced in reinforcement aspect ratio when undergoing breakage during deformation process [29, 40].

2.1.3 Factors Influencing MMC Properties

An accurate prediction of MMC physical and mechanical properties such as thermal conductivity, thermal expansion, density, strength, stiffness, toughness, ductility, wear resistance is difficult as they involve many different factors [21, 29]. Among governing factors is the specific combination of reinforcement with matrix material. For example: aluminium reinforced with different ceramics will result in a large number of composites system with a wide variety of physical or mechanical properties. Other factors which include the influence of the reinforcement in terms of shape, size and morphology, percentage of volume fraction, distribution, form, efficiency of bonding between the matrix/reinforcing phase and the processing conditions all contribute to the MMCs properties [30, 32].

The processing technology of MMCs has matured recently. Significant improvements have been achieved to produce desired MMC properties [31]. On the other hand, problems in providing a reasonable estimate of strength and stiffness in continuous and discontinuous MMCs do exist due to the following reasons [21, 29]:

1. The presence of the reinforcement produces changes in the microstructure of the matrix and therefore to the overall properties of the MMC.

2. The reinforcement may result in an existing residual stress in the MMC, which increases the mechanical properties of the composite.

3. In discontinuous reinforcement, the strengthening mechanism operating is complex and is effected by factors including reinforcement size, shape and volume fraction.

4. Reactions between matrix and reinforcement can lead to degradation of the matrix and the reinforcement and/or diminishment of composite mechanical properties.

2.1.4 Aluminium Based MMCs

Aluminium alloys are the most widely investigated matrix material for use in MMCs, more so than others such as magnesium, titanium, iron, nickel and copper alloys. In addition, it also has the highest market value among different metal based MMCs used in commercial applications [35]. This popularity as a matrix material can be attributed to [30, 36, 32]:

- Its low density, good corrosion resistance, low electrical resistance, with reasonably high thermal conductivity, the availability of a wide alloy range and heat treatment capability which result in MMCs with attractive combinations of strength, ductility and toughness;
- Its low cost relative to other light structural metals (magnesium and titanium);
- Its current dominance of the aerospace market;
- Its introduction and acceptance in the automotive engine market and
- Its overall versatility in term of properties and processing flexibility.

The aluminium matrix alloys grouped in accordance with the Aluminium Association system generally employed are listed in table 2.2 [47, 48]. Those aluminium alloys series, which have shown superior characteristics and have been used widely on commercial application in both research and industry are listed in table 2.3 [1, 30, 37]. Table 2.4 [1, 27, 29, 32] lists examples of aluminium matrix composites in terms of commercial application area. Tables 2.5 and 2.6 [27, 29, 32, 33] are the typical mechanical properties of commercial aluminium alloys and their composites. The yield and ultimate strengths of aluminium based Silicon Carbide composite reinforced with SiC MMCs is showed in figure 2.2.

Alloy Group	Designation
Al-Cu	AA2219
Al-Cu-Mg-Si	AA2009, AA2014, AA2048, AA2124
Al-Si-Mg	A359
Al-Mg	A356, AA5082
Al-Mg-Si-Cu	AA6061, AA6082, AA6090
Al-Zn-Mg-Cu	AA7075, AA7090, AA7091
Al-Li-Cu-Mg-Zr	AA8090

Table 2.2. Various aluminium alloy groups used as matrix materials, listed in accordance with Aluminium Association system [47, 48].

Alloy Group	Superior Characteristic
Al-Cu-Mg (2xxx)	Provide excellent combination of strength and damage tolerance.
Al-Mg-Si-Cu (6xxx)	Improve corrosion resistance for severe environments.
Al-Zn-Mg-Cu (7xxx)	Offer high strength potential, which is suited for aerospace applications.
Al-Fe-Li (8xxx)	Show good wettability characteristics and provide the opportunity for higher temperature performance.

Table 2.3. Aluminium alloy groups, which have shown superior characteristics on commercial application [1, 30, 37].

Reinforcement types	Continuous fibres	Short fibres/ Whiskers	Particulates
Aeronautical/ Military	• Fins • Missile body casings • Compressor blades • Launch tubes	• Support strut • Telescope strut	• Metal mirror optics • Satellite solar reflector • Wing panel • Precision component
Automotive		• Piston crown • Combustion bowl • Connecting rod • bearing	• Connecting rod • Cylinder liners • Brake disc • Brake callipers • Drive shaft • Tire spikes
Sport			• Tennis rackets • Skis • Bicycle frame • Wheel rims • Golf club heads

Table 2.4. Examples of aluminium matrix composites and their commercial application [1, 27, 29, 32].

Table 2.5. Typical properties of some commercially available aluminium matrix composites [18, 27, 29, 32, 33].

Composite	Yield Strength (MPa)	Ultimate Tensile Strength (MPa)	Elongation %	Young Modulus (GPa)	Supplier
Al-Cu					
2014/Al_2O_3/10_p (T6)	483	517	3.3	84	Duralcan, Alcan
2014/Al_2O_3/15_p (T6)	476	503	2.3	92	Duralcan, Alcan
2014/Al_2O_3/20_p (T6)	483	503	1.0	101	Duralcan, Alcan
2014/SiC/15_p (T6)	466	493	2.0	100	Cospray, Alcan
2618/SiC/12_p (T6)	460	532	3.0	98	Cospray, Alcan
2124/SiC/17.8_p (T4)	400	610	5-7	100	BP
2124/SiC/25_p (T4)	490	630	2-4	116	BP
2124/SiC/20_p (T4)	405	560	7	105	DWA Composite Spec.
Al-Mg_2Si					
6061/Al_2O_3/10_p (T6)	296	338	7.5	81	Duralcan, Alcan
6061/Al_2O_3/15_p (T6)	317	359	5.4	87	Duralcan, Alcan
6061/Al_2O_3/20_p (T6)	359	379	2.1	98	Duralcan, Alcan
6061/Al_2O_3/20_p (T6)	305	330	3.4	85	Cospray, Alcan
60601/SiC/15_p (T6)	342	364	3.2	91	Cospray, Alcan
60601/SiC/15_p (T4)	405	460	7.0	98	DWA Composite Spec.
60601/SiC/20_p (T4)	420	500	5.0	105	DWA Composite Spec.
60601/SiC/25_p (T4)	430	515	4.0	115	DWA Composite Spec.

Al-Zn-Mg					
7075/SiC/15$_p$ (T651)	556	601	3	95	Cospray, Alcan
7049/SiC/15$_p$ (T6)	598	643	2	90	Cospray, Alcan
7090/SiC/20$_p$ (T6)	665	735	2	105	DWA Composite Spec.
AL-Li					
8090/SiC/13$_p$ (T4)	455	520	4	101	Cospray, Alcan
8090/SiC/13$_p$ (T6)	499	547	3	101	Cospray, Alcan
8090/SiC/17$_p$ (T4)	310	460	4-7	103	BP
8090/SiC/17$_p$ (T6)	450	540	3-4	103	BP
Al-Si					
356/SiC/10$_p$ (T61)	287	308	0.6	82	Duralcan, Alcan
356/SiC/15$_p$ (T61)	329	336	0.3	91	Duralcan, Alcan
356/SiC/20$_p$ (T61)	336	357	0.4	98	Duralcan, Alcan
380/SiC/10$_p$ (F)	245	332	1.0	95	Duralcan, Alcan
380/SiC/20$_p$ (F)	308	356	0.4	114	Duralcan, Alcan
Mg-Al-Zn					
AZ91/SiC/9.4$_p$	191	236	2	47.5	Dow
AZ91/SiC/15.1$_p$	208	236	1	54	Dow
AZ61/SiC/20$_p$	260	328	2.5	80	Dow

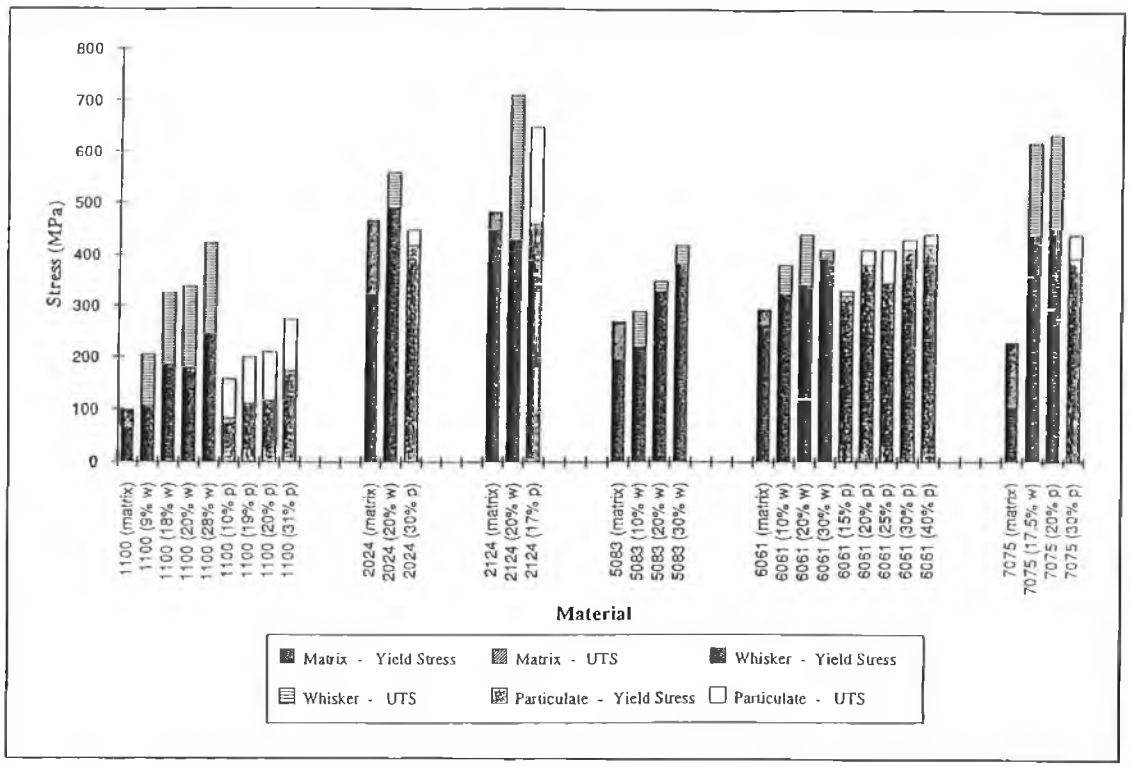

Figure 2.2. The yield and ultimate strengths of aluminium based SiC MMCs [88]

Alloy	Yield Strength, (MPa)	Ultimate Tensile Strength, (MPa)	Elongation, %	Young Modulus, (GPa)	Reference
2024 (T6)	390	480	10.4	75	20
2124 (T6)	325	470	12	72	9
2618 (T6)	370	470	9	74	20
6061 (T6)	364	383	13.5	70.4	11
6082 (T6)	337	359	19.6	69	21
7075 (T6)	505	570	10	72	9
8090 (T6)	415	485	7	80	34
A356 (T6)	206	284	10.4	75	20
A357 (T6)	275	343	10.0	72	20
AZ61	157	198	3.0	38	32
AZ91	168	311	21	49	32

Table 2.6. Typical unreinforced aluminium alloy properties.

2.2 MMC Processing

In an effort to optimise the structure and properties of MMC materials, several different processing methods have been developed over the last twenty years [36, 47]. In general, MMCs materials are produced in different combinations and product due to the multitude selection of matrix, reinforcement material and the type of reinforcement available. The MMC fabrication methods can vary considerably, depending on whether they are aimed at continuous or discontinuous MMC production. Generally the MMC fabrication methods are categorised in two types as stated below according to whether they are primarily based on treating the metal matrix in a solid or liquid form [37, 49]:

1. Solid phase fabrication methods: Powder metallurgy, Diffusion bonding, Hot rolling, Extrusion, Drawing, Explosive welding, Pneumatic impaction etc.

2. Liquid phase fabrication methods: Liquid metal infiltration, Squeeze casting, Compo casting, Pressure casting, Spray co deposition etc.

Liquid phase fabrication usually is more efficient than solid phase fabrication due to the fact that the solid phase fabrication requires longer time [30]. Various matrix forms are used for different fabrication methods. In general, powder is used in the pneumatic impaction and powder metallurgy routes, where as liquid matrix material is used in the processes of liquid metal infiltration, squeeze casting, compocasting etc. Other matrix forms are used such as the molecular form in vapour deposition and metal foils in diffusion bonding, rolling, extrusion etc [18, 21].

In order to produce fine and superior MMCs with the best mechanical properties in any kind of production route, certain requirements are essential such as [41, 49]:

1. The production route has to be as flexible as possible in terms of matrices and reinforcements to which it can be applied.

2. The production route should be capable of producing components with a high degree of reproducibility at minimum product variability at minimum cost and maximum productivity.

3. Any proposed process route should be amenable to scale-up.

4. Flexibility in the range of reinforcement size, shape and volume fraction which can be accommodated is highly desirable.

5. The reinforcement should be distributed in a controlled manner in the metal matrix.

6. The final component should have a minimal porosity, ie full density.

7. The reaction at the reinforcement/matrix interface has to be well controlled in order to promote an optimum bonding strength and to avoid reinforcement degradation.

8. The reinforcement has to be incorporated into the matrix without any breakage, which is particularly important in producing continuous fibre and whisker reinforcement MMCs.

9. Subsequent post-fabrication heat treatment should be allowed for.

In the following sub-section, an overview of the main fabrication routes is presented. There are currently six manufacturing process that have reached industrial status and these are: the powder metallurgy route, diffusion bonding, liquid metal infiltration, squeeze casting, compocasting and spray co-deposition. They compete to produce the lowest cost material with the best mechanical properties [29, 47].

2.2.1 Powder Metallurgy Route

Powder metallurgy (PM) was the most common method for fabricating MMCs and also the first method developed to overcome the difficulties in wetting ceramic particles with molten metal [21, 32]. It has allowed an improvement in reinforcement distribution and also an increase in reinforcement volume fraction up to 55% over other fabricating methods of MMCs processing. For these reasons, many researchers all over the world now focus on PM processing methods for the production of MMCs [40, 50].

Figure 2.3 shows the flow chart of the general powder metallurgy route [30]. In the powder metallurgy process, metal powder with ceramic reinforcements (particulates or whiskers) is first blended and fed into a mould of the desired shape. The objective of the blending is to form a uniform reinforcement distribution throughout. The mixture is then further compacted under high pressure. In hot pressing, the die is simultaneously heated to a temperature which is below the metal melting point but enough to develop significant solid state diffusion or sintering in order to facilitate the bonding between metal powder and ceramic reinforcements. The pressing process is followed by the removal of any undesirable gasses from within the compact (degassing) and the subsequent sealing of the container (canning). The container is then stripped, revealing the final consolidated part. Alternatively, after blending the mixture can be pressed directly by cold pressing which is followed by a separate consolidation stage [40, 51].

The advantages and disadvantages of the powder metallurgy route over other production routes are listed below [32, 52].

1. It is suitable for any alloy to be used as the matrix.

2. By using rapidly solidified material, non-equilibrium alloys can be used for the matrix. This is essentially important for the high temperature application

products as the rapidly solidified alloys have superior elevated temperature strength than conventional alloys.

3. It minimises the reaction between the matrix and reinforcement by using solid state processing, and allows any type of reinforcement used in the fabrication process.

4. It allows a high volume fraction of reinforcement to be incorporated during the process thus producing a high strength, high stiffness modulus and minimising the coefficient of thermal expansion of the composite.

5. Its production route is relatively complex which involves a huge quantity of highly reactive, potentially explosive powder and a limited product form can be achieved.

6. The blending step is a time consuming, expensive and potentially dangerous operation. In addition, to achieve an even distribution of particulate throughout the product is difficult and the use of powder requires a high level of cleanliness to avoid inclusion incorporation into the product which would have a deleterious effect on fracture toughness, fatigue life etc.

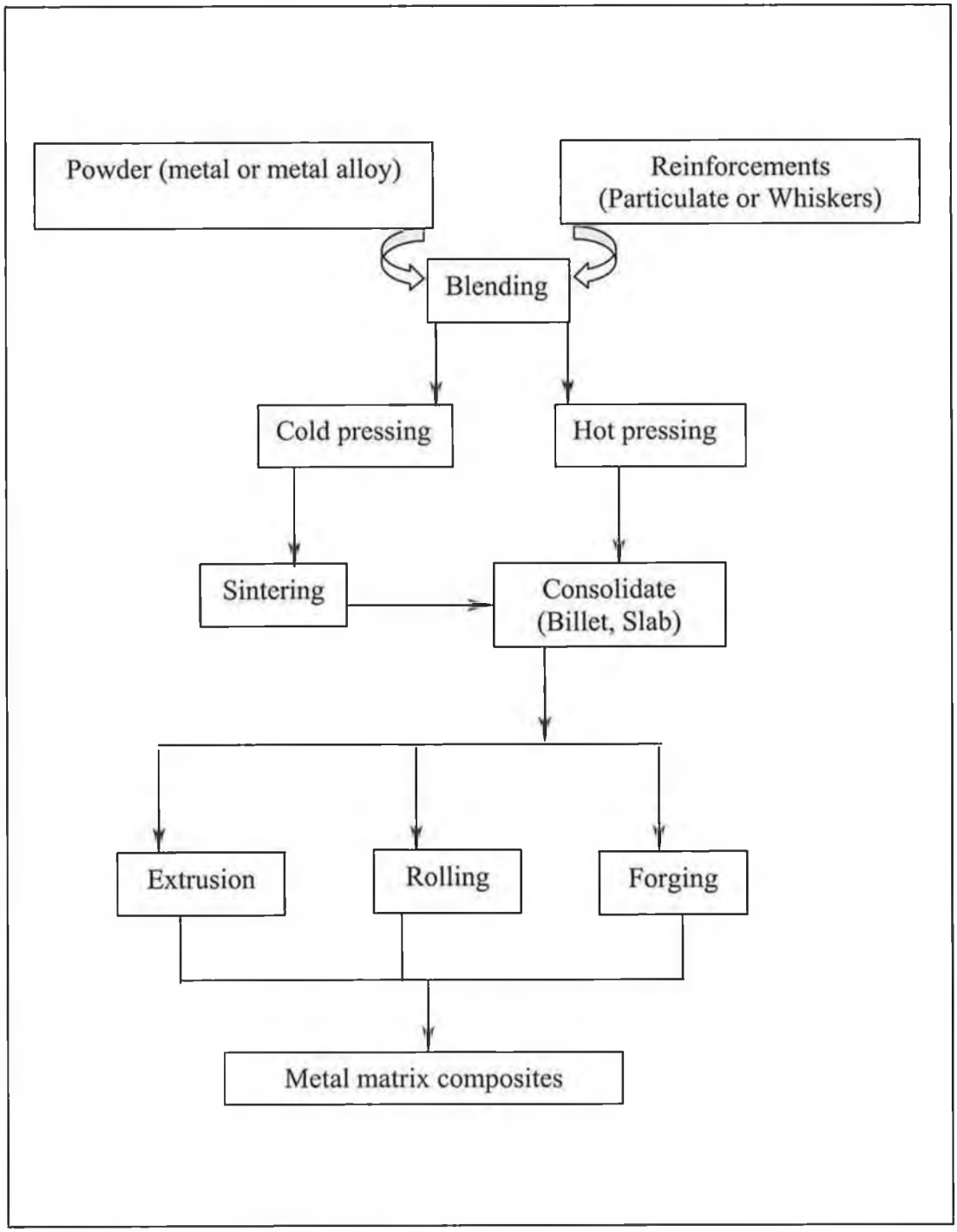

Figure 2.3. Flow chart for the powder metallurgy fabrication route [30].

2.2.2 Diffusion Bonding

Diffusion bonding is normally used to manufacture fibre reinforced MMC with sheets or foils of matrix material [24]. The process involves the metal or metal alloys in the form of sheets and the reinforcement material in the form of fibres. These are chemically surface treated to improve the effectiveness of interdiffusion. The fibres are placed on the metal foil in a predetermined orientation and bonding takes place by press forming directly. The fibres are sometimes coated by plasma spraying or ion plating to enhance the bonding strength before diffusion bonding. After bonding, secondary machining work is carried out at the end of the fabrication process [11, 30].

The diffusion bonding process in vacuum conditions is more effective than in atmospheric conditions, but in general, most methods require temperatures of 900 °C over several hours [40]. The reinforcement used with matrices of aluminium or titanium are normally filaments of silicon or boron. Titanium matrix composites are found to be particularly suited to the diffusion bonding process because of the ease with which the surface oxide layer on titanium can be broken down at relatively low temperatures [40].

2.2.3 Liquid Metal Infiltration

The basic principle of the infiltration process is to infiltrate a porous preform of reinforcement material with a molten matrix material in order to produce a composite material [29, 40]. The infiltration process can be categorised in three different ways, and can be done under atmospheric pressure, inert gas pressure, or in vacuum [18, 40]. Amongst these, vacuum infiltration is the best way to fabricate MMCs because the fibres surface activity is higher and thus better wettability can be achieved [30]. This technique has been applied in fabricating MMCs of the type Al_2O_3 whisker reinforced with aluminium matrix alloy [40].

In the process of MMC by vacuum infiltration, aluminium oxide fibre PF (Polycrystalline fibre) is used. As the first step PF yarn is made into a handleable PF tape with a fugitive organic binder. PF tapes are then laid in the desired orientation, fibre volume, shapes and then inserted into a casting mould of steel. The fugitive organic binder will be burned away and the mould is infiltrated with molten metal, which is allowed to solidify. Metal matrix alloys such as aluminium and magnesium have been used in this liquid infiltration process due to their relatively low melting points. The application of this process is restricted because of the wettability problem of reinforcements with all liquid metals and the degradation of many fibres at high temperatures [53].

2.2.4 Squeeze Casting

Due to the fact that most of the reinforcement materials such as silicon carbide, carbon and alumina do not wet properly in molten metals, it is difficult to fabricate composites by infiltration processing. In contrast, in the squeeze casting technique, the molten metal is forced-infiltrated into the fibre bundles or performs expelling all absorbed and trapped gasses.

The process of squeeze casting starts with a fibre or particulate preform which is preheated to several hundred degrees centigrade, which is below the melting temperature of the matrix and then set into a metal die. Matrix metal such as aluminium or magnesium is then heated to its melting temperature and then squeezed into the fibre preform by a hydraulic pressure (70-200MPa) press to form the mixture of fibre and molten metal. This is followed by solidification under high pressure (70 to 100MPa). The high pressure applied is to assure that the metal wets the fibres and forces the molten metal to flow into the preform, filling it completely [1, 40]. The result of this process is that a reaction zone and voids will not develop at the interface of the matrix alloy and reinforcement. It is generally applicable to composites using all types of reinforcement such as Al_2O_3/Al, SiC_w/Al and C/Mg composites [54].

Squeeze casting has overcome the problems of other casting methods including sand, gravity mould, pressure and investment casting [30]. This process can be used for large scale manufacturing, but it requires careful control of processing variable including fibre and liquid metal preheat temperature, metal alloying elements, melt quality, time lag between die closure and pressurisation, pressure level and duration. Imperfect controls of this process variable will results in various defects including perform deformation, fibre degradation, oxide inclusion and other common casting defects. They are other limitations of this process, which are the size of parts that may be cast due to the high pressure requirement, as well as the small range of shapes that can be cast [29, 55].

2.2.5 Compocasting

Compocasting is the improved process of slush or stir casting which also is the most economical method to fabricate composite with discontinuous reinforcement (chopped fibre, whisker and particulate) when compared to PM, diffusion bonding or high pressure squeeze casting [36, 40].

The compocasting process starts with a metal alloy being placed in the system with a blade assembly in place. The chamber is then evacuated and the alloy is superheated above its melting temperature and stirring is initiated. Reinforcement is added, stirring is continued to promote wetting between the reinforcement and matrix. The melt is then superheated to above its liquidus temperature and bottom poured into a graphite mould. The increased time at lower temperatures after addition will help in promoting wetting and improve bond formation. Finally, the melt which contained the non-metallic substance is then transferred into the lower die-half of the press and the top die is brought down to shape and solidify the composite by applying an appropriate pressure [41, 54].

2.2.6 Spray Co-deposition

The technique of spray co-deposition was developed by Alcan which aims to concentrated primarily on SiC as the reinforcing element and to investigate the possibility of manufacturing MMCs on an economic scale. To date a number of researches on spray co-deposition have been reported [29].

The primary step in this process is that the alloy to be sprayed is melted by induction heating in a crucible. The crucible is then pressurised and metal is ejected through a nozzle into an atomiser where, at the same time, particles are injected into the atomised metal and deposited on a preheated substrate placed in the line of flight. A solid deposit is built up on a collector. The deposited is removed from the substrate for subsequent rolling when it is cold. The final shapes of the products depend on the atomising condition, the shape and the motion of the collector [18, 30, 56].

The disadvantages of this processing technique include the difficulties in avoiding high level of porosity, inhomogeneous reinforcement distribution and the poor control of volume fraction of the reinforcement phase. Moreover the processing problems include high cost of the gas atmospheres required, large amounts of waste composite powder and the need for extra secondary processing such as machining. However, the advantages of this production route over other competitive routes are the improvement in both microstructure and properties, the efficiency of the process and the production in large quantities of high quality MMCs. In addition, low level of segregation, minimisation of interfacial chemical reaction and the effect of high rates of solidification have maintained the interest in this processing route [32, 40, 56].

2.3 Fatigue and Fracture Behaviour of MMCs

Fatigue is the progressive, localised, permanent structural change that occurs in materials subjected to fluctuating stresses and strains that may result in cracks or fracture after a sufficient number of fluctuations [57, 58]. Fatigue fractures are caused by the simultaneous action of cyclic stress, tensile stress and plastic strain. If any one of these three is not present, fatigue cracking will not initiate and propagate. A fatigue crack is started by cyclic stress, whereas crack propagation is produced by tensile stress. In general, this phenomenon has attracted attention because progressively more and more is demanded from machine parts in term of speeds of operation and loads to be sustained.

The process of fatigue failure consists of three stages [10, 59-60]:

Stage I - Initial fatigue damage leading to crack nucleation.
Stage II - Progressive cyclic growth of a crack (crack propagation) until the remaining uncracked cross section of a part becomes too weak to sustain the loads imposed.
Stage III - Final, sudden fracture of the remaining cross section.

Since early 1980 much research on MMCs fatigue properties has been carried out over the world. This is due to the fact that more than ninety percent of practical failures in engineering structure materials are related to fatigue failure [5]. On the other hand, the well known superior properties of MMCs over its corresponding matrix materials are widely accepted in commercial applications.

In the following sub-sections, the fatigue mechanisms of MMCs are outlined in order to provide an overview of the fatigue and fracture behaviour of MMCs. Due to the use of the particulate ceramics reinforced metal matrix composites (PMMCs) in the present experiment research, the review mainly concentrates on PMMCs but where relevant, fibre or whisker reinforced material is included.

2.3.1 Fatigue Crack Nucleation

It is well established in practice that the fatigue process is very dependent on the surface state [57, 61-62]. Fatigue life is strongly affected by material surface finish and surface treatment; hence fatigue is a surface-sensitive process. In fact, fatigue cracks frequently nucleate on the surface of a metal or composite [61]. The nucleation as well as the entire fatigue process is partly controlled by the cyclic-plastic deformation. Therefore, crack nucleation is expected to occur in the spot where highest cyclic-plastic deformation is experienced.

There are many engineering components, which are subjected to complex states of stress or strain because of their use in high speed and high load applications. In considering their applications, it includes the stress concentration when it was subjected to bending or twisting load, which lead to stress gradients with the highest stress on the surface [15, 62]. Even in axial loading, a small degree of eccentricity is practically unavoidable, then caused a small bending or twisting moment and consequently producing stress concentration in the surface layer.

Besides these macroscopic factors of stress concentration on the surface, there are also microscopic stress concentrators, which are effective under uniaxial loading. These microscopic stress concentrators such as dislocations formed during the plastic deformation, second phase particles like inclusions and precipitates also showed their effect at the surface layer on metal alloy and its composites [57, 63]. A further overview of fatigue crack nucleation is presented in the following sub-sections which include: cyclic deformation effects, metallurgical effects and the factors influencing crack nucleation.

2.3.1.1 Cyclic Deformation Effects

The fatigue crack nucleations in PMMCs have been studied using different methods or techniques such as surface and fracture surface observation during and after cyclic tests [5, 66]. The types of fatigue tests usually applied are pull-push, three and four-point bending and ramp-up fatigue. These tests involve specimen samples with good surface finish or treatment and sometimes carefully polished surfaces is needed in order to develop the surface morphology throughout the tests [61]. Under the cyclic fatigue testing, various specific locations have been observed where the fatigue crack nucleation may occur preferentially on the specimen surface [20, 66]. These are: I) at the ends of loading of the individual particles, especially those particles with high aspect ratio II) in the matrix region between closely aligned particles in the loading direction and III) at the region of metallurgical defects.

Pull-push uniaxial fatigue test showed that when the strain is increased from zero to 0.0525, a micro crack was formed in the matrix between two closely distributed particles and as the cumulative strain increased to 0.095, the crack is further developed [60]. Similar development of crack nucleation can be seen where cracks were formed at the loading ends of several particles in the same test. Various fatigue cracks have been detected at the loading end of particles which appear to occur by a different micro mechanism such as by interface-decohesion, crack initiated from the particle tip and crack initiation in the matrix [4, 67]. The other nucleation site of fatigue cracks observed by Kumai et [68] is in large reinforcing particles, in which he believed the high stress applied is equal to the actual stress on the large particle due to the requirement of deformation compatibility. These cracked particles may be the first stage causing the fatigue crack nucleation under cyclic loading.

2.3.1.2 Factors Influencing Fatigue Crack Nucleation

The factors that influence fatigue crack nucleation in most engineering structures in metal alloy or MMCs are outlined below [69-71]:

- *Surface roughness:*

The surface finish of specimen must be free from any surface scratches, which will act as stress concentrators and thus shorten the nucleation stage.

- *Different phase and chemical composition of surface layer:*

The formation of a chemical compound on the surface layer after processes such as surface quenching, coating, machining etc, may have both beneficial and detriment effects.

- *Residual stress:*

Macroscopic residual stress can be detected on specimen surfaces after almost all types of surface treatment. The tensile residual stress will enhance the nucleation stage while compressive residual stresses inhibits the nucleation process.

- *Corrosive environment:*

The influence of gaseous or aqueous environments on metal surface will promote fatigue crack nucleation such as increasing the slip activity in the surface layer of the cycled metal.

2.3.1.3 Metallurgical Effects

Because of the complicated factors involved in the complex production route in producing PMMCs, more processing defects are usually found in these materials than in conventional alloys. The processing defects are categorised in two major types [14, 29]: I) casting cavities such as interdendrite porosities and II) unwetted particle clusters. It has been concluded that various casting defects like interdendrite shrinkage and unwetted interfaces between the metal matrix and ceramics particles will cause the initiation of multiples cracks. Thus, fatigue cracks may start in multiple directions in which those defects are found.

Healy and Beevers [18] have concluded similar behaviour as mentioned above where the porosity associated with the initiation of fatigue cracks is generally greater than 25μm in diameter, and this will tend to occur near clusters of SiC particulate. Cluster associated crack nucleation have also been discussed by Lloyd [66] and further confirmed by Hall et al [14].

As the development of the processing techniques has reached more mature status in recent years, fewer and fewer metallurgical defects are found in PMMCs products, specially in those materials extruded after casting.

2.3.2 Fatigue Crack Propagation

Studies of fatigue crack propagation behaviour of PMMCs have been conducted during the past decade [69, 72]. In general, studies of fatigue propagation characteristics can be carried out in two way: (i) fracture mechanics behaviour studies in terms of fatigue crack growth rate as a function of the applied stress condition and (ii) investigation of micro mechanisms using scanning electron microscopy.

The plain-strain fracture toughness, K_{IC} value for many PMMCs is of the order of 15MPam$^{1/2}$ and the threshold strain range, ΔK_{th} value of the order of 3-5MPam$^{1/2}$ which is greater than most monolithic alloys [63]. The crack-growth rate curves generally exist over a narrow range of stress intensity range, ΔK. On the other hand, the fatigue crack growth behaviour is associated not only with the matrix, but also affected by others factors, for examples the size, shape, properties, distribution and percentage of volume fraction of the particles reinforcements as well as the loading and environment conditions. As a result, the fatigue crack propagation behaviour of PMMCs is uncertain and changeable from different reinforcement and matrix as compared to the unreinforced alloys. Others factors such as interface strength or bonding of particles-particles or particles-matrix are taken into consideration in order to understand the behaviour fatigue crack propagation, and also interior stress distribution pattern [73-75].

2.3.2.1 Fatigue Crack Growth and Stress Relationship

Fatigue crack growth behaviour usually refers to the plot of fatigue crack growth rate (da/dN) against stress intensity range (ΔK). Based on the da/dN vs ΔK plot, the fatigue crack propagation process for MMCs and metal alloy are divided into three parts [69, 73-75]: stage I – near threshold stage, stage II – stable propagation stage and stage III – final fast propagation stage as shown in figure 2.4.

In stage I, both MMCs materials and metal alloys have similar trends in terms of crack growth rate. However, addition of reinforcing particles in the matrix may result in a change of crack growth mechanism [74]. In general, the fatigue threshold level of MMCs is higher than the corresponding monolithic alloy. Despite that, MMCs materials show low fatigue crack propagation rate and thus experience higher crack growth resistance compare to the conventional alloy. The near threshold fatigue crack growth rate in MMC materials is also affected by the load ratio. With the increase of load ratio; threshold levels will be decreased because the degree of crack closure is depend on the magnitude of applied load [74, 76].

The difference in near-threshold behaviour between reinforced and unreinforced alloys is controlled by the significant effect of reinforcement on crack closure levels. Influence of reinforcement size, content of reinforcement and its effect of the fatigue threshold levels in SiC_p/6061 composite show that the composite with 5 and 15 percent volume fraction of SiC have higher fatigue threshold than the matrix alloy. While the alloy reinforced with coarse particles showed a better resistance to the near-threshold fatigue crack growth [74, 78].

Stage II generally illustrates a slightly higher crack growth rate in MMCs compared to the monolithic alloy. Also the respective curves have a different shape in this region; it is generally concave upward in monolithic alloy and concave downward in MMC materials [77]. This differences eventually leads to a considerable difference in the crack growth rate between the two materials.

Stage III shows that MMCs composites have faster propagation rates over the monolithic alloy and a "shooting-up" phenomenon is observed before the final fracture [76].

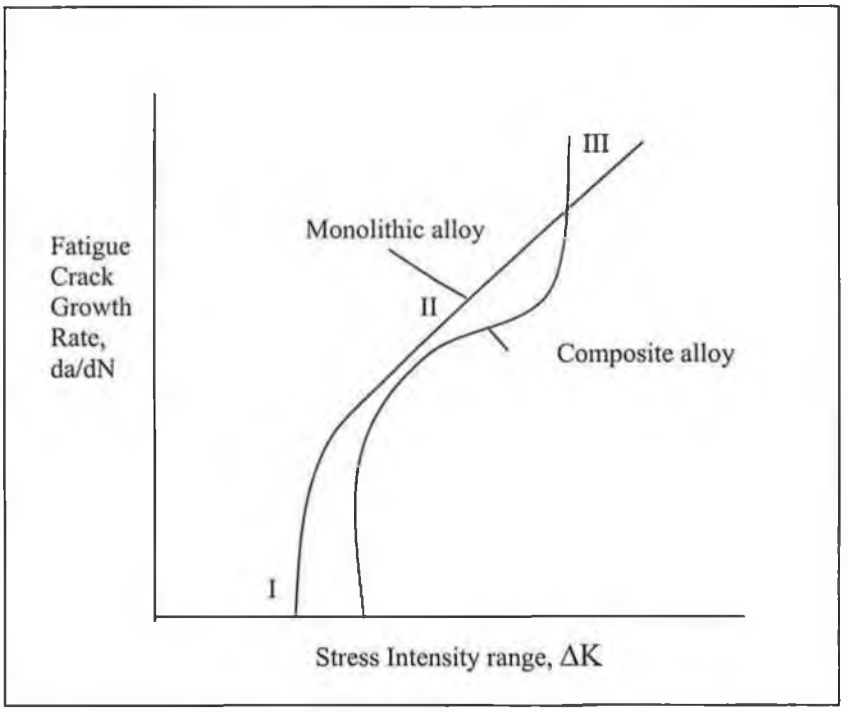

Figure 2.4. Comparison between the variation in fatigue crack propagation rates with ΔK for unreinforced and particulate reinforced MMCs.

2.3.2.2 Micro-mechanics of Fatigue

In PMMCs material, the existence of the particles may either assist or resist the fatigue crack propagation as mentioned previously. The behaviour is dependent on multiple factors, mainly the particle size, volume fraction of the reinforcement, interparticle distance, microscopic distribution of the reinforcement, stress concentration distribution and the degree of clustering of the particles [63]. The effect of particulate reinforcement on the real stress distribution in the matrix or around the fatigue crack tip has been studied extensively [77-79].

An early approach to understanding the interaction between fatigue cracks and reinforcing particles was to analyse the stress distribution for a finite crack with the existence of an inclusion [80]. Results showed that a large difference in stiffness between the matrix and the particle would yield a larger reduction in the stress intensity. Experimental study and analysis of Shang and Ritchie [81] has shown that the larger the average particle size, the higher the threshold stress intensity factor range or ΔK. With a different methodology, a different expression in predicting the threshold ΔK value as follow has been developed [82]:

$$\Delta K_{th} = \sigma_f \{(4\pi/3)D_p [(1-f_p)/f_p] \}^{1/2}$$

Where σ_f is the yield strength of the matrix, f_p and D_p are the volume fraction and the average size of the reinforcing particles respectively. This expression has been shown to provide accurate results when compared to the experimental results from a limited number of PMMCs [5].

Kassam et al [83] used a finite element calculation to study the effect of particle cluster-crack tip interaction on the actual stress distribution at the crack tip. He found that the particle clustering around a metal matrix grain at the crack tip has the effect of suppressing the plastic deformation inside the cluster region, and also the redistribution of stress has caused plastic deformation, which is outside the cluster

region. Particle clustering can lead to poor wetting inside the clusters, leading to poor fatigue properties such as easy crack nucleation [5]. The uniformity of particle distribution is one of the most critical parameters for fatigue resistance in PMMCs.

2.3.3 Fatigue Life

Fatigue lives of material represent the time for a flaw to initiate and propagate to failure. The most frequent method used to evaluated the fatigue life of a material is to plot a Wohler curve also called the S-N curve. An S-N curve is where, cyclic stress amplitude is plotted against the log number of cycles to fractures for a material.

Fatigue lives of PMMC could be affected by many metallurgical variables for a particular application. These variables included reinforcement volume fraction, types, orientation, ageing condition reinforcement size, matrix alloy used in composites etc.

Comparison of Matrix and Composite Behaviour

Many investigators have found that, in stress-controlled fatigue tests on unnotched samples, the fatigue lives of PMMC are generally longer than those of conventional alloys [10, 84], and this has been recognised as one of the benefits of the composites. Figure 2.5 shows stress versus fatigue life behaviour of aluminium and its composite [69]. It can be seen that in high cycle fatigue region, the material's strength is the major factor in affecting the fatigue life. However, superior fatigue strength and life in PMMCs are consider under certain loading condition, materials, environment and an assumption that no processing defects are present.

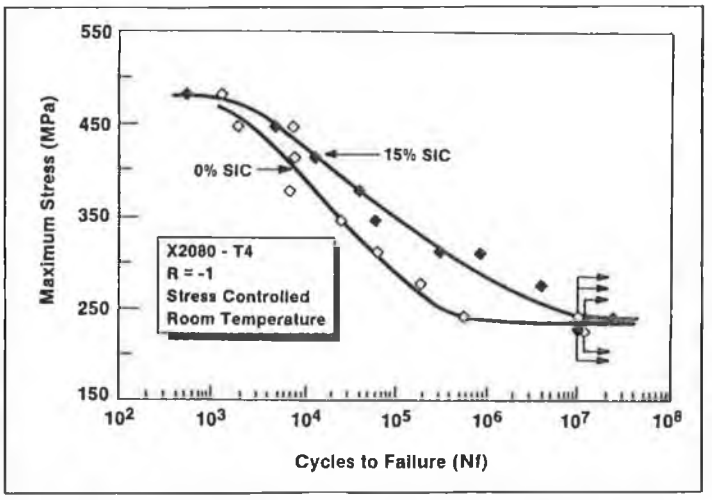

Figure 2.5. Fatigue life behaviour of aluminium and its composite [69].

Volume Fraction and Particle Size

An increase of the reinforcement volume fraction in an aluminium composite directly increases the overall fatigue strength as well as fatigue lifetime. This can be attributed to the decrease of elastic and plastic strains that resulted from the increasing modulus and apparent work hardening [14, 85, 86]. Studies from axial loading fatigue experiments found that the fatigue strength is only weakly increased by increasing volume fraction [87] while significant improvements in fatigue strength have been reported by other investigators in rotating bending techniques [6, 61]. It is also shown that decreases of particle size significantly improve fatigue behaviour as illustrated in figure 2.6 (a) and (b) [14].

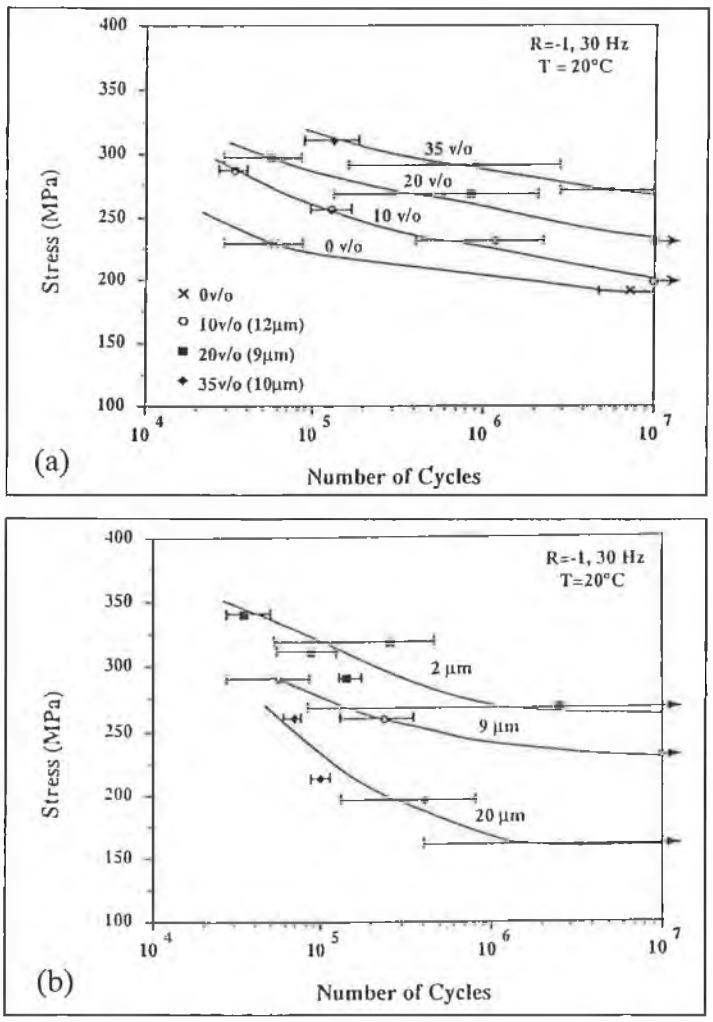

Figure 2.6. Effect of (a) volume fraction on fatigue life of 2124/SiC_p (9-12μm)-Peak aged (b) particle size on fatigue life of 2124/SiC_p (20 vol%, 5μm)-Peak aged [14].

Reinforcement Types

Reinforcement type plays an important role in controlling fatigue properties of composites. It may provide good interfacial bonding between matrix and reinforcement, which improves the fatigue strength and fatigue endurance limit. It is observed that different composite systems with same matrix alloy, which are produced the same processing route, demonstrate different fatigue behaviour, and different fatigue lifetimes. This can be seen in the S-N diagram of stress amplitude against cycles to failure for particle and whisker-reinforcement aluminium alloy 6061 in figure 2.7 [84]. In general, whisker reinforcement gave better fatigue lives than other discontinued SiC reinforced composites.

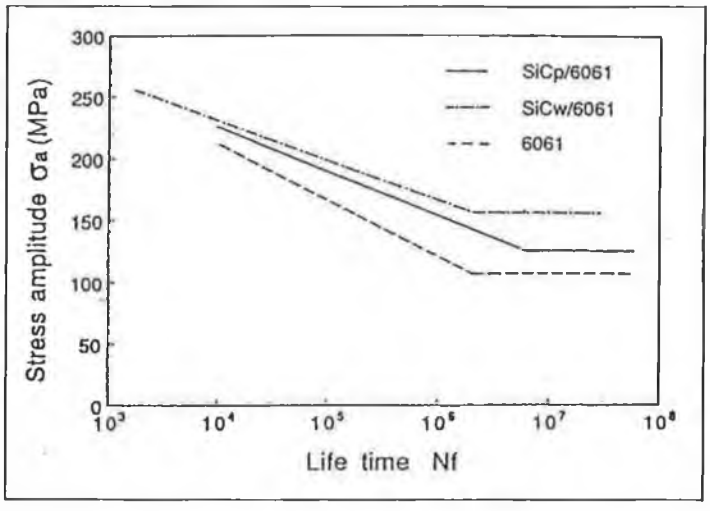

Figure 2.7. Fatigue behaviour of aluminium 6061 alloy, SiC-particulate and SiC-whisker reinforced in peak aged condition [84].

Specimen Orientations and Ageing Condition

The effects of specimen orientation and ageing conditions under stress-controlled testing on stress-life behaviour of SiC reinforced in aluminium based alloy is shown in figure 2.8 (a) and (b) [5, 14]. It indicated that specimens in longitudinal direction (L) showed higher fatigue strength than in the transverse direction (T) for both composite and conventional alloys. Furthermore, aging condition at peak aged shown pronounced fatigue strength compared over original aged, under aged and natural aged condition.

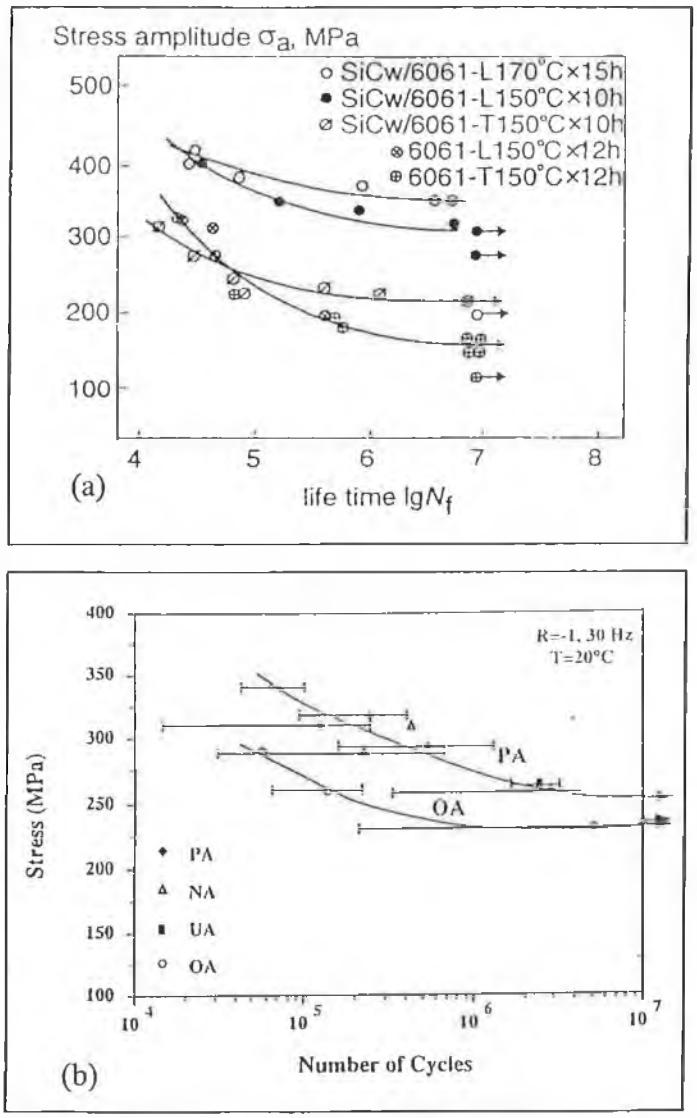

Figure 2.8. The effect of (a) specimen orientation on fatigue life behaviour of aluminium 6061 alloy and SiC_W/6061 composite (b) ageing condition on fatigue life behaviour of 2124-SiC_p (20 vol%, 5 μm) [5, 14].

Chapter 3: Experimental Work

A study has been made to understand the dynamic and cyclic fracture behaviour of the aluminium alloy 6061 and its composites, which is discontinuously reinforced with 15% volume fractions of silicon carbide particulate at average size of 30μm.

Two tests were conducted: tensile and fatigue tests on both aluminium alloy 6061 and aluminium composite, 6061/SiC_P/15% in obtain the tensile properties and fatigue life behaviour.

The following chapter concentrates on describing the experimental work, which was involved in this research project. It also includes the procedures and analysis of the tests, materials and equipment used.

3.1 Materials

Two materials have been investigated in this study in order to compare their mechanical properties. Specifically stress-strain, and fatigue life behaviour were considered. A commercial aluminium alloy 6061 was selected as the matrix material and aluminium alloy 6061 matrix reinforced with SiC particles (SiC_P) with average size of 30μm and a volume content of 15% as the composite. The chemical compositions of the matrix alloy and the composite are listed in table 3.1. Due to the method used in energy disperse X-ray analysis (EDX),it was not possible to restrict analysis to the matrix areas of the composite. Therefore, the tabulated silicon content of 12.5% includes the SiC particles.

SiC_P–reinforced AA6061 was supplied by Aerospace Metal Composites, AMC, Farnborough, England. The composite was fabricated by powder metallurgical processing. Prealloyed aluminium alloy powders were blended with finer SiC particles, packed into an aluminium can, densified by degassing and vacuum hot pressing, followed by hot extrusion at 450°C to a 14mm diameter bar. The extruded materials were subsequently solution heat treated at 535°C for 1 hour, cold-water quench, aged for 6 hours at 185°C (heat treatment T6). Same production route and heat treatment was applied on unreinforced alloy as in its composites.

Matrix Composition (Wt Pct)	**Si**	**Fe**	**Cu**	**Mn**	**Mg**	**Cr**	**Zn**	**Ti**	**Al**
AA6061	0.8	0.7	0.4	0.15	1.2	0.35	0.5	0.15	Bal
AA6061/SiC_P/15%	12.5	0.28	0.3	0.04	0.55	0.04	0.13	0.02	Bal

Table.3.1. Compositions (Weight Percentage) of unreinforced 6061 matrix (from supplier information), and 6061 reinforced with 15 percentage SiC (from EDX analysis).

Samples of the aluminium alloy composite were mounted and polished using standard metallography methods to facilitate examination of the microstructure under both optical and a scanning electron microscope (SEM). Subsequently, the microstructure and distribution of the SiC particles were studied using image analysis software called BUEHLER, Omnimet Enterprise (86100) Quantitative Image Analyser.

The fracture surfaces of both tensile and fatigue tests were examined using a Leica (Leo) Stereoscan 440 a scanning electron microscope (15KV) to determine the predominant fracture mode, and to characterised the fine-scale topography of the fatigue fracture surface.

3.2 Mechanical Testing

All mechanical tests were performed on a closed-loop servohydraulic fatigue test machine. Specimen preparation for both tensile and fatigue tests was similar. Both materials were machined parallel to the extrusion direction from as-received bar, using diamond-tipped cutting tools in a computer numerically controlled (CNC) lathe. The final surface preparation was a longitudinal hand polish using 1000 grit silicon paper to 0.2μm, so as to remove all circumferential scratches and machine marks. The cylindrical fatigue specimen geometry conformed to a BS3518 standard [98] and had a gauge diameter of 8mm and gauge length of 30mm as shown in figure 3.1. The length-to-diameter ratio of the fatigue specimen was chosen so as to ensure that the specimen would not buckle under compressive stress. The geometry of the tensile specimen was identical.

Tensile testing was conducted to failure at a constant rate displacement of 2mm/min on smooth cylindrical tensile specimens of gauge length 30mm and diameter 8mm at room temperature. A 20.16mm gauge length extensometer (figure 3.12) was used to monitor specimen strain during testing. Load and strain data were digitally recorded throughout the test.

Fatigue tests were performed on a 100KN servo-hydraulic machine equipped with 100KN load cell. The load train was given a precision alignment to minimise specimen bending. Tests were conducted at push-pull fully reverse, total-stress-controlled, at stress ratio, R = -1 and 0.1 at variety stress level. The stress function chosen was a sinusoidal waveform at 30Hz, and all tests were performed at room temperature with an average range of humidity 46%- 50%. All specimens were tested to fracture into two separate pieces, unless the specimen did not fail at 1×10^7 cycles. The test results were evaluated and plotted in stress-strain curves and S-N diagrams using "S-Plus mathematics analysis" software as described in chapter 4.

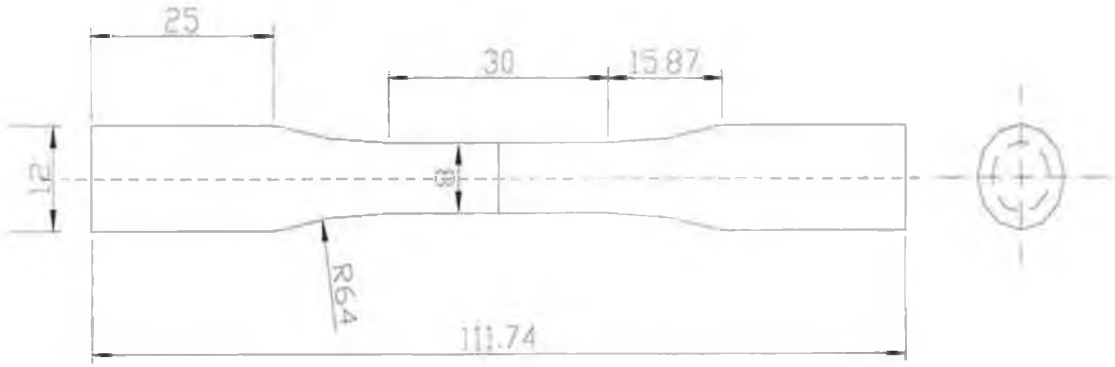

Name : Ping H Lim	Dimension : All Dimensions in MM	Title : Smooth Cylindrical Un-notch Fatigue Tests Specimen.
Date : 01-05-01	Material : Aluminium AA6061 & AA6061/SiC_p/15%	
Scale : Not to scale	Tolerance : +/- 0.01mm	

3.3 Mechanical Testing Equipment

Whether simple or complex, all fatigue-testing machines consist of the same basic components: a load train, controller, sensors and monitors. In general, the test system is loaded through the load train, which grips the test specimen; the test is then controlled by the controller. The sensors feed data back to the controller, and finally communicates with the investigator by means of the read-out devices. E.g.: monitors (LCD).

The present fatigue tests were conducted using a computer controlled closed-loop ESH servo-hydraulic 100KN fatigue-testing machine. The machine, shown in figure.3.2, is an axial fatigue-testing machine. Tension and compression loads can be applied to the unnotched specimens. This closed-loop servo-hydraulic system offers optimum control, monitoring and versatility in fatigue testing systems. It works by continually sensing the controlled and uncontrolled parameters during the test in order to establish a feedback loop to the servo- controller, where the feedback signal is then compared to the desired control input. The controller then automatically adjusts the drive system to correct and minimise the difference.

In this chapter, the major components of the computer controlled closed-loop servo-hydraulic fatigue-testing machine, used in the present fatigue tests, are described. A schematic diagram of the major components is shown in figure 3.3.

Figure 3.2. Computer controlled closed-loop ESH Servo-hydraulic 100KN fatigue testing machine.

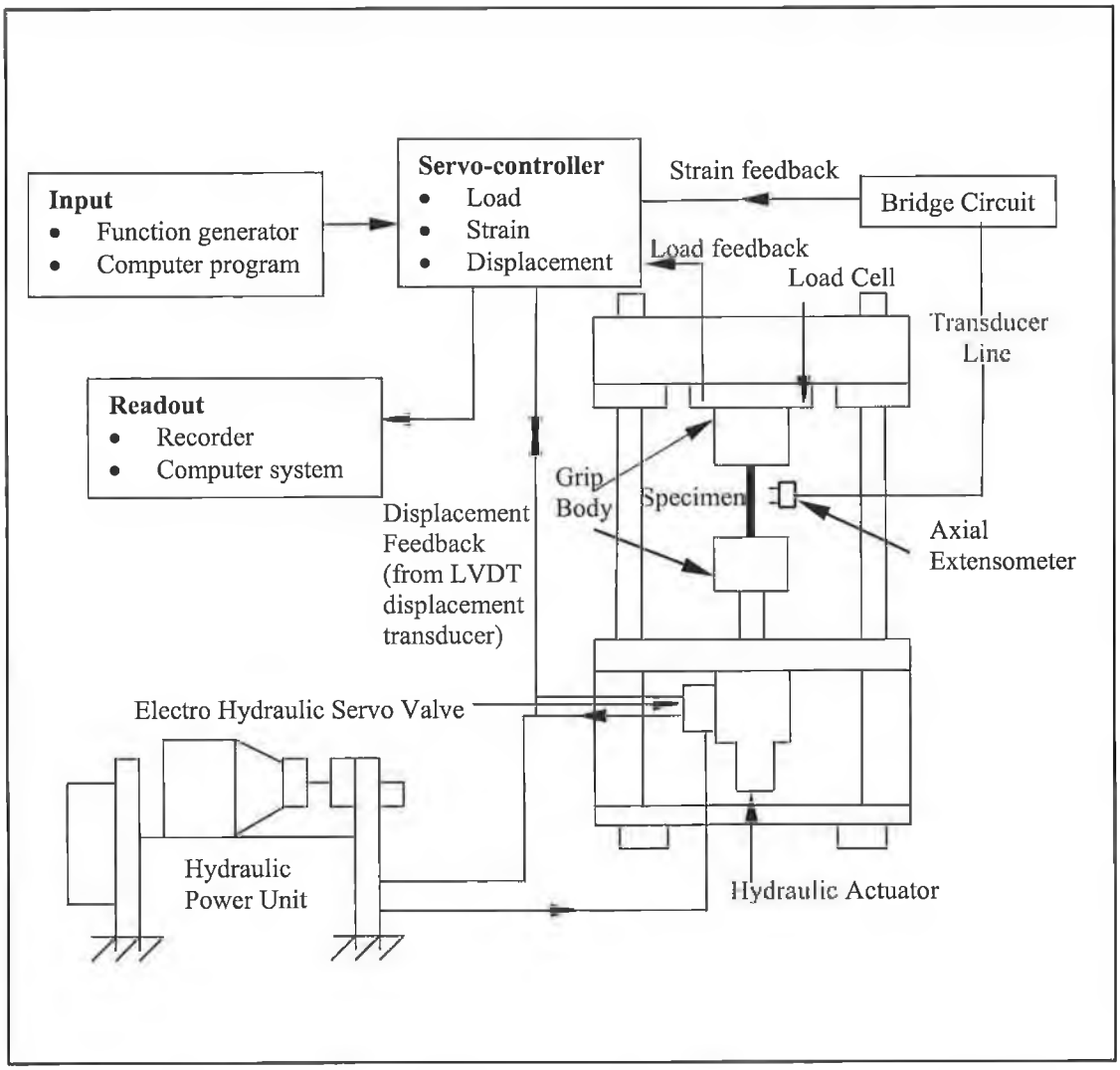

Figure 3.3. Schematic diagram of the major components of a computer controlled, closed-loop, servo- hydraulic fatigue machine.

3.4 The Load Train

The load train consists of:

I) Load frame

II) Gripping devices

III) Test specimen

3.4.1 Load Frame

A load frame used in fatigue testing of materials and small components supplies the reacting forces, which oppose the force exerted by the drive system. It also supports the specimen and sensors associated with the specific test. Load frames can vary in capacity, both in load and space for access to the specimen and grips, in rigidity, convenience of use and alignment sensitivity. Typically, the load frame must support the drive system, grips, specimen and all required sensors for control and read-out.

The load frame used in the present experimental fatigue work is an ESH model, shown in figure 3.2. The load frame is an independent floor-standing unit with solid steel upper and lower crossheads. The upper crosshead is friction clamped to two hard chromium plated ground columns. The upper crosshead also has hydraulic unclamping interlocks. Two hydraulic lifting cylinders at the sides of the load frame are used to adjust of the working daylight space.

A full capacity fatigue rated strain gauge load cell is mounted on the upper crosshead. A double-ended, double-acting electro-hydraulic servo actuator is mounted in the enclosed base below the bottom crosshead. The actuator is fitted with a manifold on which is mounted a servo-valve, accumulator and high-pressure filter. A Linear Voltage Differential Transformer (LVDT) displacement transducer is mounted concentrically within the actuator. Table 3.2 lists the specification of the load frame of the ESH servo-hydraulic fatigue testing machine.

Table 3.2. Specification of the load frame of the ESH servo-hydraulic fatigue testing machine.

Frame capacity	+/- 250 KN*
Actuator Load capacity	+/- 100KN
Load ranges	+/- 100 KN, +/- 50KN, +/- 20 KN, +/- 10 KN
Accuracy	Current British Standard Grade 1 on all four ranges
Actuator stroke	+/- 50mm
Distance between columns	600mm
Vertical daylight	Up to 1000 mm maximum between tool mounting faces

* The frame capacity of +/- 250 KN means that it would be possible, at some time in the future if required, to fit an actuator having a capacity of +/- 250 KN into the frame instead of the +/- 100 KN actuator.

3.4.2 Load Cell

The strain gauge load cell is the most widely used force-measuring and feedback device in closed-loop fatigue machines. When an external force is applied to the device, this causes elastic deformation of an internal member such as a metal column or beam, to which a strain gauge bridge has been attached. An electronic signal that is proportional to the resistance change in the bridge, and therefore to the applied force, can thus be produced. Load cells may be obtained to measure tension, compression, or both and to detect forces along one or several axes.

The strain gauge load cell was used in the present mechanical and fatigue tests. It was supplied with the actuator and calibrated as part of regular servicing by ESH testing limited. It is a precise strain gauge device which is matched in capacity to the actuator to provide a long fatigue life, high overload capacity and side load resistance. Table 3.3 shows the ESH strain gauge load cell specification.

Model / Series Number	986080 S200/313	
Capacity	100	kN
Full Range Output	1.76	Mv / Volt
Non-Linearity	-	+/- % Full Range Output
Hysteresis	-	% Full Range Output
Zero Balance	-	Mv
Excitation	19.666	Volt DC
DVM Model / Series Number	FLUKE 8842A Certificate No. 12449	

Table 3.3. ESH strain gauge load cell specification.

3.4.3 Gripping Devices

Proper gripping is not simply the attachment of the test specimen in the load train. A special specimen gripping mechanism must be incorporated into the load train. The gripping devices used in the present fatigue testing are provided by ESH testing limited - they are a self-aligning type as show in figure 3.4. The grip bodies, grip insert along with the specimen being tested can be seen. Figure 3.5 shows the grip inserts used for round specimens. The shape and size of the gripping bodies are designed in such a way so as to prevent backlash while passing through zero load and to prevent buckling of the test specimen at maximum compressive load when performing tension-compressive testing.

Figure 3.4. Gripping devices.

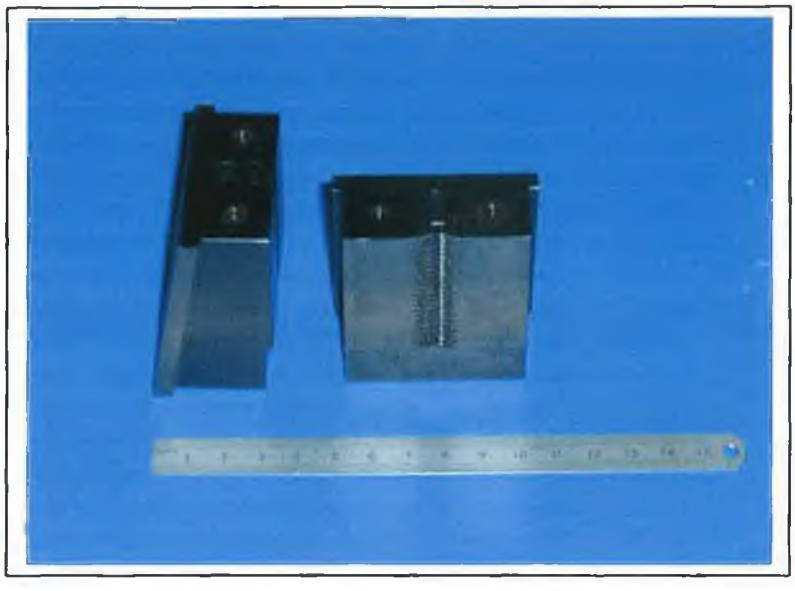

Figure 3.5. Grip inserts for round fatigue specimens.

3.4.4 Test Specimens

A specimen represents a sample of a metal or alloy. Testing of samples serves to determine and compare the basic fatigue characteristics of different materials. The design of axial fatigue test specimens used in the present test is a cylindrical shape with tangential blending between the test section and the grip ends. The current test specimen materials are an aluminium alloy AA6061 and an aluminium/silicon carbide composite, AA6061/SiC_p/15% with average particles size of 30μm. These specimens are shown in figures 3.6 and 3.7.

The axial fatigue test specimen has three areas: the test section or gauge length and the two grip ends. The grip ends have a constant diameter, which are designed for the grip inserts seen in figure 3.5. The function of the grip ends is to transfer load from the test machine grips to the test section in the axial fatigue tests. The test section of the specimen is reduced in cross-section to prevent failure in the grip ends during the test. The transition from the grip ends to the test area is designed with large, smooth blended radii to eliminate any stress concentration in the transition.

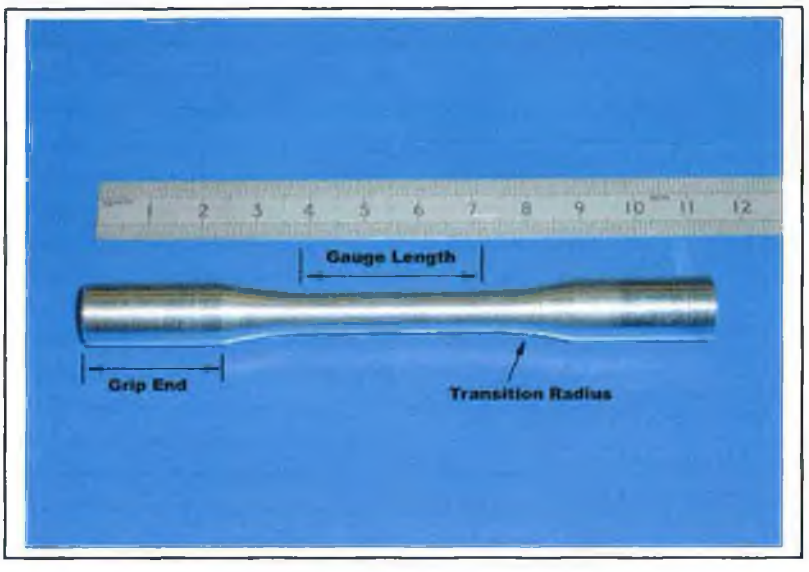

Fatigue 3.6. Aluminium alloy AA6061 fatigue test specimen.

Figure 3.7. Aluminium silicon carbide AA6061/SiC_p/15% fatigue test specimen.

3.4.5 Hydraulic Power Unit

The Hydraulic Power Unit is provided by ESH Testing limited and is a free standing unit which requires no special foundations. It is shown in figure 3.8. The ESH power units are designed for operation at pressures up to 290 bar a full range pressure control valve and gauge are fitted. The main parts of the unit are a vertical pump/motor combination mounted on top of an oil reservoir together with a control box, filter block, isolator valve and pressure gauge. The control box is equipped with relief valve, check valve, dump valve and accumulator. Full flow filters in both pressure and return line are present to ensure the total cleanliness of the oil in the servo hydraulic system in order to give the best performance and long servo valve life possible.

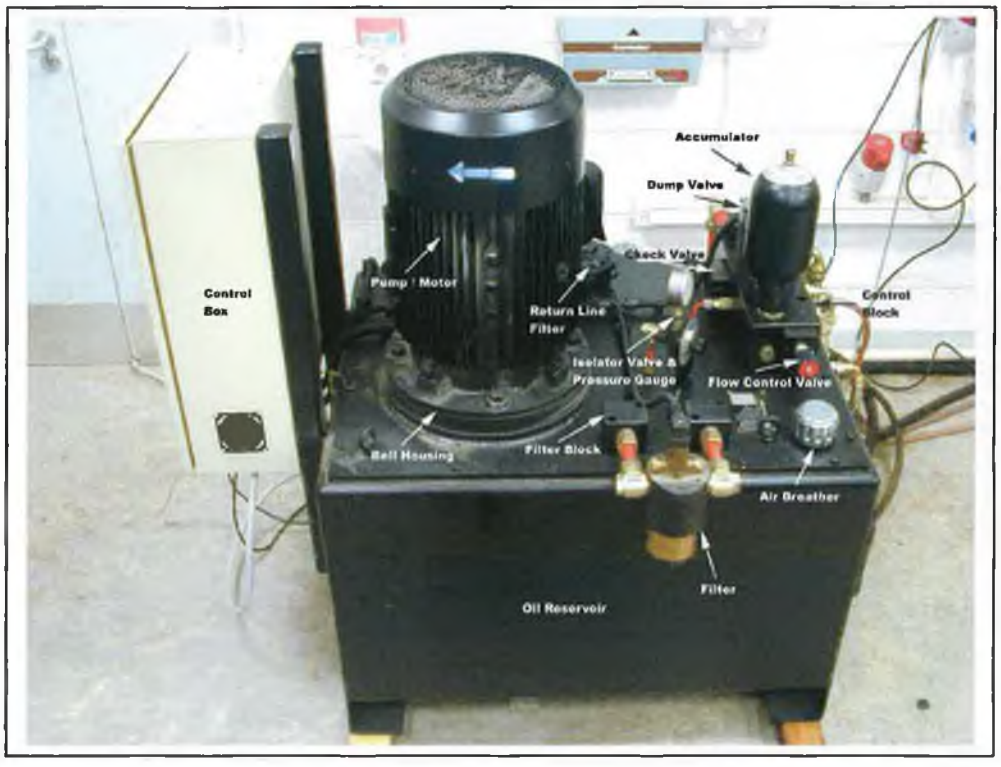

Figure 3.8. Hydraulic Power Unit.

The hydraulic pump is coupled to the electric motor using a flexible shaft coupling. Also included is a pump suction element, relief valve, air breather, check valve, and pressure gage. A heat exchanger for oil cooling is provided by a water modulating valve, an electrical shut-off solenoid and temperature gages. Inspection covers are positioned for ease of inspection and maintenance. The motor control is connected to a pair of float switches that shut off the motor if the fluid level is either too low or too high. A temperature sensor shuts off the motor if the oil reaches 125 degrees F. When the motor shuts off, the water solenoid also shuts off the flow to the heat exchanger. The hydraulic power unit comes with a remotely mounted control box that features the ON button, Safety Stop button with security key, check fluid light, and high temperature warning light.

The servo-valve is used to control the volume and direction of flow of hydraulic fluid between the hydraulic power supply and the hydraulic actuator. It converts an electrical signal into a mechanical action by changing the direction of fluid flow in the actuator through the twist of a small electro-magnetic torque motor. Table 3.4 shows the specification of the hydraulic power unit used for the specified servo-hydraulic fatigue machine.

Table 3.4. Hydraulic Power Unit specification.

Hydraulic fluid type	Shell Tellus 37
Hydraulic reservoir capacity	205 litres
Hydraulic oil flow	23 litres/minute
Maximum working pressure	25 MPa
Normal working pressure	25 MPa
Pressure line filter element number	UCR 63013
Return line filter element number	R6121
Accumulator pre-charge pressure	Between 19 and 21 MPa
Maximum cut-out temperature setting for reservoir thermostat	60°C
Electric motor	11 kW
Electric power	380/415 Volt 50Hz 3-phase

3.4.6 The Programmer

The programmer supplies the command signal to the system. This command signal is a digital signal, which incorporates two function generators, analogue devices and computer programs. Two software programs were used in performing the experimental fatigue testing. They are the ESH Block Editor program and the ESH Block Run program, their user interface is shown in figures 3.9 (a), 3.9 (b) and 3.10. The Block Run and Block Editor programs work together to enable the generation and automatic execution of a complex sequence of test parameters. They allow the operator to build up a sequence of test program blocks with the following parameters defined for each block.

- Control mode (either in Stress, Strain or Displacement)
- Target level (either in Stress, Strain or Displacement)
- Ramp rate
- Mean level
- Cyclic frequency
- Waveform
- Frequency
- Amplitude
- Block duration (time/cycles)
- Data gather (in Stress, Strain, Displacement and time)

The Block Run program uses the Virtual Control Panel (VCP) program to provide access to the digital control system features through a PC, and thus avoids manual operation of the control system. Up to 20 different blocks may be created and saved as a program. Programs can be run any number of times, and in any sequence. The data gather option can be set in any block and appropriate load, stroke, and extension time data will be saved to disk during, and at the end of the test.

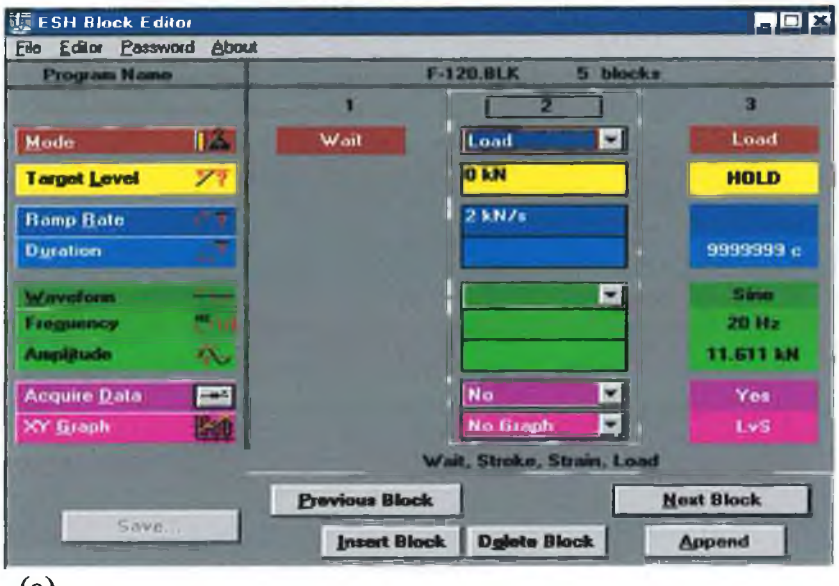

(a)

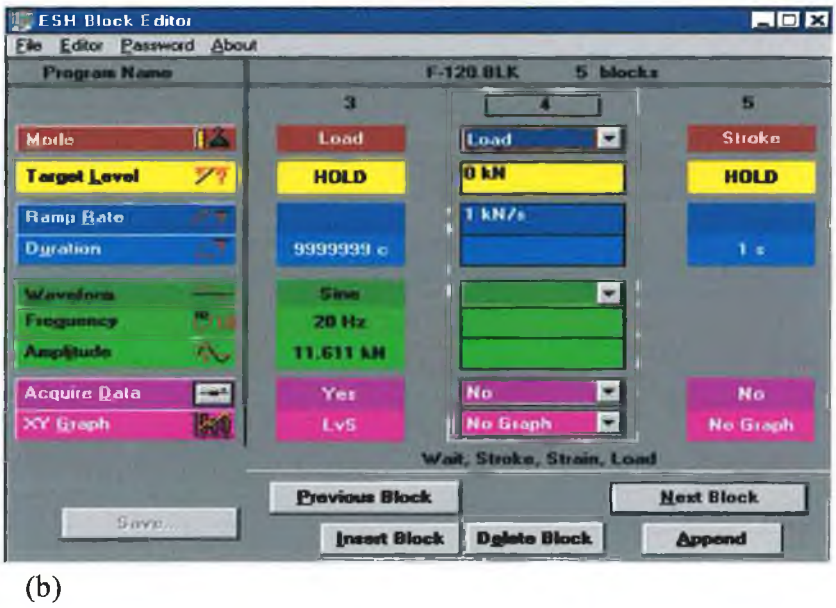

(b)

Figure 3.9. (a) and (b) ESH Block Editor Program Interface.

Figure 3.10. ESH Block Run Program Interface.

3.4.7 Servo-controller

In a closed-loop servo-hydraulic fatigue system, the objective of the Servo-controller is to command the test system to follow programmed test parameters such as load, strain or displacement. Such elements as constant or variable amplitude, mean level, type of waveform, frequency and number of cycles to be completed must also be controlled to optimise system performance. The output as a time-dependant signal will then be received by the drive system, which converts the signals to a force or displacement or strain-time excitation. That excitation is then directly transferred to the specimen being tested.

The drive system is the most significant feature of a closed-loop servo-hydraulic fatigue system. It is usually electrically powered with the motor drive ensuring that the hydraulic pumps provide pressure to control the motion and force of the hydraulic piston actuator accurately.

A servo-controller also incorporates numerous other compensatory features such as:

- Adjusts the gain or proportional band of the system.
- Controls or modify the feedback from signals error in improved stability of the tests.
- Controls and adjust the command signal (in stress, strain or displacement).
- Monitors the system error signal, as well as warning when an error occurred on the system.
- Has the capability to select various command and feedback signals in stress, strain or displacement mode.
- Has auxiliary functions such as recorder signal conditioning, calibration and system start up and shutdown.

In the present experimental work, the ESH digital control system is operated using the Virtual Control Panel (VCP) program provided by ESH testing limited. The VCP program acts as a common channel of communication between application and the controller, and allows complete control of the digital control system from an IBM compatible PC. The ESH Digital Control System consists of three modes of control: Load, Strain and Displacement with other operating parameters, feedback values and warning messages which are presented to the operator on a liquid crystal monitor display or PC. In addition, the upper part of the display gives a continuous indication of the command value for the control mode in use, and the three feedback values. Also, the maximum and minimum value for each feedback is always shown and may be reset to the current feedback values at any time.

Other control parameters are shown in the lower part of the display, which are grouped into 5 separate menus (see Figures 3.11 (a)-(e)). The control of all parameters is accomplished by selecting the required parameter on the screen using the cursor key and altering its state or value using softkeys as appropriate. The LED buttons on the liquid crystal monitor display are provided as safety interlocks which sense conditions such as overload, clogged filters or control system failure. Each interlock provides a warning lamp, which prevents hydraulic pressure being applied when an error is present on the control system. The digital control system always starts in stroke control and no other mode can be selected unless the hydraulic pressure is on. For safety purposes, the control system reverts to stroke control if the hydraulic pressure is lost or turned off at any time.

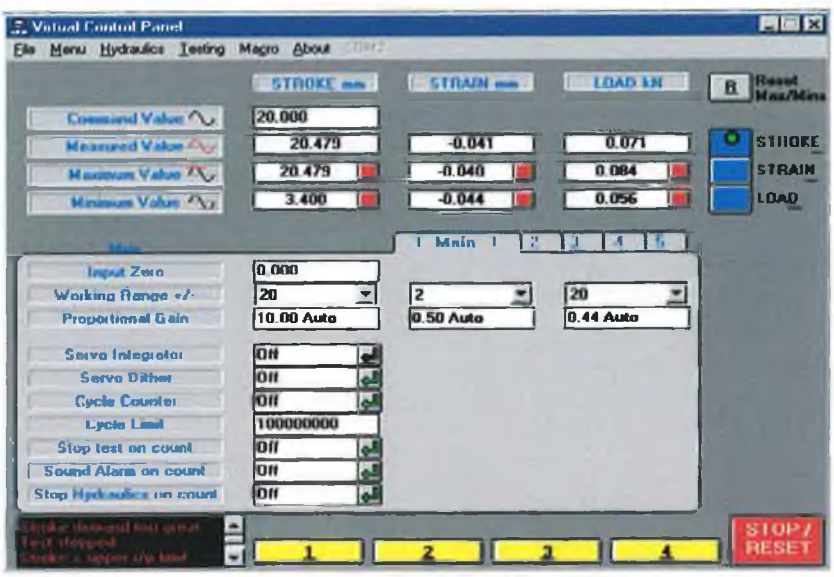

Figure 3.11. (a) Main menu.

Figure 3.11. (b) Limits menu.

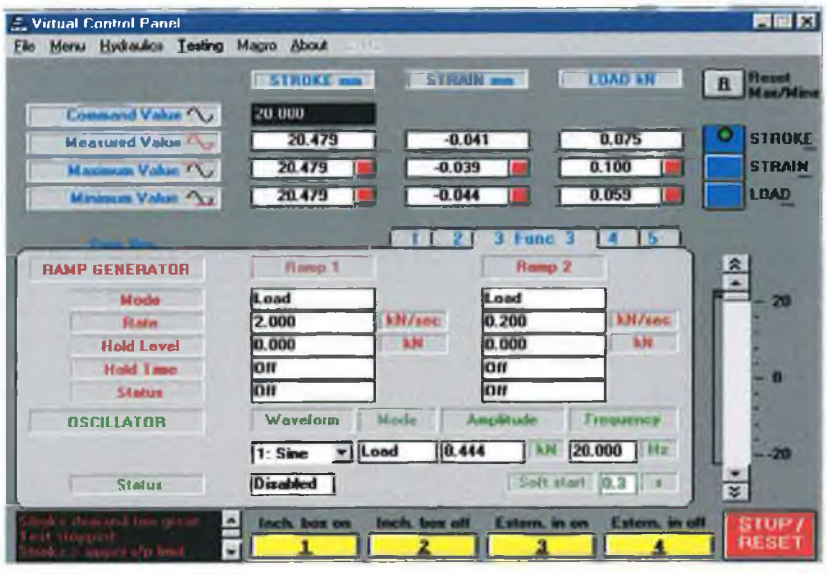

Figure 3.11. (c) Function generator menu.

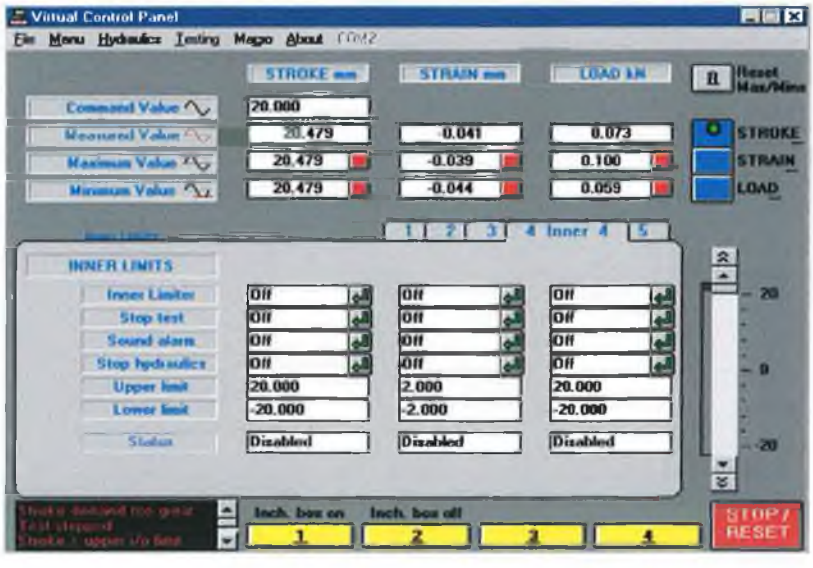

Figure 3.11. (d) Inner Limit menu.

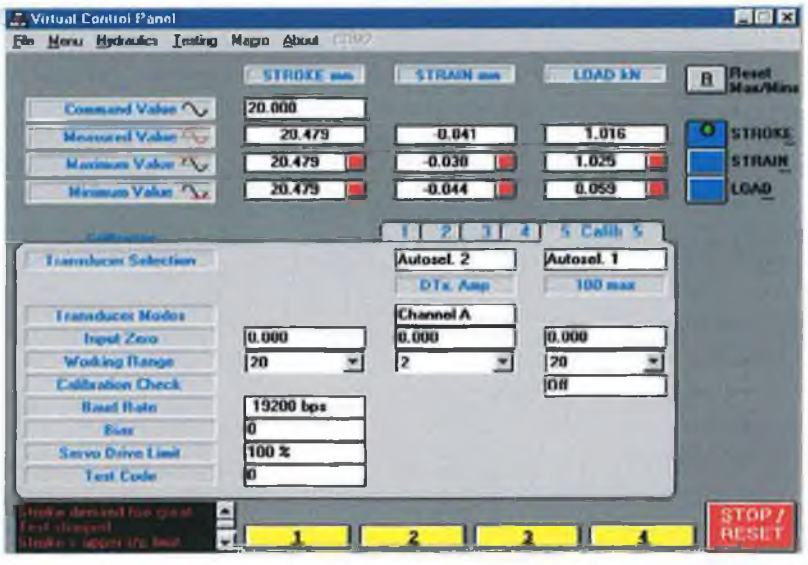

Figure 3.11. (e) Calibration menu.

3.4.8 Sensors

Sensors are used to measure load, strain, displacement, deflection and cycle count on the fatigue testing system. One of the functions of the sensors is to provide an output signal to the controller, which is transmitted to a readout device as in the case of uncontrolled parameters. Also it allow communication with the investigator. Sensors such as the strain gauge load cell that is inserted in the load train, Linear Voltage Differential Transformer (LVDT) displacement transducer and axial extensometer were the major devices used during the present mechanical fatigue testing.

3.4.8.1 Linear Variable Differential Transformers (LVDT)

The LVDT is an electromechanical device, which provides an output voltage proportional to the displacement of a movable core. It consists of a transformer with a primary and secondary coil, wound to a common cylindrical form, and a core which is oriented axially within the hollow body of the transformer.

3.4.8.2 Axial Extensometer

In mechanical testing of AA6061 Aluminium and its composite, an axial extensometer, model EXA20-5 with gauge length 20mm (as shown in figure 3.12) was used for the measurement of extension. The axial extensometer consists of a basic unit, two edges, two stroke limiting blocks, a set of clamping springs and a gauge block or a locking pin. The axial extensometer was provided, calibrated by ESH limited Ltd by proved of a certificate for it as shown in Appendix A and was checked regularly. Table 3.5 listed the technical data of the EXA20-5 axial extensometer.

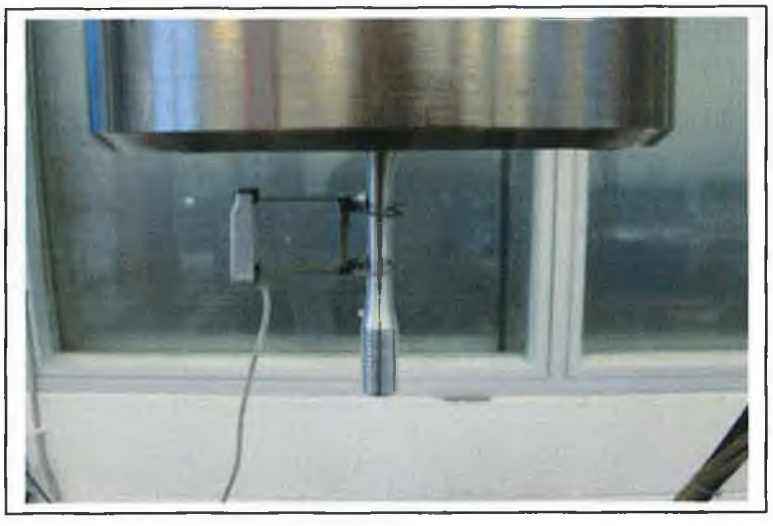

Figure 3.12. An extensometer on tensile specimen.

Model type	**Gauge length [mm]**	**Displacement range [mm]**	**Measuring Error of Full Scale [+/- %]**		
EXA 20-5	20	+/- 5	0.35		
Natural Frequency [Hz]	**Activation Force [N]**	**Weight [g]**	**Dimensions**		
			L [mm]	**W [mm]**	**H [mm]**
100	3	9	34	10	45

Table 3.5.Technical data of axial extensometer EXA 20-5.

Characteristic of EXA20-5 axial extensometer:

- Easy-to-apply clamping to ensures a reliable fitting on both smooth and uneven surface.
- It has a special distance gauge for quick and precise fixing of the gauge length.
- It has a flexible connection cable with fixed wiring.
- It has a high natural frequency, thus disturbance-free strain measurement is guaranteed.

3.5 Test Procedures

Tensile Test Procedure

Tensile testing were carried out on the 100KN ESH servo-hydraulic fatigue testing machine at a tensile deformation, constant displacement rate of smooth cylindrical specimens. The strain measurements were obtained with the used of ESH axial extensometer over a 30mm gauge length sample as shown in figure 3.12. Load and strain data were digitally recorded throughout the test. The tensile testing procedures carried out followed the ASTM test standard [99]. Tests procedures are described below:

1. Determine the diameter of test sample at the centre of the reduce section and measure its cross-section area.
2. Set up machine setting, select programming mode, click on PC monitor to display ESH Block Editor Program interface. Set first block as **'Waite'** in program name: **Mode**.
3. Select **'Stroke'** in second block with **'Target level'** 40mm at **'Ramp rate'** 2mm/min. Select **'Yes'** for the **'Acquire data'** and **'XY graph'** section.
4. Third block is set to **'Stroke'** and **'Hold'** for 5 second. Next, save the file name as 'tensile test.blk'.

5. Open ESH Block Run Program Interface, retrieve program name: 'tensile test.blk'. Insert result file name, file path, specimen details and click on run test icon.
6. Fit specimen on the gripping end, place axial extensometer on sample gauge length. Zero force the specimen, follow further instructions till the end of test.

Fatigue Test Procedure

Fatigue testing of the samples were conducted on the same machine as mentioned in tensile test procedure. Two stress ratios, (R = minimum stress/maximum stress) have been selected which performed in tension/compression range, R = -1 and tension/tension range, R = 0.1. Fatigue testing were carried out in sine waveform (fatigue stress cycle) as shown in figure 3.13, at 30Hz and at room temperature.

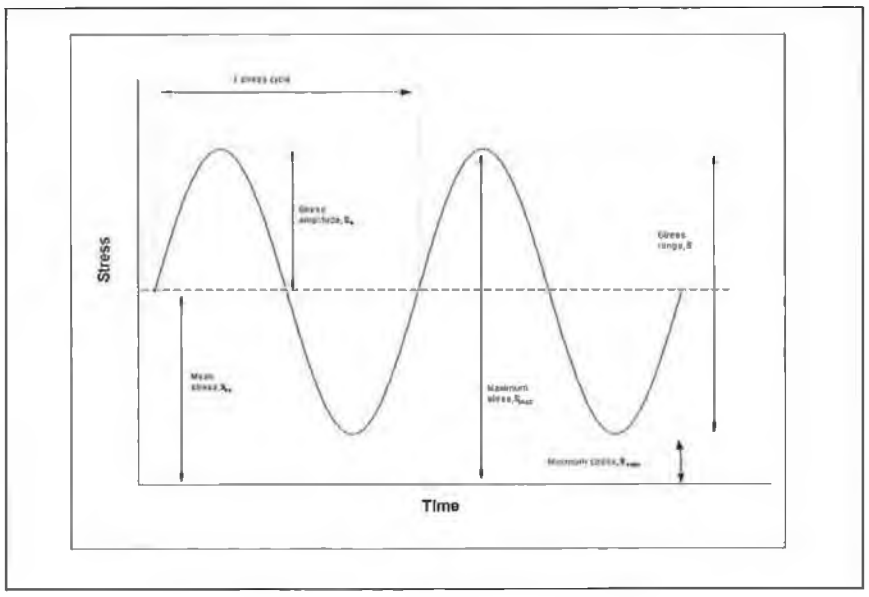

Figure 3.13. Fatigue stress cycle.

The fatigue testing procedures are as follow:

1. Examine fatigue tests specimen, make sure the specimen surfaces are free from scratches.
2. Set up machine setting, select programming mode, click on PC monitor to display ESH Block Editor Program interface. Set first block as **'Waite'** in program name: **Mode**.
3. Select **'Load'** in second block with **'Target level'**, 0KN at **'Ramp rate'**, 2KN/s, select **'No'** for the **'Acquire data'** and **'XY graph'** section.
4. Third block is set to **'Load'** and **'Hold'** for certain amount of cycles at **'Sine'**, **'30Hz'** and select a value of **'Stress amplitude'**. Next, save the file name as 'fatigue test.blk'.
5. Open ESH Block Run Program Interface, retrieve program name: 'fatigue test.blk'. Insert result file name, file path, specimen details and click on run test icon.
6. Fit specimen at gripping end, zero force the specimen, follow further instructions till the end of test.

Chapter 4: Experimental Results and Discussions

Results of and observations on the experimental programme are described in this chapter. The results are based on both mechanical tensile and fatigue tests. The materials used were aluminium alloy 6061, and 6061 composite reinforced with 15 volume % of silicon carbide particles, as described in chapter 3.

Both tensile and fatigue tests were carried out on a number of samples to ensure accuracy of the test results. Three samples of both aluminium alloy and its composite were tested for each tensile test condition. Fatigue tests involved at least 2 specimens at each stress level, up to 6 different stress levels at each stress ratio. These tests are categorised into two groups. Those at stress ratio R = -1 (fully reversed tests in tension and compression), and those at stress ratio R = 0.1 (tension-tension tests). The total numbers of aluminium alloy fatigue specimens tested are 35, and 18 aluminium composites alloy specimens.

Mechanical property behaviour is illustrated by stress-strain curves, and fatigue lifetime characteristics are presented as stress amplitude–cycles to failure (S-N) diagrams. While results for the aluminium alloy and its composite are compared to one another, the behaviour of both is also compared with relevant published data.

4.1 Tensile Properties

Table 4.1 and 4.2 show the experimental data in average from three samples for tensile tests on aluminium alloy 6061 and its composite respectively. The investigated tensile samples were produced by Powder metallurgical processing methods. The stress-strain curves were plotted, and are presented in figure 4.1.

Time (s)	Stroke (mm)	Elongation Δl (mm)	Load, P (kN)	Strain, e	Stress, S (MPa)	True Strain, ε	True Stress, σ (MPa)
0	0	0	0	0	0	0	0
0.11	0.049	0.024	3.125	0.00119	62.170	0.00119	62.2445
0.59	0.171	0.049	7.715	0.00243	153.486	0.002427	153.859
1.15	0.269	0.076	12.329	0.003769	245.28	0.003762	246.204
1.7	0.391	0.102	16.357	0.005059	325.415	0.005046	327.061
2.3	0.537	0.141	18.555	0.006993	369.143	0.006969	371.725
2.84	0.635	0.195	18.579	0.009672	369.621	0.009625	373.195
3.4	0.757	0.276	18.628	0.013689	370.595	0.013596	375.669
3.95	0.854	0.356	18.555	0.017657	369.143	0.017503	375.661
4.5	0.928	0.434	18.725	0.021526	372.525	0.021297	380.544
5.05	1.05	0.503	18.848	0.024948	374.972	0.024642	384.327
5.59	1.123	0.569	18.848	0.028221	374.972	0.027831	385.554
6.09	1.245	0.625	19.018	0.030999	378.354	0.030528	390.083
6.64	1.367	0.686	19.018	0.034024	378.354	0.033458	391.228
7.19	1.465	0.749	19.067	0.037149	379.329	0.036476	393.421
7.73	1.587	0.81	19.14	0.040175	380.781	0.039389	396.076
8.29	1.733	0.871	19.238	0.0432	382.731	0.042293	399.265
8.78	1.807	0.93	19.263	0.046126	383.228	0.045094	400.905
9.33	1.904	0.993	19.311	0.049251	384.183	0.048077	403.105
9.88	2.002	1.057	19.36	0.052425	385.158	0.051097	405.357
10.43	2.1	1.12	19.238	0.05555	382.731	0.054062	403.992
10.98	2.222	1.191	19.238	0.059072	382.731	0.057393	405.340
11.53	2.319	1.262	19.287	0.062593	383.706	0.060712	407.723
12.08	2.441	1.33	19.458	0.065966	387.108	0.063881	412.642
12.63	2.563	1.406	19.311	0.069735	384.183	0.067411	410.974
13.18	2.661	1.477	19.36	0.073257	385.158	0.070698	413.374
13.73	2.808	1.555	19.263	0.077125	383.221	0.074296	412.785
14.28	2.905	1.636	19.238	0.081143	382.731	0.078019	413.787
14.83	3.003	1.716	19.311	0.085111	384.183	0.081682	416.881
15.38	3.076	1.799	19.311	0.089227	384.183	0.085469	418.463
15.91	3.247	1.885	19.165	0.093493	381.279	0.089377	416.925
16.47	3.32	1.97	19.214	0.097709	382.254	0.093225	419.603
17.02	3.442	2.058	19.067	0.102073	379.329	0.097193	418.048
17.57	3.54	2.151	18.872	0.106686	375.450	0.10137	415.505
18.18	3.662	2.261	18.725	0.112142	372.526	0.106288	414.301
18.73	3.76	2.341	18.603	0.11611	370.098	0.109849	413.070
19.28	3.857	2.439	18.408	0.12097	366.219	0.114195	410.520

Table 4.1. Tensile test data in average from three samples for aluminium alloy 6061.

Time (s)	Stroke (mm)	Elongation Δl (mm)	Load, P (kN)	Strain, e	Stress, S (MPa)	True Strain, ε	True Stress, σ (MPa)
0	0	0	0	0	0	0	0
0.06	0.024	0.012	2.637	0.000595	52.93942	0.000595	52.97093
0.95	0.146	0.039	8.74	0.001934	174.3559	0.001932	174.6932
1.82	0.293	0.073	13.794	0.003621	274.903	0.003614	275.8983
2.7	0.439	0.139	15.381	0.006894	306.4757	0.006871	308.5886
3.57	0.562	0.22	15.82	0.010912	315.2094	0.010853	318.6488
4.4	0.659	0.3	16.211	0.014879	322.9882	0.01477	327.7941
5.34	0.854	0.393	16.235	0.019492	323.4656	0.019305	329.7707
6.21	0.903	0.474	16.431	0.02351	327.365	0.023237	335.0612
7.09	1.099	0.561	16.528	0.027825	329.2947	0.027445	338.4572
8.02	1.245	0.662	16.577	0.032834	330.2696	0.032307	341.1137
8.9	1.343	0.752	16.553	0.037298	329.7921	0.036619	342.0927
9.78	1.465	0.857	16.602	0.042506	330.7669	0.041627	344.8264
10.66	1.636	0.967	16.626	0.047962	331.2444	0.046847	347.1314
11.54	1.685	1.074	16.528	0.053269	329.2947	0.051898	346.8358
12.42	1.855	1.199	16.577	0.059468	330.2696	0.057767	349.9101
13.3	2.026	1.326	16.309	0.065767	324.9378	0.063695	346.3081
14.17	2.148	1.455	15.942	0.072165	317.6365	0.06968	340.5589

Table 4.2. Tensile test data in average from three samples for aluminium composite 6061/SiC_P/15%.

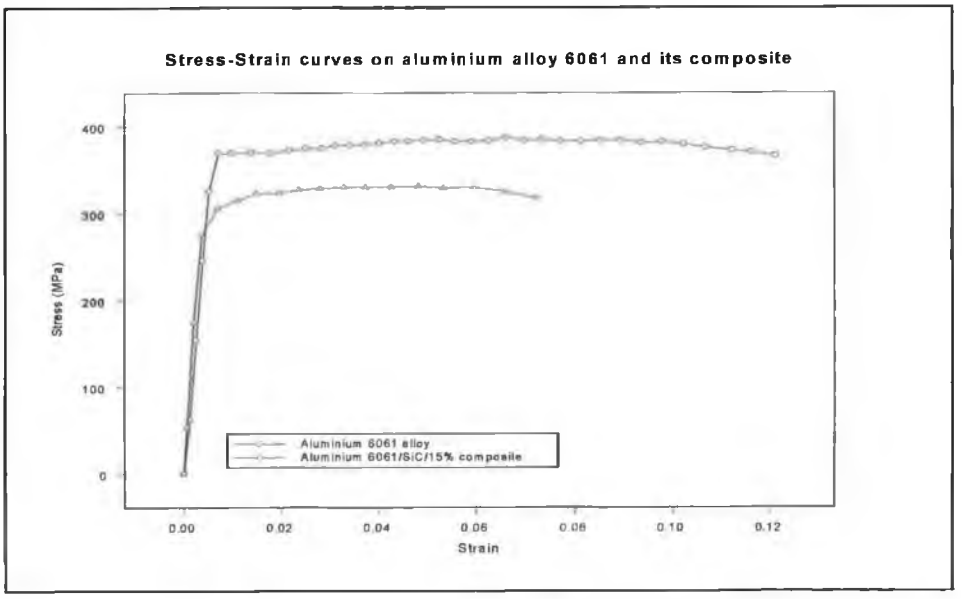

Figure 4.1. Engineering Stress-Strain curves for aluminium alloy 6061 and its composite.

In table 4.3 the tensile properties of the present test materials are presented, and compared with those published elsewhere for 6061 and its composite.

Materials	Average particle size (μm)	Yield Strength $\sigma_{y2\%}$ (MPa)	Ultimate tensile Strength σ_{Utl} (MPa)	Young Modulus E (GPa)	Total Elongation (%)	Processing Route	Ref
AA6061	-	363.08	378.1	68.08	19.35	PM + Hot extrusion + T6	Present work
AA6061	-	374	399	69	12.5	PM + Hot extrusion + T6	7
AA6061	-	243	290	68.5	15	PM + section rolled + T6	89
AA6061/ SiC_p/15%	30	284.49	331.24	90.67	8.12	PM + Hot extrusion + T6	Present work
AA6061/ SiC_p/15%	4.5	390	450	93	5	PM + Hot extrusion +T6	7
AA6061/ SiC_p/15%	3.5 - 5	378	421	88.3	6.7	PM + Hot extrusion + T6	90

Table 4.3. Various mechanical properties of aluminium alloy 6061/15% SiC composite and the aluminium alloy 6061.

The present results for AA6061 are well within the range of other published data. Quite close agreement is seen with other values for Young's modulus [7, 89], and the strength is comparable to that of other 6061 material subjected to a similar heat treatment process [7]. It is worth noting however that strength values for the alloy can vary quite significantly depending on heat treatment, as can ductility [7, 89]. The present material exhibits particularly high ductility (over 19%) compared to equivalent materials (eg 12.5% [7]).

The present results for the composite material are also compared with other published data in table 4.3. Unfortunately it was not possible to compare exactly 'like with like',

as available data is for materials with smaller size reinforcement, produced by different manufacturers, but with the same matrix alloy, same volume fraction of SiC particle and subjected to the same heat treatment. It has been proposed that the aluminium matrix used is the most important factor affecting yield strength and ultimate tensile strength of these SiC/Al composites [54], so the data presented are considered to be valid. Nevertheless some variation in tensile properties is likely due to the other differences.

The composite under study has a typical value of Young's modulus for this material (around 90 GPa), and exhibits slightly higher ductility (over 8%, compared to 5-7%) than the others tested [7, 90]. Its strength is seen to be relatively low however, with yield strength being approximately 285 MPa, as compared to values of 378-390 MPa measured for similar materials. This is also reflected in the ultimate tensile strength values, which, at approximately 330 MPa, are much lower than those of 420-450 MPa for other 6061/SiC composites.

The differences in mechanical properties between the current composite and others tested could be attributed to many factors as seen in table 4.3. These include variation in manufacturer, differences in SiC_p size (which was larger in the present composite), and different ageing conditions used. These aspects are believed to have caused the relatively low yield and ultimate tensile strength in the current composite, compared to those reported by other researchers [14, 91-93].

The Stress-Strain curves of figure 4.1 illustrate that the present aluminium alloy 6061 has higher ductility than the composite, which failed in a more brittle manner. In fact, the composite material has only 42% the ductility of the matrix alloy (8.12% as compared with 19.35%). It is also clear that the matrix alloy is stronger. The addition of the reinforced SiC particles did not improve strength in the composite over the conventional alloy, but rather decreased it. The decreases in yield strength and ultimate tensile strength were 21.6% and 12.4% respectively.

From table 4.3 however it is also seen that the SiC-reinforced aluminium alloy 6061 composite exhibits a much higher elastic modulus, E. There was a 33.18 % increase (from 68 GPa to over 90 GPa) in the Young Modulus of the alloy when reinforced with SiC particles. These results are summarised in figure 4.2.

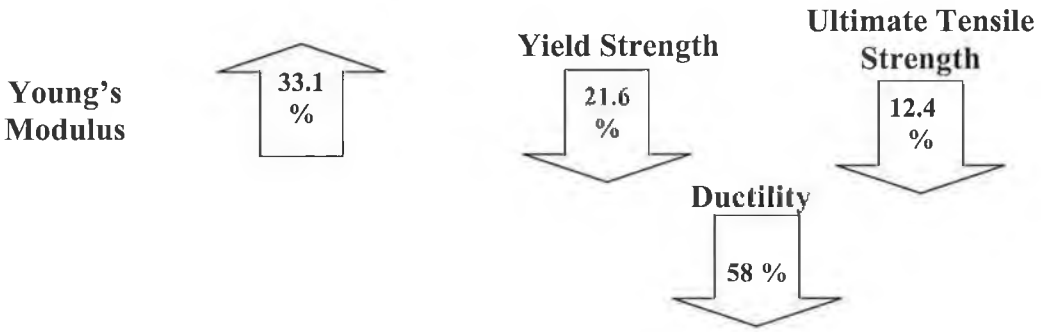

Figure 4.2. The effect of 15% SiC, 30μm, particle reinforcement on mechanical properties of aluminium alloy 6061.

Looking to the data published in [7] for a similar matrix material and its composite, a comparable reduction in ductility is seen (a 60% reduction from 12.5% to 5%), in conjunction with an almost 35% improvement in Young's modulus. However, the same loss in overall strength is not seen, and indeed the composite yield strength and ultimate tensile strength are both higher than the monolith material (by 4% and 13% respectively). This correlates with the present composite material's poor strength properties commented upon earlier.

A low strain was recorded from the tensile property test for the composite in question. An increase in Young modulus resulted, this is assumed to be related to the differences in volume fraction of strengthening precipitates. On the other hand, the decrease of tensile ductility in composites is pronounced. Notably, unreinforced alloy demonstrated a distinct yield point. The addition of particle reinforcement to a matrix alloy without improvement in mechanical properties is not a common phenomenon.

Similar results indicating the lower composite strength but higher composite modulus than the unreinforced alloy have been reported for aluminium based composites [14, 15]. This result might due to that the matrix alloy and a composite was produced by different manufacturer but in same processing method and heat treatment. Hence, it was not possible to compare both materials in terms of their tensile properties.

4.2 Fatigue Lifetime Behaviour

The materials investigated for fatigue-lifetime and fracture behaviour were the same as those used in the tensile property tests. Fluctuating load tests, as described in the previous chapter were carried out to analyse the fatigue behaviour of both the conventional and composite alloy. In all, twenty-seven 6061 specimens were fatigue tested, and seventeen 6061 matrix composite were tested.

The results from these tests are presented and discussed in a number of sections. Results are tabulated, and are also plotted as maximum stress level versus the logarithm of number of cycles to failure, the so-called S-N diagrams. The endurance limit, σ_e is defined according to the literature as the stress level at which a specimen does not fail until 1×10^7 cycles [14].

Initially results for aluminium alloy 6061 are presented. These include its fatigue-lifetime behaviour at mean stress of zero, i.e. stress ratio R = -1. The effect of mean stress is then seen by comparison with results for alloy 6061 at R = 0.1. Data are compared with those available in the literature for this alloy. The relevant results and plots are given on tables 4.1, 4.2 and 4.3 and figures 4.2 to 4.6.

The second results section presents the equivalent results for the composite material. Its fatigue lifetime behaviour is detailed, both at stress ratio R = -1 and R = 0.1, and is compared with available published results for similar materials. The S-N plots are presented in figures 4.7 to 4.10.

In completing the experimental results, the behaviour of the alloy material is compared with that of the composite as shown in figures 4.11 (a) and (b). Table 4.4 and 4.6 list the fatigue-lifetime results for this comparison.

The S-N diagrams were generated using " S-plus 2000 mathematics software", and this was also used to calculate and draw a best fit curve from the experimental data. The S-N diagram was plotted from fatigue results in two-dimensional data where the curve-fitting plots display a regression line with scatter plot of the associated data points. The regression lines are generated using an ordinary least-squares analysis to calculate y values for given values of x. The best curve-fitting plots for the S-N diagram used was so called "Power curve-fitting plot".

4.2.1 Fatigue Lifetime Behaviour of Matrix Alloy

Results of fatigue tests on specimens of the 6061 aluminium alloy are given in tables 4.4 and in figures 4.3. At R = -1, multiple tests were carried out, whereas at R = 0.1, two tests at each stress were done due to the availability of specimens are limited.

Stress Ratio, R = -1					
Stress Range (MPa)	**Maximum Stress (MPa)**	**Minimum Stress (MPa)**	**Mean Stress (MPa)**	**Stress Amplitude (MPa)**	**Cycles to Failure, N_f**
636.6	318.3	-318.3	0	318.3	1.16×10^3, 2.7×10^3
576.9	288.47	-288.47	0	288.47	1.12×10^4, 1.31×10^4 1.37×10^4, 2.78×10^4 3.24×10^4
484	242	-242	0	242	3.26×10^4, 3.55×10^4 4.77×10^4, 1.18×10^5
400	200	-200	0	200	7.88×10^4, 2.65×10^5 3.68×10^5, 5.27×10^5
340	170	-170	0	170	1.55×10^5, 4.27×10^5, 8.16×10^5, 3.16×10^6
280	140	-140	0	140	5.2×10^6, 6.1×10^6, 8.53×10^6, 1×10^7 – did not fail

Stress Ratio, R = 0.1					
Stress Range (MPa)	**Maximum Stress (MPa)**	**Minimum Stress (MPa)**	**Mean Stress (MPa)**	**Stress Amplitude (MPa)**	**Cycles to Failure, N_f**
322.3	358.1	35.81	196.96	161.15	4.2×10^4, 6.5×10^4
304.38	338.2	33.82	186.01	152.19	1.14×10^5, 2.22×10^5
286.2	318	31.8	174.9	143.1	3.16×10^5, 4.23×10^5
259.62	288.47	28.847	158.66	129.81	7.93×10^5, 8.2×10^5
217.8	242	24.2	133.1	108.9	2.36×10^6, 3.27×10^6
198	220	22	121	99	9.5×10^6, 1×10^7 – did not fail

Table 4.4. Fatigue lifetime of aluminium alloy 6061 at stress ratios, R = -1, and 0.1.

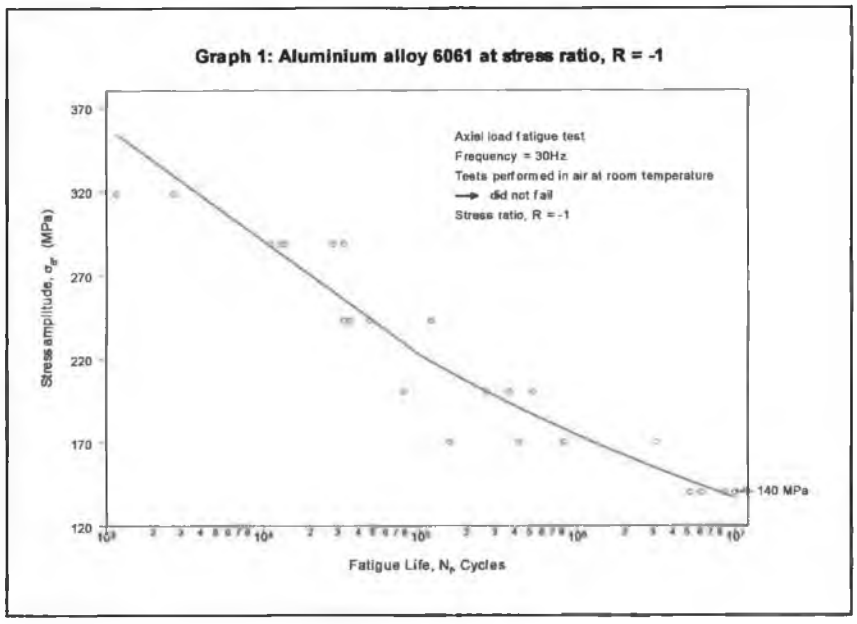

Figure 4.3. S-N curve on aluminium alloy 6061at stress ratio of R = –1.

Figure 4.3 shows general trend of the S-N curve on aluminium alloy 6061 at stress ratio of R = –1. The diagram is plotted with the number of cycles to failure as the abscissa and stress amplitude as the ordinate. A logarithmic and linear scale is used respectively for the number of cycles to failure and stress amplitude in scatter plot. Curve of the plot is best fitted by "Power curve-fitting plot" within the mathematics software S-Plus 2000 as mentioned previously. All statistics data points are adjusted appropriately for best curve fits.

The 6061 result showed a fatigue limit after reached 1 x 10^7 cycles, which was 140MPa. Although fatigue limits are not generally observed in aluminium alloys, the present fatigue test limit was set in the range of 1 x 10^7 cycles in terms of considered the cost and time consumed. The highest fatigue lifetime gap was observed at stress amplitude 200MPa and 170MPa, which was 85% and 95% respectively. While higher and lower stress amplitude experienced smallest fatigue lifetime gap fewer than 65%. Intermediate stress amplitude at 242MPa showed a 72% difference of fatigue lifetime.

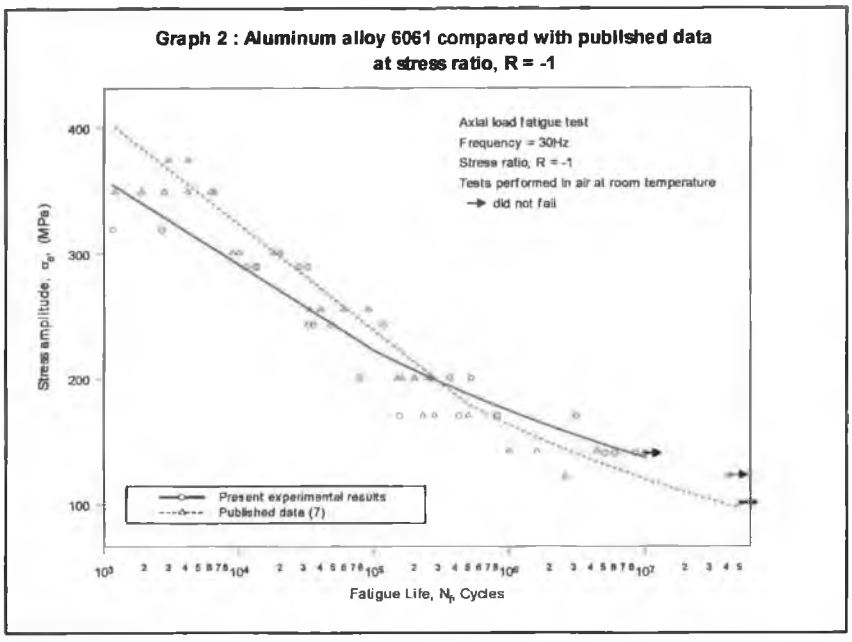

Figure 4.4. S-N curves on aluminium alloy 6061 compared with published data.

To investigate the validity of the results of the fatigue tests, figure 4.4 was plotted. The plot scatter method was the same as used in figure 4.3. Here the experimental results for 6061 are compared with available published data for this material under fully reversed (R = -1) axial loading. The data used in the plot are presented in Appendix B. The published data used for comparison was taken from the International Journal of Fatigue, November, 1993 [7], and the fatigue tests were carried out in a similar way to those used for the present material. All tests were tested in axial push-pull loading at stress ratio, R = -1, using sinusoidal waveform and at room temperature. Other published sources are not used to compare with present results due to differences in material, fatigue test techniques, or differences in stress ratio or environment [4, 6, 20, 94]. A linear scale is used for stress amplitude and a logarithmic scale for the number of cycles to failure. As can be seen in figure 4.4, the curve-fit on both data sets was similar.

Figure 4.4 shows no significant difference in fatigue lifetime (in cycles) at intermediate and high stresses regions for the current material and published data. At low stresses, the current experimental results show a slightly longer lifetime, but the differences are minimal. Current material showed a higher endurance limit than published material at fatigue lifetime after 1 x 10^7 cycles, which was 140 MPa and 100 MPa respectively.

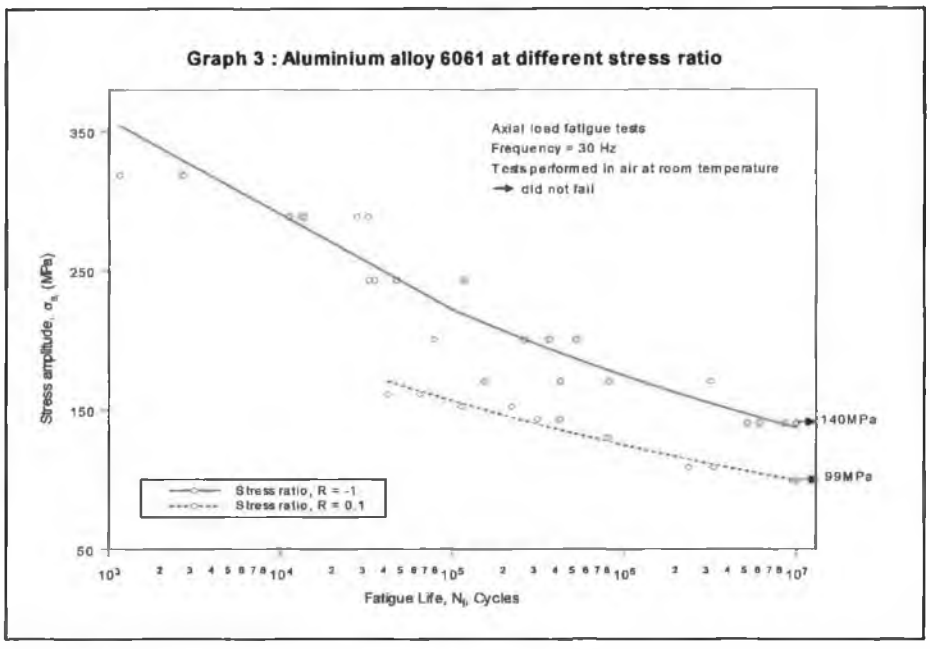

Figure 4.5. Effect of mean stress on aluminium alloy 6061.

Figure 4.5 shows the effect of mean stress on fatigue response for 6061 aluminium alloy. The curve fit method was the same as applied in previous figures. It is clear from the graph that changing from a tension/ compression test (stress ratio, R = -1) to a tension/tension tests (R = 0.1) reduces material life, at a given stress amplitude. An increase in mean stress, σ_m has caused a decrease in the corresponding fatigue life. The trend seen in the graph is the same as those published in the ASM International fatigue data book: light structural alloys [95], and is typical of mean stress effects in metals. Therefore the conventional mean stress relationships can be used to analyse the results.

There are four mathematical relationships, which have been proposed for the effect of mean stress on the fatigue behaviour of materials subjected to various stress ratios, namely [96]:

1. Goodman's linear relationship
2. Gerber's parabolic relationship
3. Soderberg's linear relationship
4. The elliptic relationship

The Goodman's and Gerber's relationships are used to analyse the current results due to the widespread use of these relationships for behaviour where the mean stress level is between zero, and the tensile strength of the alloy [97]. First one was the modified Goodman relationship which assumed that the effect of mean stress is linear over this range: second is the Gerber relationship which was considered the variation to be parabolic as shown in figure 4.6. The fatigue tests data from the unreinforced matrix material are presented on that figure in the format of a Goodman-Gerber diagram, where:

Goodman's linear relationship:

$$\frac{\sigma_a}{\sigma_N} + \frac{\sigma_m}{\sigma_u} = 1$$

$$\sigma_a = \sigma_N\left(1 - (\sigma_m/\sigma_u)\right)$$

Gerber's parabolic relationship:

$$\frac{\sigma_a}{\sigma_N} + \left(\frac{\sigma_m}{\sigma_u}\right)^2 = 1$$

$$\sigma_a = \sigma_N\left(1 - (\sigma_m/\sigma_u)^2\right)$$

and σ_a is the stress amplitude, σ_N is stress amplitude below which $N_f > 10^7$ cycles at R = -1, σ_m is the mean stress and σ_u is the ultimate tensile strength.

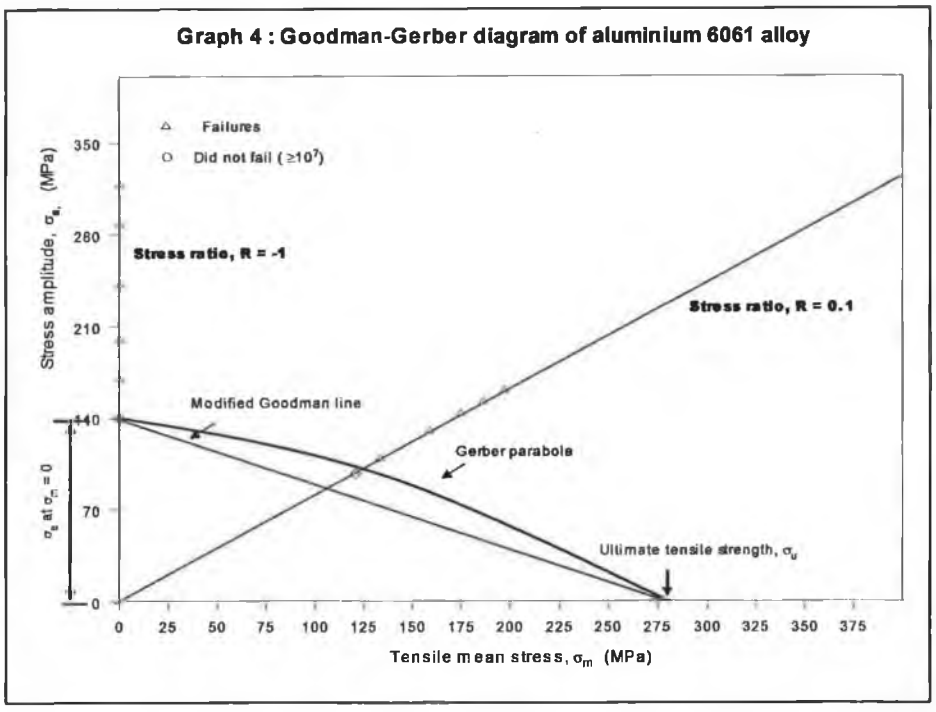

Figure 4.6. Goodman's – Gerber's diagram of aluminium 6061 alloy.

The Goodman's - Gerber's diagram of the unreinforced material is shown in figure 4.6, which indicates that the response of the material lies somewhere between the bounds set by the Goodman and Gerber prediction. However the Goodman equation provides the closest correlation for this alloy.

Table 4.5. Unnotched axial fatigue strength at cycles to failure for 6061 aluminium alloy.

Specimen	Stress ratio, R	Fatigue strength at maximum stress (MPa) at cycles of :				
		1×10^3	10^4	10^5	10^6	1×10^7
Unnotched round 6061 alloy	0.1		358.1	338.2	242	220
	-1	318.3	288.47	242	170	140

Based on the curve fit through the experimental data, the fatigue strength (maximum stress) of the 6061 alloy at given numbers of cycles to failure is shown in table 4.5 above. The ratio of the fatigue strength to ultimate tensile strength at 10^7 cycles for the unreinforced matrix is 0.37 at stress ratio –1, and is 0.58 at stress ratio 0.1.

At a stress ratio of –1, the material demonstrated a higher fatigue strength at all maximum stress levels, as well as better fatigue endurance limit than at R = 0.1 Stress ratio 0.1 exhibited better ratio on maximum fatigue strength over the ultimate tensile strength as high as 0.95 compared to 0.84 at Stress ratio of -1.Fatigue endurance strength was also pronounced over stress ratio –1. There were 220MPa and 140MPa respectively.

4.2.2 Fatigue Lifetime Behaviour of MMC Material

Table 4.6 shows the experimental results of fatigue data on 6061 composite at two different stress ratio. Fatigue tests were conducted using the same test procedures and conditions as applied to the 6061 alloy. Again, at stress ratio, R = -1 each stress level was applied to at least two specimens. At stress ratio R = 0.1 only one specimen was tested at each stress level due to the lack of availability of specimens.

Stress Ratio, R = -1					
Stress Range (MPa)	**Maximum Stress (MPa)**	**Minimum Stress (MPa)**	**Mean Stress (MPa)**	**Stress Amplitude (MPa)**	**Cycles to Failure, N_f**
576.9	288.47	-288.47	0	288.47	1.5×10^3, 2.54×10^3
484	242	-242	0	242	1.73×10^4, 1.28×10^4 2.32×10^4
400	200	-200	0	200	3.78×10^4, 1.56×10^4 1.58×10^4
340	170	-170	0	170	2.52×10^5, 7×10^4 3.61×10^5
280	140	-140	0	140	1×10^7 – did not fail, 1×10^7 – did not fail
Stress Ratio, R = 0.1					
Stress Range (MPa)	**Maximum Stress (MPa)**	**Minimum Stress (MPa)**	**Mean Stress (MPa)**	**Stress Amplitude (MPa)**	**Cycles to Failure, N_f**
286.2	318	31.8	174.9	143.1	5.6×10^4
259.6	288.47	28.84	158.66	129.8	1.3×10^5
217.8	242	24.2	133.1	108.9	1.76×10^5
198	220	22	121	99	1×10^6
180	200	20	110	90	1×10^7 – did not fail

Table 4.6. Fatigue lifetime of alloy 6061 composite at stress ratios, R = -1, and 0.1.

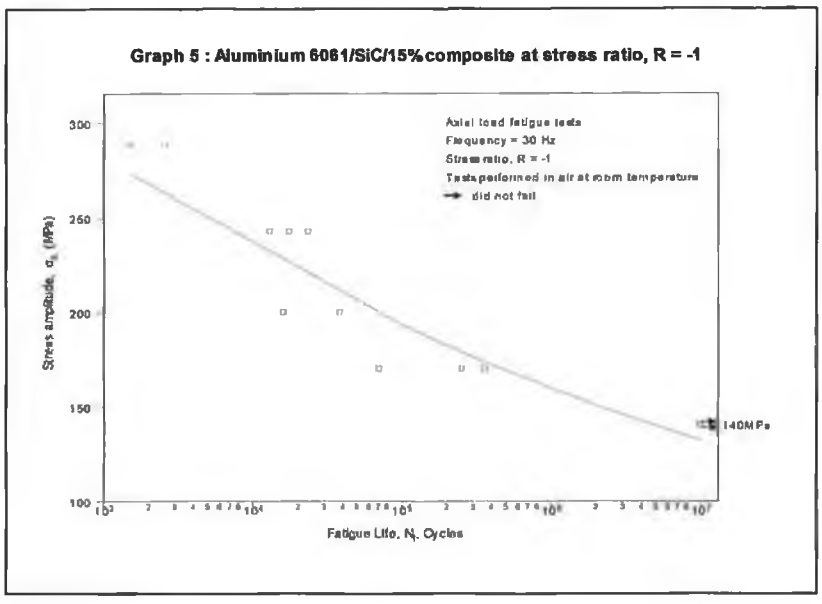

Figure 4.7. S-N curve of aluminium 6061/SiC/15% composite at stress ratio, R = -1.

Figure 4.7 shows the composite fatigue lifetime curve at stress ratio -1. Fatigue strength in low fatigue region, which is < 1 x 10^4 cycles is not pronounced and fatigue lives in intermediate stress amplitude at 242MPa and 200MPa are in the range of 1 x 10^4 cycles. In the high cycle fatigue regime, at 1× 10^7 cycles, the composite material shows a maximum stress level at140MPa.

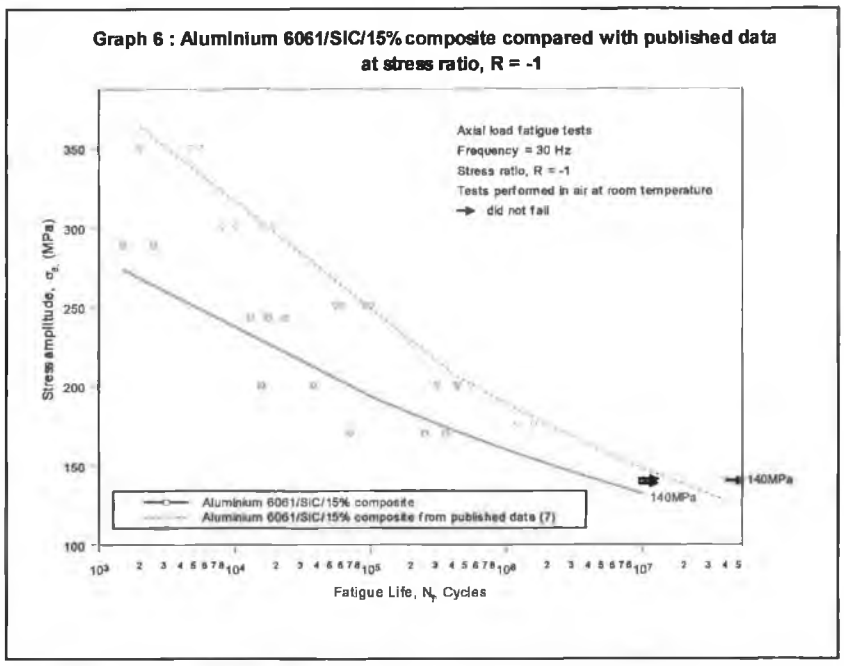

Figure 4.8. Comparison of 6061/SiC/15% composite with published data at stress ratio, R = -1.

In order to further investigate the results of the composite fatigue tests, figure 4.8 is plotted. Here the experimental results for 6061 composites are compared with available published data for this material under fully reversed (stress ratio, R = -1) axial loading. The data for this plot are given in Appendix B. The published data used is from the same source [7] as mentioned in preceding section in figure 4.4. Both composites were manufactured by same processing route (a powder metallurgical process followed by hot extrusion), have the same volume fraction of SiC particles, (15%) and underwent T6 heat treatment.

Figure 4.8 shows that the current composite experiences much poorer fatigue response compared to published results, although does exhibit the same fatigue endurance limit at 140MPa. The highest fatigue strength at low fatigue region is also lower than the published value as 288MPa compared to 350MPa respectively. These differences can be due to certain factors that affected the tensile property and fatigue lives such as

different in average SiC-particles size, produced by different manufacturer which might induced different processing and heat treatment stages as illustrated in table 4.3.

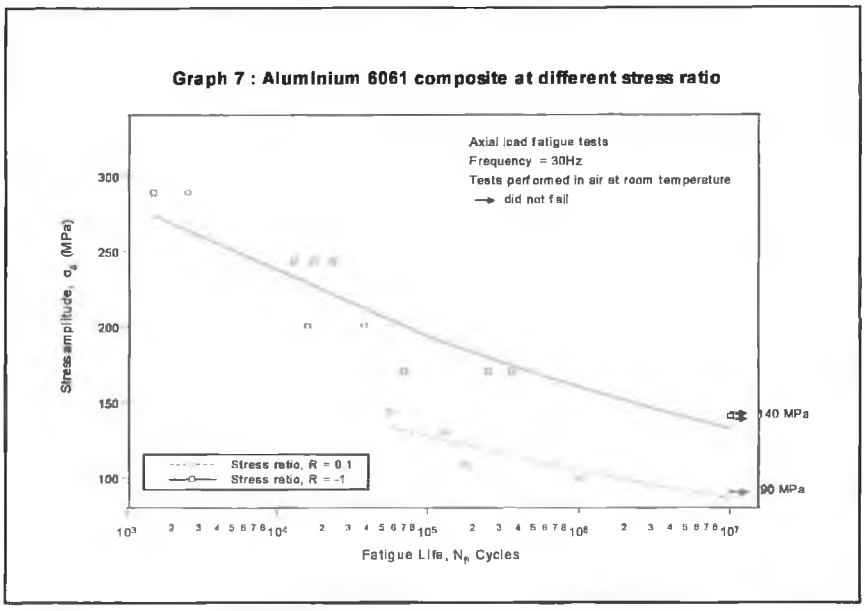

Figure 4.9. Comparison of aluminium 6061/SiC/15% composite at stress ratio, R = -1 and 0.1.

Figure 4.9 shows the effect of stress ratio 0.1 and –1 on fatigue response of the composite of 6061 aluminium alloy. Stress ratio 0.1 produced higher fatigue strength at every stress level as well as better fatigue endurance limit over ratio –1 for this material. The figure also showed a similar trend as showed in 6061 aluminium alloy to which an increased on mean stress, σ_m has caused a decreased in the correspondent shorter life.

The Goodman's- Gerber's diagrams of the composite material is shown in figure 4.10, which shows that the responses of the MMC materials lies somewhere between the bounds set by the Goodman and Gerber prediction. However the Goodman equation provides the closest correlation for the composite.

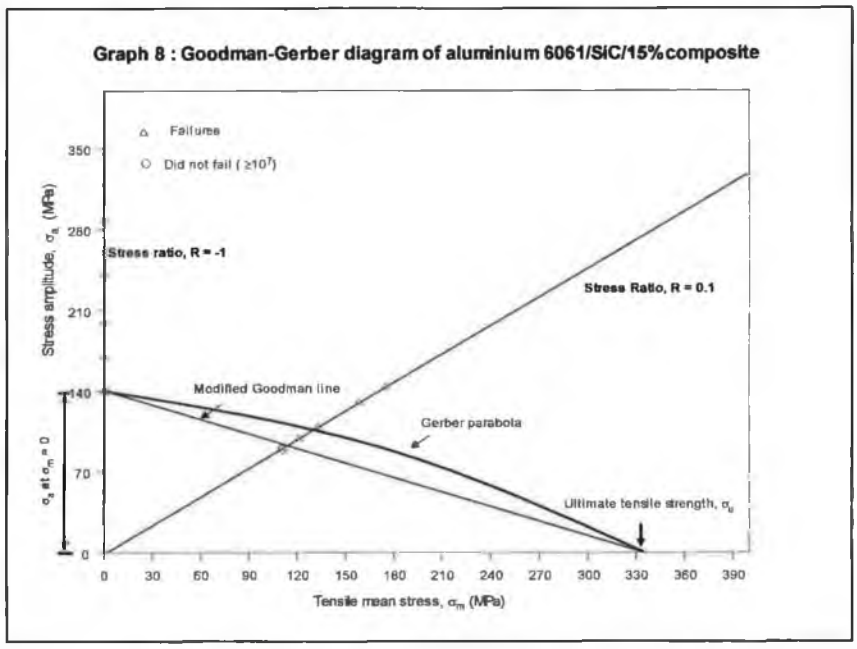

Figure 4.10. Goodman's - Gerber's diagrams of 6061/SiC/15% composite.

Specimen	Stress ratio, R	Fatigue strength (MPa) at cycles of :				
		10^3	10^4	10^5	10^6	1×10^7
Unnotched round 6061/SiC_P/15% composite	0.1		318	288.47	220	200
	-1	288.47	242	170	-	140

Table 4.7. Unnotched axial fatigue strength at cycles of failure for 6061 composite.

Based on the curve fit through the experimental data, the fatigue strength of the 6061 composite at given numbers of cycles to failure is shown in table 4.7. The ratio of the fatigue strength at 10^4 cycles to ultimate tensile strength for the composite is 0.42 at stress ratio –1, and at 10^3 cycles is 0.63 at stress ratio 0.1.

4.2.3 Comparison Between Alloy and Composite Fatigue Behaviour

The fatigue response of unreinforced and reinforced 6061 aluminium alloy is shown for two stress ratio, R –1 and 0.1 in figure. 4.11 (a) and (b), where the stress amplitude is plotted against total fatigue life in cycles (N_f). In general, results from the smooth cylindrical bar testing indicated that, at a constant stress level, the addition of SiC did not improve the unnotched fatigue lives significantly over those of the unreinforced 6061 aluminium matrix at stress ratio –1 and 0.1 as can be seen in table 4.3.

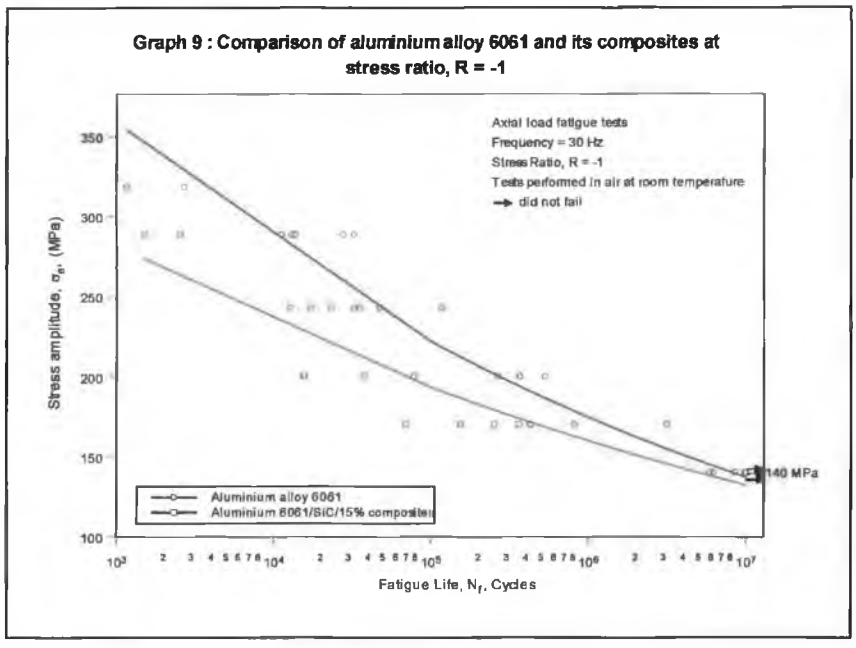

(a)

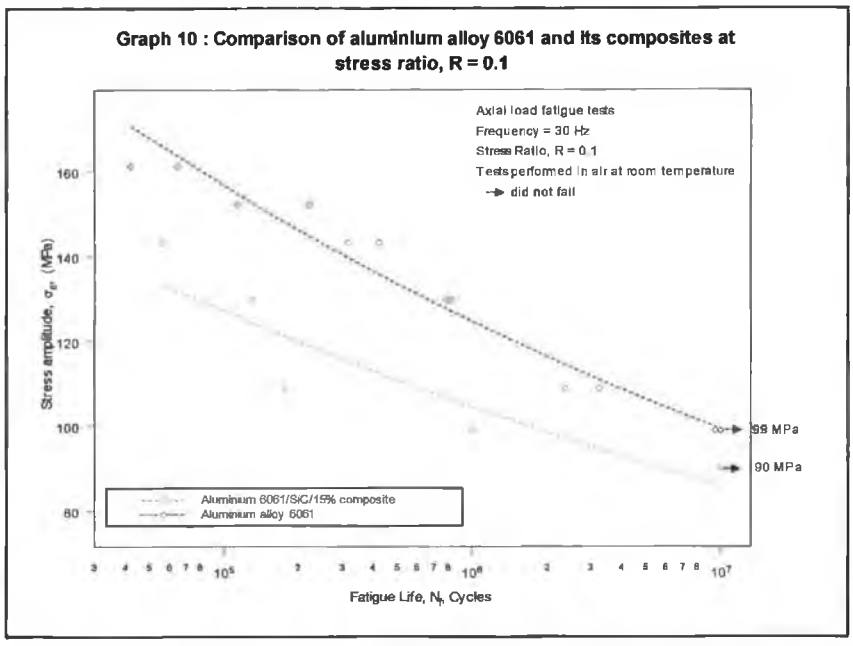

(b)

Figure 4.11. Fatigue response of (a) unreinforced and (b) reinforced 6061 aluminium alloy at stress ratio (a) R = -1 and (b) 0.1.

At a stress ratio of –1, the fatigue-lifetime of the composite is shorter than the unreinforced alloy in the low to high fatigue life region of 10^3 to 10^6 cycles. The gap of fatigue life for both materials was smaller and an improvement of the fatigue life can be seen at stress level 170MPa. However, it must be noted that the composite has a longer life at 170MPa.

Similar trend of fatigue life patterns was seen at the stress ratio of 0.1. Again, the composite showed an inferior in fatigue lives over the conventional alloy. There was a difference in fatigue strength; there is 220MPa and 200MPa for the matrix alloy and composite respectively.

In general, the inferiority in fatigue life of 6061 composite when compared to 6061 alloy is not common, however can be attributed to a number of factors. Reasons of inferiority in composite fatigue lives are discussed at the followed section 4.3: Fractographic investigation.

4.3 Fractographic Investigation

This section continues from previous results and discussion sections in focusing on the microstructure and fracture surfaces of AA6061 aluminium alloy and its particle reinforced composite tested in tension and fatigue.

Metallographic and fractographic observations are presented for both materials tested and are discussed in this section. Observations also rely upon macro and microscopic studies of the specimens, and the relationship between the matrix alloy and its interface or reinforcement in order to explain the mechanical and fatigue properties.

Initially the composite alloy was studied. Specimens were cut in sections followed by standard metallographic polishing and finally were observed under an optical microscope and quantitative imaging analysis applied to images obtained. The aim of this metallographic investigation was to observe the composite structure and the distribution of SiC_P in the composite alloy. Quantitative imaging analysis was used to study the average size, volume fraction and amount of SiC_P in specific areas of the composite.

Fracture surfaces of samples from tensile and fatigue tests were investigated using a scanning electron microscope (SEM). Different magnifications of fracture surfaces were observed, and used to explain the fracture behaviour of the matrix alloy and composite.

Metallography of the Test Materials

Figure 4.12 (a) and (b) are the optical micrographs of the MMC material. They show the distribution of SiC particles in this aluminium composite in the cross-sectional plane, and in the longitudinal direction (which is parallel to the extruded direction) respectively. These micrographs are selected from the regions of the sample, where there is an even distribution of SiC particles.

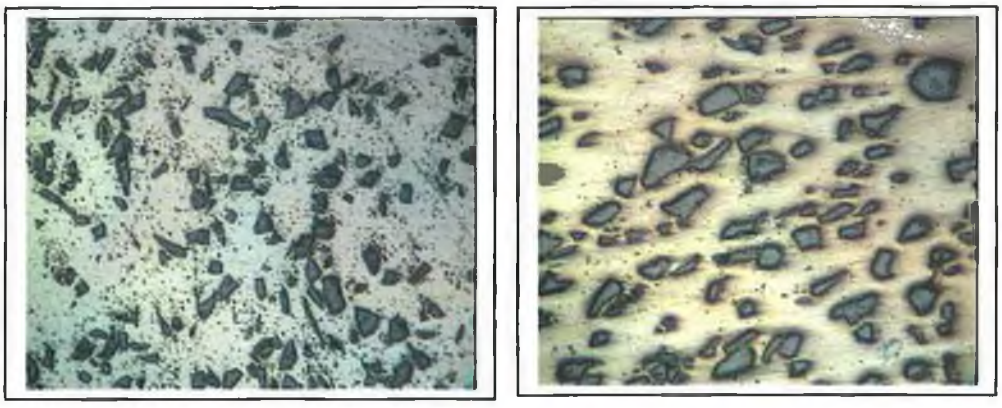

(a) (b)

Figure 4.12. Optical micrographs of particle distribution for AA6061/SiC_P/15%, (a) cross-section plane and (b) longitudinal plane [magnification = 100x].

In order to quantify this distribution, an optical micrograph taken in cross-section was then analysed using quantitative imaging analysis software as mentioned previously and the results are shown in figure 4.13. The imaging analysis software was used to detect, highlight and finally categories the sizes of SiC particles. The presence of small particles on micrographs in figure 4.12 is caused by the silicon cloth used during the polishing process.

The results show the mean SiC particle size in the composite is 17.12μm, with maximum and minimum particle sizes of 36.37μm and 4.27μm respectively in the total area of 218615μm^2. The highest percentage of particles (at 23.4%) are in the range 17-20μm, which are followed by particles ranging from 14-17μm, which constitute 21.5% of all particles. Particle sizes of 20-30μm and 30-34μm constitute 24% and 1.8% of the total particles in the field respectively.

These results do not correlate well with the manufacturer data, which states an average particle size of 30μm. One possible reason for this may be non-uniform distribution of SiC particles throughout the composite arising from the powder processing route (eg. Poor mixing can cause clustering of sizes). Also, the micrograph taken represents only a small part of that cross section, so some error will exist in projecting overall particle size distribution. However, the supplier does not specify the means used to measure particle distribution, and it may be that the current study yields more accurate results.

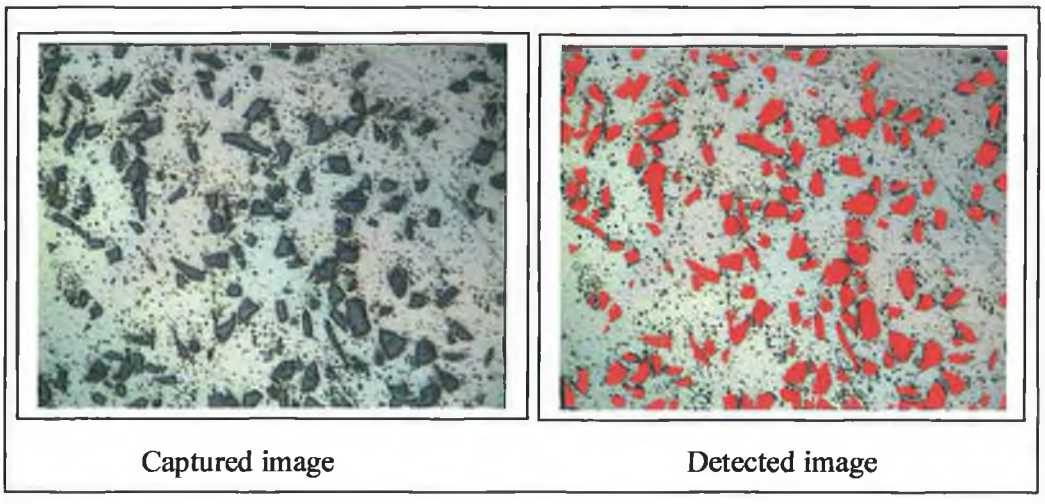

Captured image Detected image

(a)

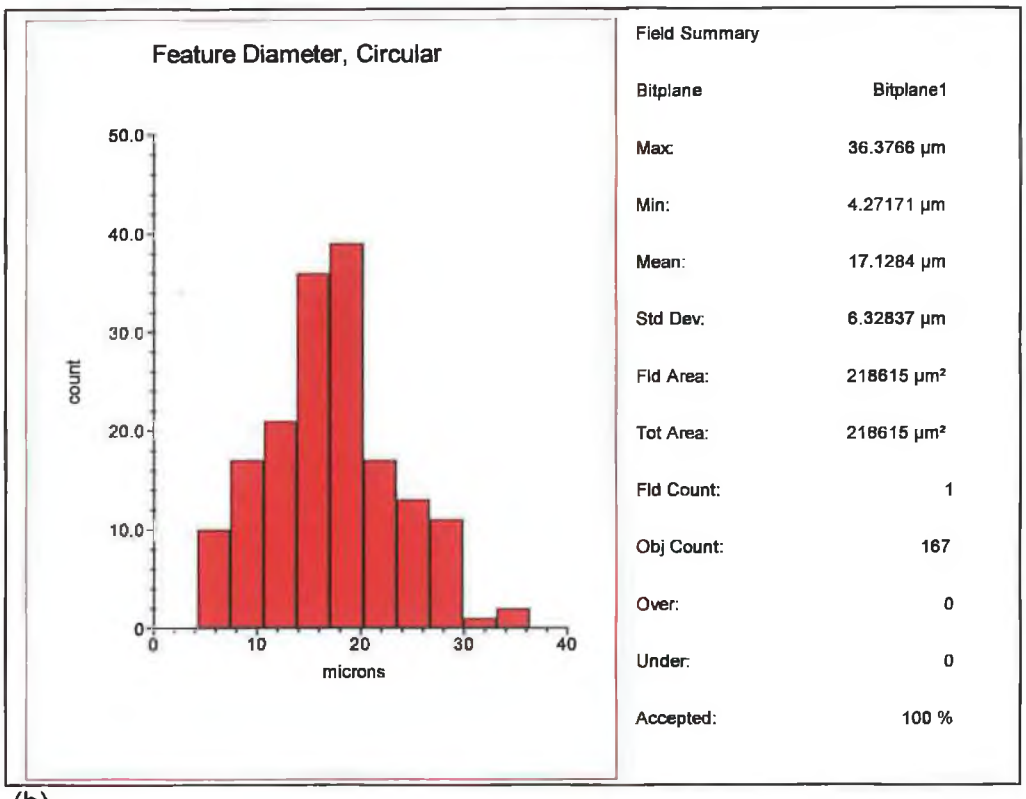

(b)

Figure 4.13. (a) Capture and detected image of the SiC_p and (b)Quantitative imaging analysis of the average SiC particle sizes in a cross-sectional plane of the test MMC material.

It is noteworthy that the SiC particles include high numbers of larger particles (>10µm). In general, a decrease in the size of SiC_P increases yield strength, and ultimate strength of the composite [14, 93]. Tensile ductility of a composite is also significantly reduced with larger sized reinforcement in artificial aged, peak aged (PA) conditions [14].

Tensile Tests

Figure 4.14 shows a photograph of typical fractured tensile specimens of 6061 alloy and its composite. The picture illustrates a low ductility 'flat and brittle' fracture in 6061 composite, while the matrix alloy exhibits a higher ductility, more 'cup and cone' type fracture. This correlates with the ductility (%) at failure results for the matrix alloy and composite, which are 19.35% and 8.12% respectively as listed in table 4.3.

Figure 4.14. Fractured tensile specimen of 6061 aluminium and its SiC composite.

Low magnification SEM macrographs of tensile specimen fracture surfaces for both materials are shown in figure 4.15 and more detailed features are shown in the higher magnification figure 4.16. Study of images at higher magnification revealed a dimpled fracture surface for both unreinforced and reinforced specimens. The fracture surfaces of the unreinforced 6061 alloy contain an even distribution of large dimples connected by sheet of smaller dimples as shown in figure.4.17 (a). This indicates a pattern resulting from microvoid nucleation, growth, coalescence and failure.

The fracture surface of the MMC contains smaller voids and dimples between the particles is shown in figure 4.17 (b). Particle cracking of many of the SiC particles was also observed on the fracture surface. In addition, evidence of the pull-out of particles coated with aluminium matrix was sometimes observed. The failure mode of the reinforced composites was predominantly through matrix ductile failure due to stress concentration near the interface region. Particle cracking occurs because of the triaxial stress and plastic strain near the brittle particle surface. Some particle pull-out seen was due to the matrix failure [93].

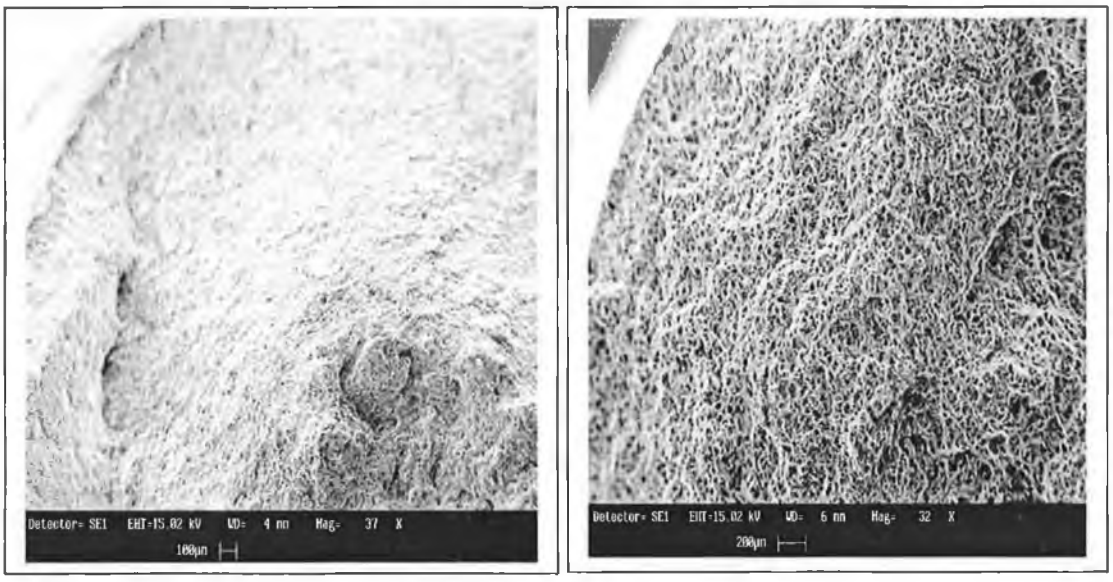

a) b)

Figure 4.15. Macrographs of tensile fracture surface of (a) 6061 aluminium (b) 6061 composite.

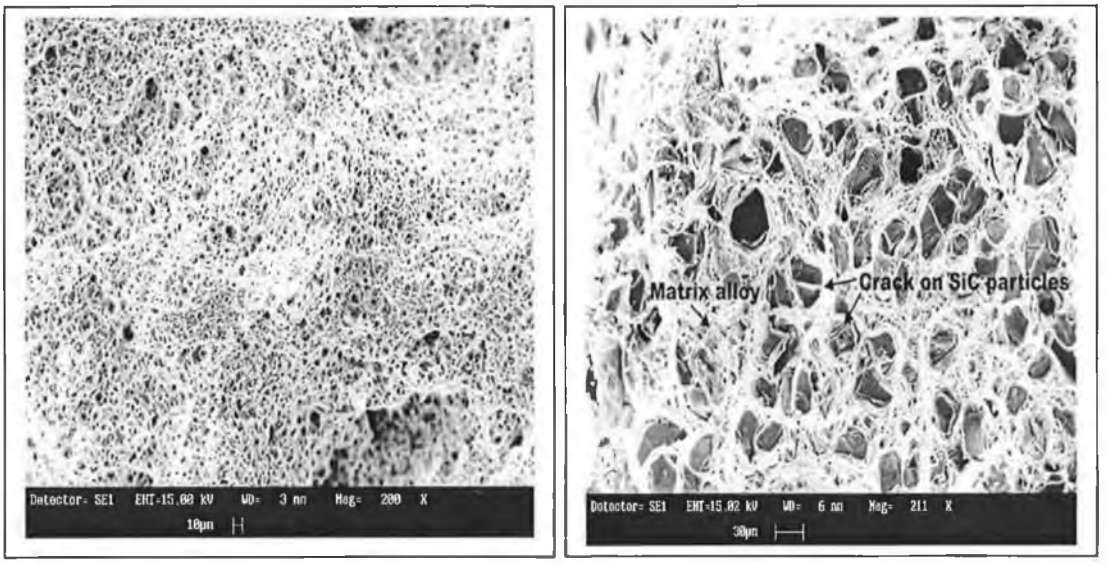

a) b)

Figure 4.16. Micrographs of tensile fracture surfaces on (a) 6061 aluminium (b) 6061 composite.

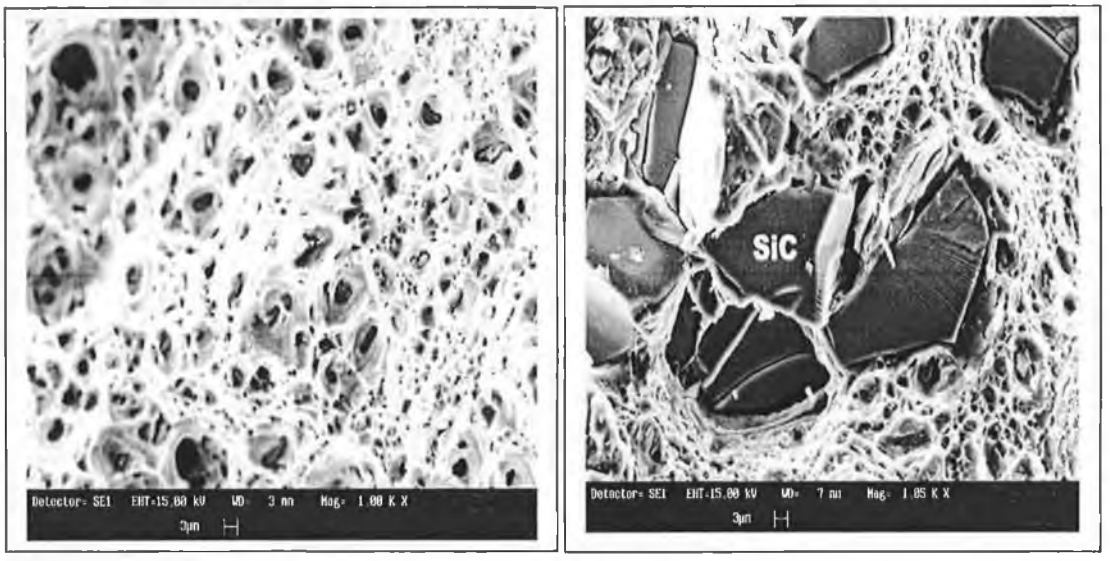

a) b)

Figure 4.17. Microvoids and dimples of a wide range of sizes on the fracture surface of (a) 6061 aluminium alloy (b) AA6061/SiC_P/15% composite.

Reinforced composite experienced larger quantities of voids and dimples which is believe in attributed to the fracture or decohesion of the SiC particles. It also believed that weak integrity and adherent formed in the interface between aluminium and SiC has reduce the effect in transferring the load from matrix to the reinforcement.

Fatigue Tests

Fracture surfaces of unreinforced and reinforced 6061 alloy specimens tested in fatigue were observed under a SEM. In general, two types of fracture areas are evident in investigating a fracture surface in smooth bar, high nominal stress unnotched specimen caused by fatigue phenomenon [96]. The areas are named as the fatigue zone and rupture zone as illustrated in figure 4.18. The fatigue zone is the area of crack propagation while rupture zone was the area of final failure.

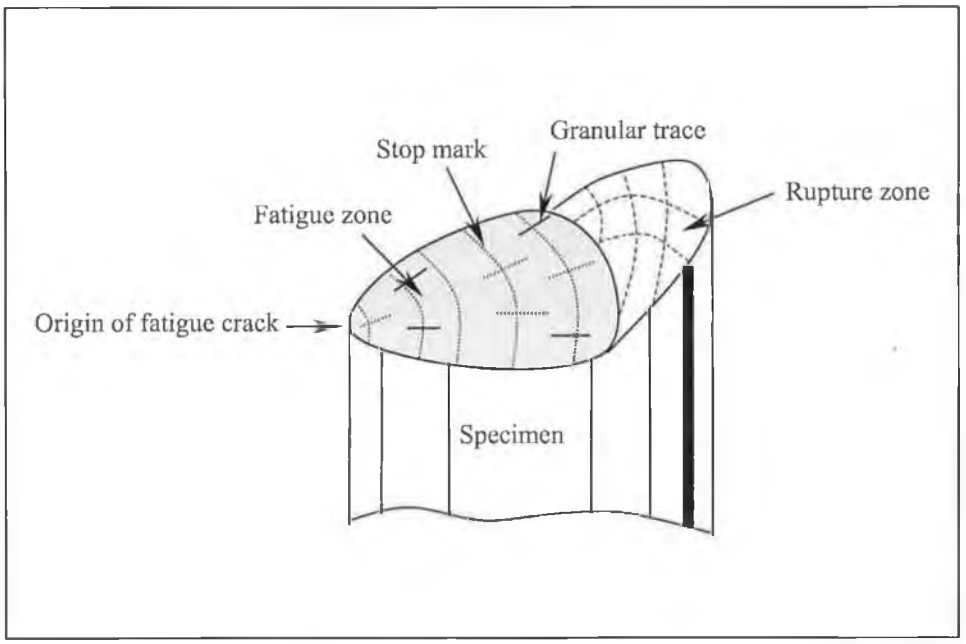

Fatigue 4.18. Schematic representation of fatigue zone and identifying marks.

6061 aluminium alloy

Figures 4.19 (a) and (b) show the fracture surfaces of unreinforced aluminium alloy, tested to failure at stress ratios –1 (tension-compression) and 0.1 (tension-tension) respectively. Both macrofractographs show the same pattern as that illustrated in figure 4.18. Arrows on the images indicate the location of the starter fatigue cracks.

As can be seen in figures 4.19 (a) and (b), the crack origin sites (shown with an arrow) are close to the specimen surface, typical results of an area of high stress concentration caused by surface imperfections. The 'granular trace', showing the progression of the fatigue crack emanating from this origin site is clearly seen in both cases. When the cracks reached a certain length, the specimen was unable to carry the applied maximum load, and broke suddenly into two separated pieces resulting in the rupture zone.

It is obvious that the relative size of the fatigue zone to rupture zone was determined by the stress level induced. This can be seen in figure 4.19 (a), where the rupture zone is relatively small compared to the fatigue zone, due to the relatively low maximum stress, which was applied. With the increased in stress applied, Figure.4.15 (b) shows a larger rupture zone compared to fatigue zone, i.e. the critical crack size leading to failure is smaller.

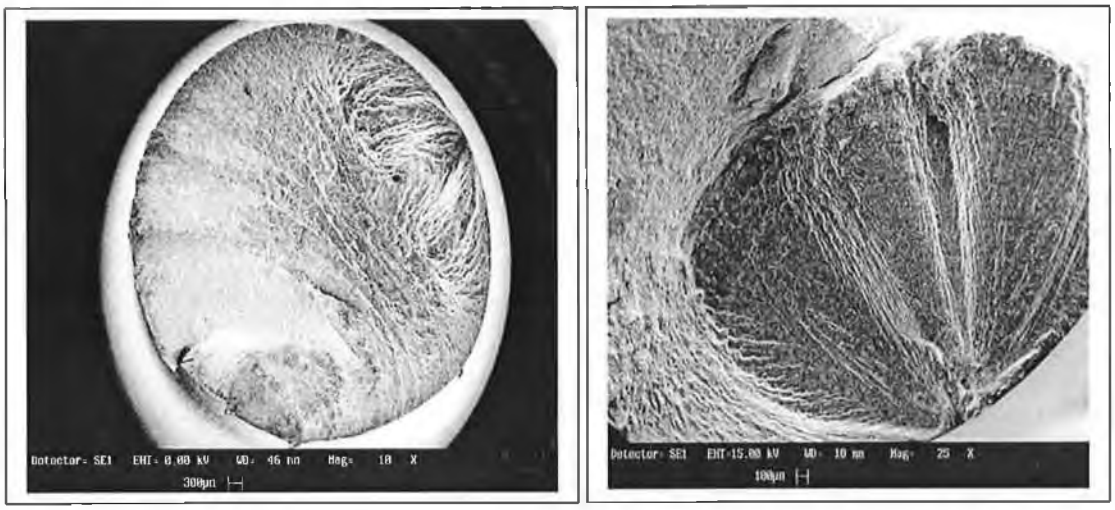

a) b)

Figure 4.19. Macrofractographs of fatigue fracture surface of 6061 aluminium alloy (a) at stress ratio –1 (σ_{Max} = 170MPa, N_f = 4.27 x 10^5 cycles), (b) at stress ratio 0.1 (b) (σ_{Max} = 318MPa, N_f = 3.16 x 10^5 cycles).

A high magnification fractograph taken in the area of fatigue crack origin indicates the formation of extrusions and intrusions in the matrix alloy subjected to alternating loading (figure.4.20).

Detailed examination of the fracture surfaces also reveal the direction of the crack growth in the fatigue zone through stop marks. It is obvious that specimens tested at stress ratio –1 have a lot of stop marks, to which indicated the variation of fast crack propagation rate due to different variation in stress amplitude with cyclic time

At low nominal stress, the fatigue fracture surface for stress ratio –1 is rather flat and shiny and has the characteristic fatigue features like 'Stop marks'. Under SEM inspection, the 'Stop marks' reveal the present of a series of parallel patterns, which are called fatigue striations, shown in figure 4.21. However the 'Stop mark' characteristics are not so clear on the fracture surfaces of samples tested at stress ratio 0.1 consequence from low stress amplitude range, not surprisingly, a relatively high ductility pattern is seen in the rupture zone (figure 4.22).

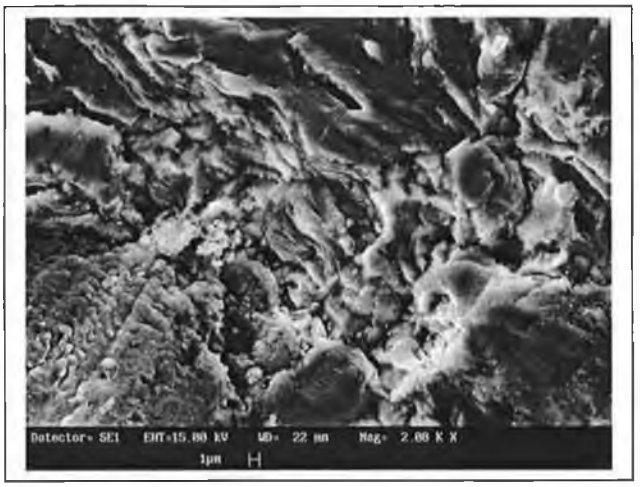

Figure 4.20. The formation of extrusion and intrusions in aluminium alloy subjected to alternating loading.

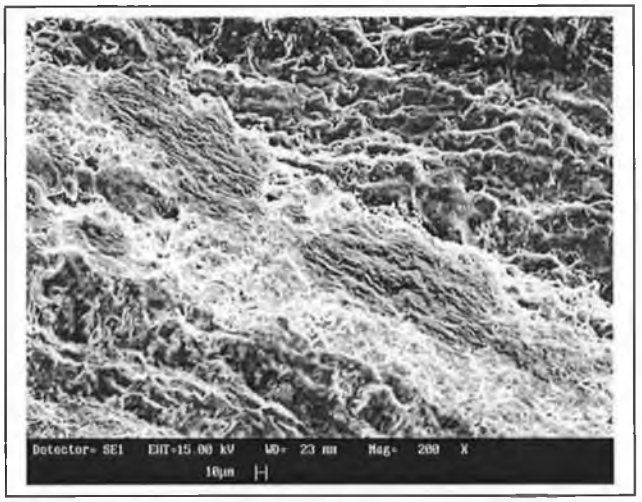

Figure 4.21. Fatigue striation on 6061 aluminium alloy.

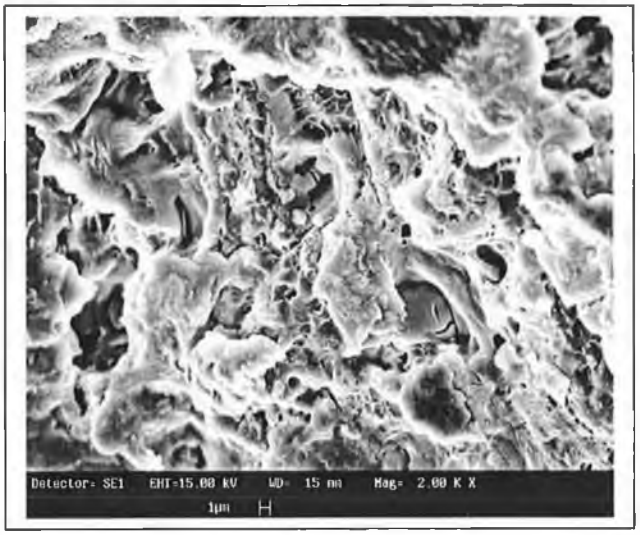

Figure 4.22. Fatigue rupture surface of AA6061.

6061 Aluminium composite

Examination of the fracture surface features under scanning electron microscope for the failed fatigue specimens was performed at low magnification to identify the fatigue and final fracture regions, and at higher magnifications to investigating the regions of a) fatigue crack initiation and b) final fracture.

For the material, which has 15% volume fraction of SiC_P reinforcement, the fracture surfaces have very similar topography whether tested at high, intermediate or low cyclic stress amplitude as shown in figures 4.23 (a) and (b). Flat fracture surfaces were observed to extend from the region of the fatigue zone to the rupture zone, which reveal the fracture was brittle. Macrographs also show more than one crack origin site, and these are indicated by arrows on the figures below. The fracture striation patterns are normal to the stress axis over the fracture surface.

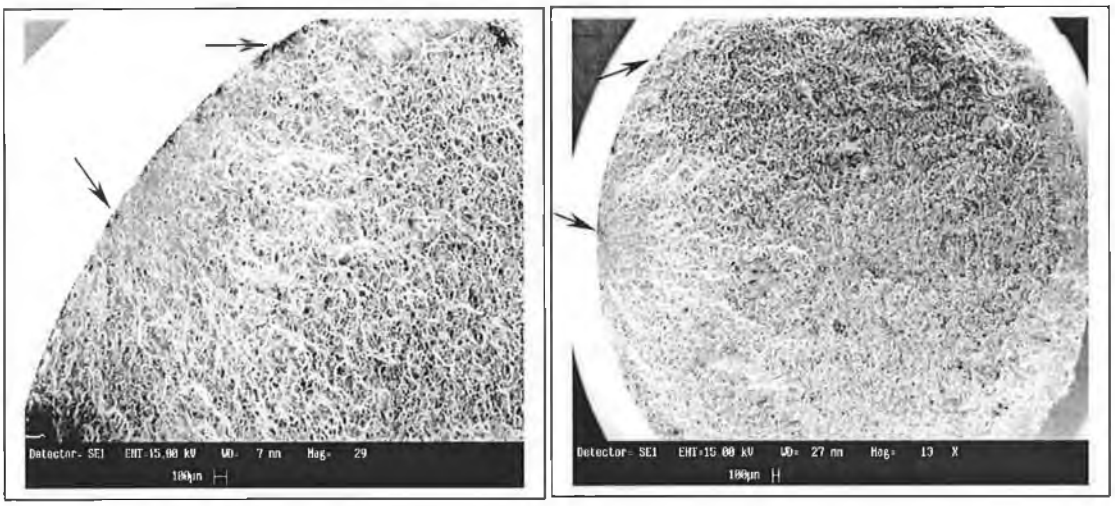

a) b)

Figure 4.23. Macrographs of fatigue fracture surface on 6061 composite (a) at stress ratio –1 (σ_{Max} = 170MPa, N_f = 2.52 x 10^5 cycles), (b) at stress ratio 0.1 (σ_{Max} = 288.47MPa, N_f = 1.31 x 10^5 cycles).

Figure 4.24 shows the fracture of larger SiC particles (>20μm) associated with SiC clusters within/near the crack initiation zone, large particles of SiC fractures are also seen. The larger SiC particles tend to crack early during the cyclic deformation while small particles tend to decohere from the matrix alloy to produce small ductile dimples [14]. It has been reported that the propensity for SiC particle fracture increases with increasing average particle size [14]. Larger particles have higher propensity to incorporate larger faults, and thus are susceptible to cracking at lower stress than small SiC particles.

Figure 4.25 shows micrograph of the fracture surface of a typical fatigue zone on present fatigue samples. The micrograph exhibited increasing amount of cracked SiC particle along crack initiation path to fast fracture surface. Under SEM fractographic observations, evidence showed matrix alloy attached on SiC particle as the result of decohesion was found, and is illustrated in figure 4.26. The decohesion indicates a low bond strength between matrix and reinforcement, which contributed to failure in the composite.

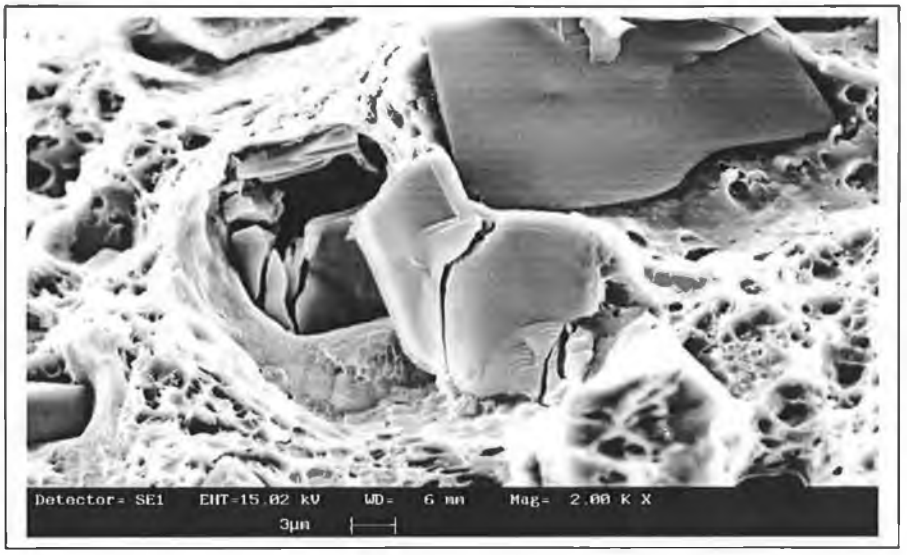

Figure 4.24. Scanning electron micrograph shows a cracked SiC particles within/near the crack initiation zone on aluminium 6061 composite.

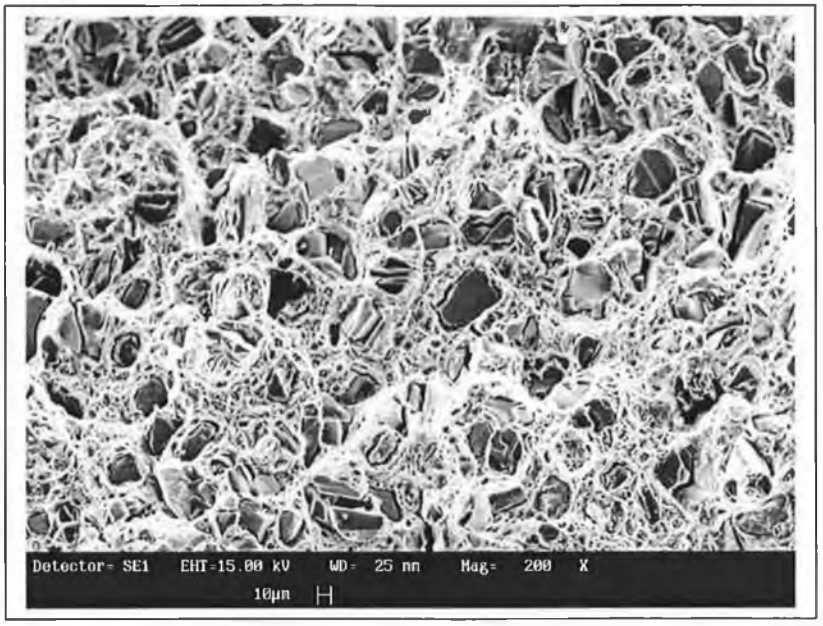

Figure 4.25. Fatigue crack on SiC particles on aluminium 6061 composite.

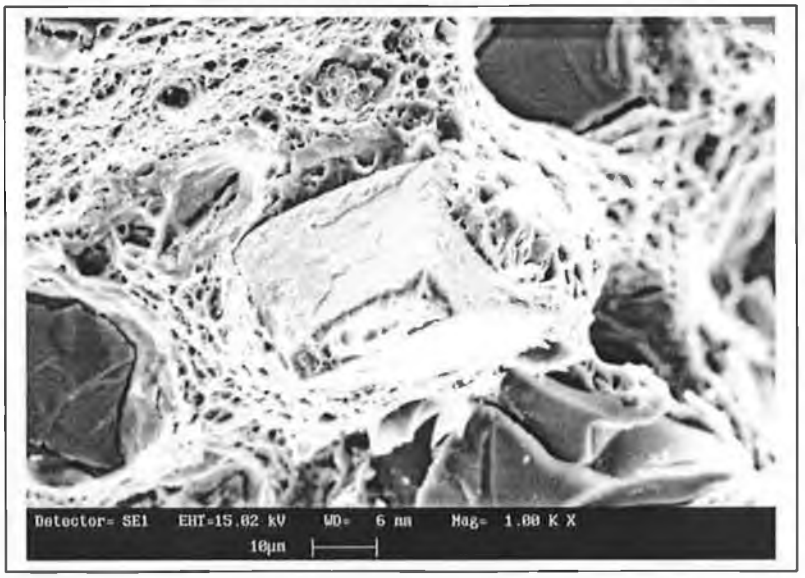

Figure 4.26. SEM fractograph of matrix alloy attached on silicon carbide particle as the results of decohesion in 15% SiC_P 6061 composite.

A combination of ductile dimple failure of the matrix and brittle failure of the reinforcing particles was observed, as shown in figure 4.27. Small SiC particle seems underneath the larger dimpled but most of the dimples are less than 1 μm in diameter. It is believed that the crack is initiated at larger coarse silicon carbide particles at low strain during cyclic deformation while fine SiC particle decohere from the matrix alloy and form voids at high strain amplitude [2]. The dimple pattern was also observed around cracked SiC particles.

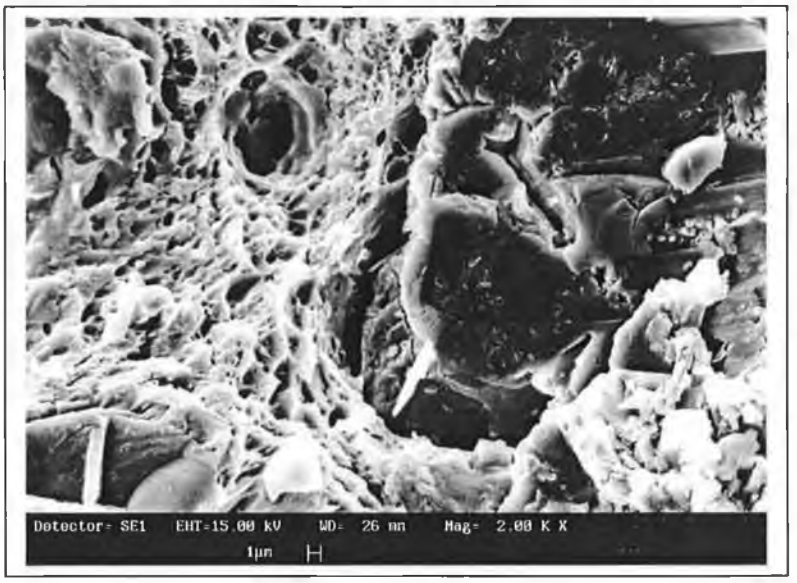

Figure 4.27. Micro voids and dimples of wide range of sizes on the fracture surface of 6061/SiC_P/15% (σ_{max} =242MPa, $N_f = 2.32 \times 10^4$ cycles).

In fatigue rupture zone, dimple patterns are rarely seen in the final failure but rather large quantities of cracked SiC particles are observed as illustrates in figure 4.28.

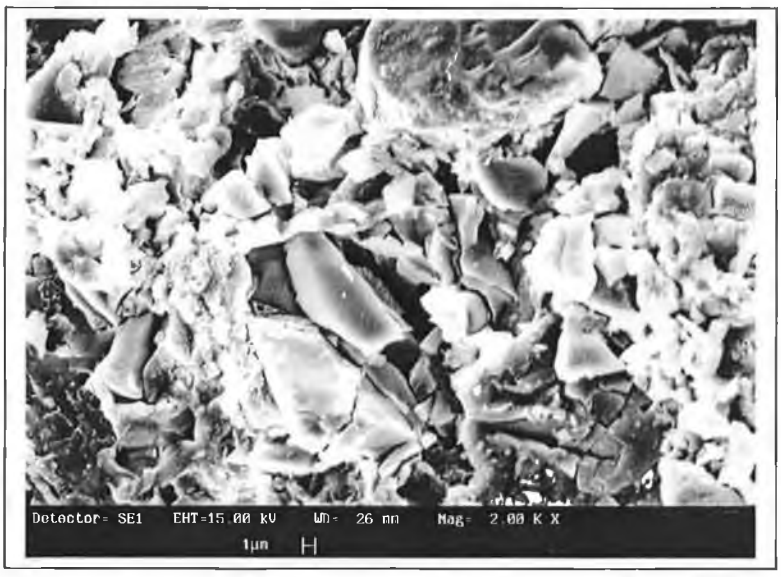

Figure 4.28. Final fracture surface of 6061/SiC_P/15%.

Chapter 5: Conclusions and Recommendations

5.1 Conclusions

- The tensile properties of the 6061 alloy studied are well within the range of other published data. On the other hand, the composite under study demonstrated relatively low strength and slightly higher ductility than data available for similar composites.

- The 6061 alloy exhibits higher ductility, better strength but lower Young Modulus then its particle reinforced composite. The addition of the reinforcement SiC particles to 6061 did not improve strength over the conventional 6061 alloy.

- The fatigue lifetime behaviour of the present 6061 alloy is similar to that seen in published literature, and no significant differences are observed in its fatigue resistance at intermediate and high stresses. While the composite showed much poorer fatigue resistance, it does exhibit the same fatigue endurance limit of 140 MPa after 1×10^7 cycles.

- The increase of mean stress at a given stress amplitude caused a decrease in the corresponding fatigue life for both conventional alloy and composite.

- The stress ratio of −1 shows better fatigue strength, fatigue endurance limit and fatigue life at all stress amplitude levels over those for a ratio of 0.1 for both materials.

The composite used in the current tensile and fatigue tests gave inferior results in terms of both tensile and fatigue strengths compared to the conventional alloy. This can be contributed to the following factors:

- The relatively large particle sizes have decreased interfacial strengths between the matrix alloy and reinforcement particles.

- The composite is not in peak-aged condition due to the fact that SiC particles can accelerate the ageing characteristics of the matrix.

5.2 Proposed Further Research

The following points are proposed for further research and development of the present field of study.

- Testing of an increased number of specimens in order to enhance the statistical accuracy of the fatigue tests result. This may require production of materials and samples in-house. This, in combination with improved quality composite material will greatly enhance the validity of results.

- A more broad systematic test programme using various combinations of reinforcement particles and alloy matrices to investigate the effects of reinforcement volume fraction, reinforcement size and heat treatment processes on mechanical strengths and fatigue behaviour of the composite compared to its conventional alloy at room temperature.

- Extension of the programme of study to include further axial fatigue tests in a variety of environments, including elevated temperatures.

References:

[1] Eliasson J., Sandstrøm R., Applications of Aluminium Matrix Composites, Key Engineering Materials, Vol. 104-107, pp 3-35, 1995.

[2] ASM Handbook, Vol. 19: Fatigue and Fracture, ASM International, Metal Park, Ohio, 1997.

[3] Thomas M.P., King J.E., Effect of Thermal and Mechanical Processing on Tensile Properties of Powder Formed 2124 Aluminium and 2124Al-SiC_p Metal Matrix Composites, Materials Science and Technology, Vol. 9, pp 742-753, September, 1993.

[4] Shan D., Nayeb-Hashemi H., Fatigue Life Prediction of SiC Particulate Reinforced Aluminium Alloy 6061 Matrix Composite using a Weilbull Distribution Model, Recent Advances in Solid and Structure, ASME, pp. 113-127, 1998.

[5] Wang Z., Fatigue of Particulate Ceramics Reinforced Metal Matrix Composites, Key Engineering Materials, Vol. 104-107, pp. 765-790, 1995.

[6] Yu W.C., Yuan J.C., Wang Z.G., Fatigue Behaviour of SiC_p/6061/Al Composite, Acta Metallurgical, Series B, Vol. 4, No. 3, pp. 201-205, Jun 1991.

[7] Hochreiter E., Panzenbock M., Jeglitsch F., Fatigue Properties of Particle-Reinforced Metal Matrix Composites, International Journal of Fatigue, Vol. 15, No. 6, pp. 493-499, 1993.

[8] Skolianos S., Mechanical Behaviour of Cast SiC_p-reinforced Al-4.5% Cu-1.5% Mg Alloy, Materials Science and Engineering, Vol. A210, pp. 76-82, 1996.

[9] Mc Danels D.L., Analysis of Stress-strain, Fracture and Ductility Behaviour of Aluminium Matrix Composites Containing Discontinuous Silicon Carbide Reinforcement, Metallurgical Transaction A, Vol. 16A, pp. 1105-1115, June 1985.

[10] Bonnen J.J., You C.P., Allison J.E., Jones J. W., Fatigue Behaviour of Discontinuously Reinforced Aluminium Matrix Composites, Proceedings of the 4th International Conference on Fatigue and Fatigue Thresholds, pp. 887-892, 1990.

[11] Papakyriacou M., Mayer H.R., Tschegg-Stanzl S.E., Groschl M., Fatigue Properties of Al_2O_3 Particle Reinforced 6061 Aluminium Alloy in the High-cycles Regime, International Journal of Fatigue, Vol. 18, No. 7, pp. 475-481, 1996.

[12] Hochreiter E., Jeglitsch F., Influence of Composition and Distribution of the Reinforcing Particles on Fatigue Properties of Metal Matrix Composites, Journal De Physique IV, pp. 1763-1767, 1993.

[13] Bonnen J.J., Allison J.E., Jones J.W. Fatigue Behaviour of a 2xxx Series Aluminium Alloy Reinforced with 15 Vol Pct SiC_p, Metallurgical Transaction A, Vol. 22A, pp. 1007-1019, May, 1991.

[14] Hall J.N., Jones J.W., Sachdev A.K., Particle Size, Volume Fraction and Matrix-strength Effects on Fatigue Behaviour and Particle Fraction in 2124 Aluminium-SiC_p Composites, Materials Science and Engineering, Vol. A183, pp. 69-80, 1994.

[15] Bhanuprasad V.V., Staley M.A., Ramakrishnan P., Mahajan Y.R., Fracture of Metal Matrix Composites, Key Engineering Materials, Vol. 104-107, Trans Tech Publications, Switzerland, pp. 495-506, 1995.

[16] Lewis C.F., The Exiting Promise of Metal Matrix Composites, Material Engineering, pp 33-37, May 1986.

[17] Schwartz M., Composite Materials Handbook, 2nd edition, McGraw-Hill Inc, 1992.

[18] Suresh S., Mortensen A., Needleman A., Fundamentals of Metal Matrix Composites, Butterworth-Heinemann, 1993.

[19] Baker C., Metal Matrix Composites, Materials world, Vol. 6, No.1, pp 22-23, 1998.

[20] Masuda C., Tanaka Y., Fatigue Properties and Fatigue Fracture Mechanisms of SiC whiskers or SiC Particulate Reinforced Aluminium Composites, Journal of Materials Science, Vol. 27, pp. 413-422, 1992.

[21] Terry B., Jones G., Metal Matrix Composites: Current Development and Future Trends in Industrial Research and Applications, Elsevier Science, 1990.

[22] Feest E.A., Exploitation of The Metal Matrix Composites Concept, Metals and Materials, Vol. 4, No. 5, pp. 273-278, 1988.

[23] Stacey M.H., Production and Characterisation of Fibres for MMC, Materials Science Technology, Vol. 4, pp. 227-239, March 1988.

[24] Chou T.W., Kelly A., Okura A., Fibre-reinforced Metal Matrix Composites. Composites, Vol. 16, No. 3, pp 187-206, July 1985.

[25] Millière C., Suéry M., Fabrication and Properties of Metal Matrix Composites based on SiC Fibre Reinforced Aluminium Alloys, Materials Science and Technology, Vol. 4, pp. 41-51, January 1988.

[26] Degischer H.P., Schulz P., Lacom W., Properties of Continuous Fibre Reinforced Al- and Mg- Matrix Composites Produced by Gas Pressure Infiltration, Key Engineering Materials, Vol. 127-131, pp 99-110, 1997.

[27] Froes F.H., Advanced Metals for Aerospace and Automotive use, Materials Science and Engineering, Vol. A184, pp. 119-133, 1994.

[28] Curran G., MMCs: The Future, Materials World, Vol. 6, No. 1, pp. 20-21, 1998.

[29] Clyne T.W., Withers P.J., An Introduction to Metal Matrix Composites, Cambridge University Press, 1993.

[30] Huda M.D., Hashmi M.S.J., El-Baradie M.A., MMCs: Materials Manufacturing and Mechanical Properties, Key Engineering Materials, Vol. 104-107, Transaction Technology Publication, Switzerland, pp. 37-64, 1995.

[31] Kevorkijan V.M., Sustarsic B., A New Production Technology for Discontinuously Reinforced Al-SiC Composites, Key Engineering Materials, Vol. 127-131, Trans Tech Publications, Switzerland, pp. 471-478, 1997.

[32] Lloyd D.J., Particle Reinforced Aluminium and Magnesium Matrix Composites, International Materials Reviews, Vol. 39, pp. 1-23, 1994.

[33] Powder Metallurgy, Vol. 7, ASM Metals Handbook, American Society for Metals, Metals Park, Ohio 44073, 1990.

[34] Knowles D.M., King J.E. The Influence of Ageing on Fatigue Crack Growth in SiC-particulate Reinforced 8090, Acta Metallurgical Material, Vol. 39, No. 5, pp. 795-806, 1991.

[35] Mummery P., Derby B., The Influence of Microstructure on the Fracture Behaviour of Particulate Metal Matrix Composites, Materials Science and Engineering, Vol. A135, pp. 221-224, 1991.

[36] Midling T., Grong O., Processing and Properties of Particle Reinforced Al-SiC MMCs, Key Engineering Material, Vol. 104-107, Transaction Technology Publication, Switzerland, pp. 329-354, 1995.

[37] Lloyd D.J. Composites: Processing, Properties and Products, The Proceeding of the 3rd International Conference on Aluminium Alloys, Norway, pp. 145-168, 1992.

[38] Kumai Shinji., King Julia E., Knott John F., Fatigue in SiC-particulate-Reinforced Aluminium Alloy Composites, Material Science and Engineering, Vol. A146, pp. 317-326, 1991.

[39] Carotenuto A., Gallo A. Nicolais L., Degradation of SiC Particles in

Aluminium-based Composites, Journal of Materials Science, Vol. 29, pp. 4967-4974, 1994.

[40] Gareth O'Donnell., Processing Optimisation and Numerical Modelling of Powder Metallurgical Aluminium Matrix Composites, Ph.D. Thesis, Dublin City University, Dublin, Ireland, 1999.

[41] Mc Kimpson M.G., Scott T.E., Processing and Properties of Metal Matrix Composites Containing Discontinuous Reinforcement, Materials Science and Engineering, Vol. A107, pp. 93-106, 1989.

[42] Webster D., Effect of Lithium on the Mechanical Properties and Microstructure of SiC Whisker Reinforced Aluminium Alloys, Metallurgical Transactions A, Vol. 13A, pp.1511-1519, August, 1982.

[43] Wu G., Zhao Y., Kono N., Watanabe H., Takahashi T., Fabrication of SiC_w-Al_2O_{3p}/6061 Alloy Composite and Its Mechanical Properties, Key Engineering Materials, Vol. 104-107, pp. 467-474, 1995.

[44] Wu G., Zhao Y., Kono N., Watanabe H., Takahashi T., Strengthening Mechanism of SiC_w-Al_2O_{3p}/6061 Aluminium Alloy Composites, Key Engineering Materials, Vol. 104-107, pp. 647-654, 1995.

[45] Voituriez C., Hall I.W., Strengthening Mechanisms in Whisker-reinforced Aluminium Composites, Journal of Materials Science, Vol. 26, pp. 4241-4249, 1991.

[46] Komai K., Minoshima K., Yoshida G., Fracture Behaviour of SiC Whisker Reinforced Aluminium Alloy under Combined Tension/torsion Loading at Room and Elevated temperatures, Proc. of ICCM-10, Whistler, BC, Canada, Part 2, Pp. 815-822, August, 1995.

[47] Srivatsan T.S., Ibrahim I.A., Mohamed F.A., Lavernia E.J., Processing Techniques for Particulate-reinforced Metal Matrix Composites, Journal of Materials Science, Vol. 26, pp. 5965-5978, 1991.

[48] Hunt W.H. Jr., Cook C.R., Sawtell R.R., Cost-Effective High Performance P/M Aluminum Matrix Composites for Automotive Applications, International Congress and Exposition, Detroit, Michigan, USA, SAE Technical Paper Series, 910834, pp. 1-11, February-March, 1991.

[49] Sritharan T., Xia K., Heathcock J., Mihelich J. Matrix/reinforcement Development for Aluminium-based Composites, Metal & Ceramic Matrix Composites: Processing, Modelling & Mechanical Behaviour, eds. Bhagat R.B, Clauer A.H., Kumar P. and Ritter A.M., The Minerals, Metals & Materials Society, pp. 13-22, 1990.

[50] Hull M., Commercial Success for MMCs, Powder Metallurgy, Vol. 41, No. 1, pp. 25-26, 998.

[51] Bhagat R.B., Emerging P/M Metal Matrix Composites, Advances in Powder Metallurgy & Particulate Materials. Vol. 9, pp. 139-146, 1992.

[52] Hunt W.H. Jr., Rodjom T.J., Discontinuously Reinforced Aluminium Materials by Powder Metallurgy Processes, Advances in Powder Metallurgy & Particulate Materials, Vol. 9, pp. 21-32, 1992.

[53] Clyne T.W., Mason J.F., The Squeeze Infiltration Process for Fabrication of Metal Matrix Composites, Metallurgical Transaction A, Vol. 18A, pp. 1519-1530, August, 1987.

[54] William G., Squeeze forms – Combines Casting with Forging, Metallurgia, pp. 228-232, Jun, 1983.

[55] Chadwick G.A., Squeeze Casting of Metal Matrix Composites using Short Fibre Preforms, Materials Science and Engineering, Vol. A135, pp. 23-28, 1991.

[56] Singer A.R.E., Metal matrix Composites Made by Spray Forming, Materials Science and Engineering, Vol. A135, pp. 13-17, 1991.

[57] ASM, 1985 Metal Handbook, Vol. 2: Failure Analysis and Prevention, ASM International, Metal Park, Ohio, 1992.

[58] Dowling, N. E., Mechanical Behaviour of Materials, Engineering Methods for Deformation, Fracture, and Fatigue, Prentice-Hall, Enhlewood Cliffs, N.J., pp. 286-288, 1990.

[59] You C. P., Bonne, J. J., Allison J. E., Proceeding of the 4th International Conference on Fatigue and Fatigue Threshold, USA, Chapman & Hall. pp. 887-892, 1990.

[60] Hurd N. J., Fatigue Performance of Aluminium Reinforced Metal Matrix Composites, Materials Science and Technology, Vol. 4, pp. 513-517, June 1988.

[61] Eftekhari A., Talia J. E., Mazumdar P. K., Influence of Surface Condition on the Fatigue of an Aluminium-Lithium Alloy (2090-T3), Materials Science and Engineering, Vol. A199, pp. L3-L6, 1995.

[62] Johnson, W.S., Metal Matrix Composites Testing, Analysis, & Failure Modes, STP 1032, American Society For Testing and Materials, Philadelphia, pp. 194-200, 1989.

[63] Staley, J.T., An Introduction to Metal Matrix Composites, McGraw-Hill, New York, pp. 242-246, 1993.

[64] Wang Z.R. Yip T.H., Stain Localisation in Particulate Metal Matrix Composites, International Harold Margolin Conference, San Francisco, USA,

Feb, 1994.

[65] Suery M., L'Esperance G., Interfacial Reaction and Mechanical Behaviour of Al Matrix Composites Reinforced with Ceramic Particles, Key Engineering Materials, Vol. 79-80, Transaction technology publication, Switzerland, pp. 33-46, 1993.

[66] Lloyd D.J., Aspect of Fracture in Particulate Reinforced Metal Matrix Composites, Acta Metallurgical Materials, Vol. 39, No.1, pp. 59-71, 1991.

[67] Park K. J., Park C.G., Kim N.J., Lee C.S., Microstructure on the Intrinsic Fatigue Properties of Al-Li 8090 Alloy, Materials Science and Engineering A190, pp. 99-108, 1995.

[68] Kumai Shinji., King Julia E., Knott John F., Short and Long Fatigue Crack Growth in a SiC Reinforced Aluminium Alloy, Fatigue Fracture Engineering Materials Structure, Vol. 13, No. 5, pp.511-524, 1990.

[69] Allison, J.E., Wayne, J.J. Fundamentals of Metal Matrix Composites, eds: Suresh S., Mortesen A., Needleman A, Butterworth-Heinemann, pp. 269-273, 1993.

[70] Sun Lizhi., Li ShouXin., Zhu Zuming., Wang Z. G., Dependence of Fracture Behaviour on SiC_p Size of Al Matrix Composites, Proceeding of ICCM-10 Whistler, BC, Canada, pp 32-36, August, 1995.

[71] De Salazar M.G., Urena A., Manzanedo S., Barrena M. I., Corrosion Behaviour of AA6061 and AA7005 Reinforced with Al_2O_3 Particles in Aerated 3.5% Chloride Solutions: Potentiodynamic Measurements and Microstructure Evaluation, Corrosion Science, Vol. 41, pp. 529-545, 1999.

[72] Ishii Hitoshi., Tohgo Keiichiro., Araki Hiroyasu., Fatigue Crack Propagation of SiC, whisker Reinforced 6061 Al Alloy Composite, Engineering Fracture Mechanics, Vol. 40, No. 4/5, pp. 821-827, 1991.

[73] Papakyriacou M., Mayer H. R., Tschegg-Stanzl S. E., Groschl M., Near-Threshold Fatigue Crack Growth Al_2O_3 Particle Reinforced 6061 Al Alloy. Fatigue Fracture Engineering Material structure, Vol. 18, No. 4, pp. 477-487, 1995.

[74] Levin M., Karlsson B., Influence of SiC Particle Distribution Prestraining on Fatigue Crack Growth Rates in Aluminium AA6061-SiC Composite Material, Material Science and Technology, Vol. 7, pp. 596-607, July, 1991.

[75] Kumai S., Yoshida K., Higo Y., Nunomura S., Effects of Dendrite Cell size and Particle Distribution on the Near-Threshold Fatigue Crack Growth Behaviour of Cast Al-SiC Composites, Acta Materials, Vol. 44, No. 6, pp. 2249-2257, 1996.

[76] Suresh S., Fatigue of Materials, Cambridge University Press, 1991.

[77] Logsdon W.A., Lian P.K., Tensile, Fracture toughness and fatigue Crack Rate Properties of Silicon Carbide Whisker and Particulate Reinforced Aluminium Metal Matrix Composites, Engineering Fracture Mechanics, Vol. 24, No. 5, pp. 737-751, 1986.

[78] Kumai S., Yoshida K., Higo Y., Nunomura S., Effects of the Particle Distribution Fatigue Crack Growth in Particulate SiC/6061 Aluminium Alloy Composites, International Journal of Fatigue, Vol. 14, No. 2, pp. 105-112, 1992.

[79] Leinum J.R., Pedersen K., Roven H.J., Effects of Crack Direction on Fatigue Crack Propagation Mechanisms in an Uncrystallized AlMgSi Alloy, The Proceeding of the 3rd International Conference on Aluminium Alloys, Norway, pp. 521-526, 1992.

[80] Niklas A., Froyen L., Wevers M., Delaey L., Acoustic Emission during Fatigue Crack Propagation in SiC Particle Al Matrix Composites, Metallurgical and Material Transaction A, Vol. 26A, pp. 319-83-3189, December, 1995.

[81] Shang Jian Ku., Ritchie R.O., On The Particle-size Dependence of Fatigue-Crack Propagation Thresholds in SiC-particulate Reinforced Aluminium Alloy Composites: Role of Crack Closure and Crack Trapping, Acta Metallurgical, Vol. 37, No. 8, pp. 2267-2278, 1989.

[82] Davison D.L., The Growth of Fatigue Cracks Through Particulate SiC Reinforced Aluminium Alloys, Engineering Fracture Mechanics, Vol. 33, No. 6, pp. 965-977, 1989.

[83] Kassam Z.H.A., Zhang R.J., Wang Z.R., Finite Element Situation to Investigate Interaction Between Crack and Particulate Reinforcement in Metal Matrix Composites, Material Science Engineering, 1994.

[84] Hasson D.F., Crowe C.R., Ahearn J.S., Cook D. C., Failure Mechanism in High Performance Materials, eds: Early J., Shives R. and Smith J, Cambridge University Press, pp. 14, 1984.

[85] Guerra-Rosa L., C. Moura Branco C., Radon J. C., Monotonic and Cyclic Crack Tip Plasticity, International Journal of Fatigue, Vol. 6, No. 1, pp. 17-84, January 1984.

[86] Miller W.S., Humphreys F.J., Strengthening Mechanisms in MMC's, The Mineral, Metal and Materials Society, pp. 125-131, 1990.

[87] Hunt W.H., Osman Jr., T.M., Lowandowski J.J. Micro-and Macrostructural Factor in DRA Fracture Resistance, JOM, pp. 30-35, January 1993.

[88] Rees D.W.A., Gatehouse W., Liddiard M, Tensile and Compressive Behaviour of a Particulate Metal Matrix Composites, Proceeding of Euroworkshop, pp.

155-168, Auguest 1995.

[89] Bhanu Prasad V.V., Prasad K.S., Kuruvilla A.K., Pandey A.B., Bhat B.V.R., Mahajan Y.R., Composite Strengthening in 6061 and Al-4Mg Alloys, Journal of Materials Science, Vol. 26, pp. 460-466, 1991.

[90] Zhao Zhou., Zhijian Song., Yingkun Xu., Effect of Microstructure on the Mechanical Properties of an Alloy 6061-SiC Particle Composite, Materials Science an Engineering, Vol. A132, pp. 83-88, 1991.

[91] Manoharan M., Lewandowski J.J., Effect of Reinforced Size and Matrix Microstructure on the Fracture Properties of an Aluminium Metal Matrix Composite, Material Science and Engineering, Vol. A150, pp. 179-186, 1992.

[92] Ko Byung-Chul and Yoo Yeon-Chul., The Effect of Ageing Treatment on the Microstructure and Mechanical Properties of AA2124 Hybrid Composites Reinforced with both SiC Whiskers and SiC Particles, Composites Science and Technology, Vol. 59, pp. 775-779, 1999.

[93] Shyong H., Derby B., The Deformation Characteristic of SiC Particulate-Reinforced Aluminium Alloy 6061, Materials Science and Engineering, Vol. A197, pp. 11-18, 1995.

[94] Bathias C., A Review of Aluminium Matrix Reinforced by Particles or Short Fibres, Material Science Forum, Vol. 217-222, pp. 1407-1412, 1996.

[95] ASM International Fatigue Data Book: Light Structural Alloys, November 1995.

[96] Failure of Materials in Mechanical Design, Analysis, Prediction, Prevention, Second edition, Collins J. A. A., Wiley-Interscience Publication, pp - 232-233, 1993.

[97] British Standard, BS 3518: Method of Fatigue Testing, Part 1: Guide to General Principle, 1993.

[98] Arsenault R.J., The Strengthening of Aluminium Alloy 6061 by Fibres and Platelet Silicon Carbide, Materials Science and Engineering, Vol. 64, pp. 171-181, 1984.

[99] ASTM Designation: E 8M-97, Standard Test Method for Tension Testing of Metallic Materials, 1997.

APPENDIX A

CERTIFICATE OF CALIBRATION

ISSUED BY The Calibration Laboratory of ESH Testing Limited

DATE OF ISSUE 25 August 1998 CERTIFICATE NUMBER 02065

NAMAS

CALIBRATION
No. 0188
No. 0188 SI

Leys Road, Brockmoor, Brierley Hill,
West Midlands, England. DY5 3UT.
Tel: 01384 480545
Fax: 01384 74974
Email: esh_testing@compuserve.com

ESH testing limited

Approved Signatory
P C RANDLE

ISSUED TO	The School of Mechanical and Manufacturing Engineering Dublin City University Dublin 9 IRELAND
LOCATION	The Calibration Laboratory of ESH Testing Limited
DESCRIPTION	A Sandner Electronic Clip Gauge Extensometer
SERIAL No	EXA 20-5 / 768
GAUGE LENGTH	20 mm ATTITUDE Vertical
INDICATOR	ESH Digital System No. 976080
CONDITIONING UNIT	ESH Clip Gauge Amp 2 No. D610
DATE OF VERIFICATION	01 July 1998

The above extensometer has been verified to the standard BS EN 10002-4 : 1995 and to ESH Technical Work Procedure No. ESH/10002-4, using verification equipment calibrated to BS EN 10002-4 : 1995.

The extensometer complied with the requirements of the standard for the following classification :

INCREASING ONLY

5.0 mm	Range	Class 1.0	5.0 mm down to 0.50 mm
2.0 mm	Range	Class 1.0	2.0 mm down to 0.20 mm
1.0 mm	Range	Class 1.0	1.0 mm down to 0.10 mm
0.5 mm	Range	Class 1.0	0.5 mm down to 0.05 mm

CALIBRATION DEVICE	Divided test piece rig no. 1823/EXT. Certificate No. NPL 97022/ EXT4/50 Dated 16 July 1997
TEMPERATURE	20 degrees Celsius.

NOTE :
Clause 7 of BS EN 10002-4 : 1995 states that under normal conditions it is recommended that verification shall be carried out at intervals of approximately 12 months. This interval shall not exceed 18 months unless the test is expected to last more than 18 months, in this case the extensometer shall be verified before and after the test. The extensometer shall be verified after each repair or adjustment which affects the accuracy of measurements.

The reported expanded uncertainty is based on a standard uncertainty multiplied by a coverage factor $k = 2$, providing a level of confidence of approximately 95 %.
The uncertainty evaluation has been carried out in accordance with UKAS requirements.

APPENDIX B

Comparison of fatigue lifetime tests of experimental aluminium alloy 6061 with the published data at Stress ratio, R = -1.

Aluminium alloy AA6061		**Aluminium alloy AA6061[7]**	
Stress Amplitude (MPa)	*Cycles to failure, N_f*	*Stress Amplitude (MPa)*	*Cycles to failure, N_f*
318.3	1.16×10^3	373.62	3×10^3
318.3	2.7×10^3		4.2×10^3
288.47	1.12×10^4	348.35	1.2×10^3
288.47	1.31×10^4		1.9×10^3
288.47	1.37×10^4		2.8×10^3
288.47	2.78×10^4		4.2×10^3
288.47	3.24×10^4		6.2×10^3
			6.5×10^3
242	3.26×10^4		
242	3.55×10^4	300	9×10^3
242	4.77×10^4		1×10^4
242	1.18×10^5		1.8×10^4
			2×10^4
200	7.88×10^4		
200	2.65×10^5		
200	3.68×10^5	254.94	3.3×10^4
200	5.27×10^5		4×10^4
			6×10^4
170	1.55×10^5		9×10^4
170	3.16×10^6		
170	4.27×10^5	200	1.5×10^5
170	8.16×10^5		1.6×10^5
			2×10^5
140	6.1×10^6		2.6×10^5
140	5.2×10^6		2.5×10^5
140	1×10^7 (Did not fail)		
140	8.53×10^6	170.33	2.3×10^5

			2.8×10^5
			5×10^5
		142.19	1×10^6
			1.6×10^6
			4.5×10^6
		121.97	2.6×10^6
			4.1×10^7 (Did not fail)
		100	5×10^7 (Did not fail)

Comparison of fatigue lifetime tests on experimental aluminium alloy 6061 composites with the published data at Stress ratio, R = -1.

Aluminium composites AA6061/SiC_P/15%		**Aluminium composites AA6061/SiC_P/15%[7]**	
Stress Amplitude (MPa)	*Cycles to failure, N_f*	*Stress Amplitude (MPa)*	*Cycles to failure, N_f*
		350	2×10^3
			4.7×10^3
			5.5×10^3
288.47	1.5×10^3		
288.47	2.54×10^3	300	8×10^3
			1×10^4
			1.6×10^4
			1.9×10^4
242	1.73×10^4	250	5.5×10^4
242	1.28×10^4		6×10^4
242	2.32×10^4		9×10^4
			1×10^5
200	3.78×10^4	200	3.1×10^5
200	1.56×10^4		4.3×10^5
200	1.58×10^4		5.5×10^5
			4.4×10^6
170	2.52×10^5		
170	7×10^4	175	1.2×10^6
170	3.61×10^5		1.6×10^7
140	1×10^7 (Did not fail)	140	4×10^7 (Did not fail)
140	1×10^7 (Did not fail)		